Wind- and Thermal-Driven Air Flows and the Buoyancy and Advection Effects on Air Exchange within Urban Environments

by

Sigurdur Petur Magnusson

(B.Sc. in Civil and Environmental Engineering
University of Iceland, 2008)

Submitted to the Department of Civil and Environmental Engineering in Partial Fulfillment of the Requirements for the Degree of

Doctor of Philosophy in the Field of Civil and Environmental Engineering

at the

MASSACHUSETTS INSTITUTE OF TECHNOLOGY

June 2014

Signature of Author.....Signature redacted.....
Department of Civil and Environmental Engineering
May 2, 2014

Certified by.....Signature redacted.....
Dara Entekhabi
Bacardi and Stockholm Water Foundations Professor of Civil and Environmental Engineering and Earth, Atmospheric, and Planetary Sciences
Thesis Supervisor

Accepted by.....Signature redacted.....
Heidi Nepf
Chair, Departmental Committee for Graduate Students

Wind- and Thermal-Driven Air Flows and the Buoyancy and Advection Effects on Air Exchange within Urban Environments

by

Sigurdur Petur Magnusson
Submitted to the Department of Civil and Environmental Engineering
May 2, 2014 in Partial Fulfillment of the
Requirements for the Degree of Doctor of Philosophy in the Field of
Civil and Environmental Engineering

ABSTRACT

Human exposure to air pollutants and thermal stress in urban areas are public health concerns. The year 2008 was the first year when more than half of the human population lived in urban areas. Studies of the urban air fluid dynamics can be applied to increase pedestrian comfort and emergency response planning. In this study we focus on thermal effects on urban air flows. The thermal effects are extended beyond what is found in the literature to better understand the thermo fluid processes within urban areas.

A field experiment on the air flow within an urban street canyon was performed to examine the relationship between the dimensionless in-canyon velocity, u/U_0, where U_0 is the free stream velocity, and the thermal conditions inside the canyon. A buoyancy parameter, B, which estimates the ratio between buoyancy forced and mechanically forced flows, is applied. The results indicate a mechanically driven flow regime for B parameters less than 0.05–0.1 (u/U_0 a constant). For larger B parameters, u/U_0 begins to increase and the flow is considered to be in the intermediate flow regime.

To further extend the buoyancy effects, computational fluid dynamics (CFD) simulations are performed. The aspect ratio (H/L, H height of the buildings and L the width between the buildings) is varied. The results show that the air flow within urban areas can be considered to be purely buoyancy driven when the B parameter is larger than about 50. For canyons with aspect ratios near unity, $\frac{u}{U_0} \approx B^{1/2}$. The buoyancy is more important in deep canyons.

The exchange rate between urban areas and the ambient air is an important factor in determining the human exposure to air pollutants. CFD simulations are developed to estimate the effects of increased buoyancy on the exchange rate and the results show how the exchange rate increases roughly with $B^{1/2}$ for purely buoyancy driven flows.

Finally, CFD simulations are performed to estimate the effects of horizontal advection on the air quality within urban areas. Under mechanically driven situations the concentration increases roughly by $n^{1/4}$ in the downstream direction, where n is the number of upstream canyons and the same amount of tracer is released inside each of the canyons.

Thesis Supervisor: Dara Entekhabi
Title: Bacardi and Stockholm Water Foundations Professor of Civil and Environmental Engineering and Earth, Atmospheric, and Planetary Sciences

ACKNOWLEDGMENTS

Writing my PhD thesis has been an enjoyable journey. First, I would like to thank my creative advisor, Professor Dara Entekhabi, for his generous contribution, challenging ideas and motivation during the last four years. His expertise and experience in the academia and role as a science team leader at NASA SMAP mission has been a real inspiration for me.

Then, I would also like to thank my outstanding thesis committee; Professor Rex Britter for all of our meetings in Singapore and at MIT and his knowledge in the field of urban air fluid mechanics, Professor Les Norford for his involvement in the field experiment executed in Singapore and his expertise on applied studies in this field, Professor Joe Fernando for his contribution and ideas about the field experiment in Singapore, for our meeting at University of Notre-Dame and for having provided one of his students, Dr. Ann Dallman, to assist on the execution of the field experiment, and Professor Roman Stocker for his comments and knowledge in the field of fluid dynamics.

Collaborating with Dr. Ann Dallman from University of Notre-Dame was an important step in choosing my thesis topic and executing the field experiment and I am thankful for our cooperation.

My research group consists of talented and ambitious individuals who will become global experts in their fields. I highly appreciate the opportunity given to get to know all of them.

Finally, I would like to thank my friends at the New England area for their invaluable friendship and my friends and family members in Iceland for all their memorable visits to Boston.

I would like to dedicate my thesis to my family in Iceland

Contents

Symbols

A_{wall}	Wall surface area	[m2]
A_{out}	Average area of flow out of the canyon	[m2]
a_1, a_2, a_3, a_4	Constants	[-]
α	Entrainment coefficient	[-]
α_t	Thermal diffusivity of air	[m2 s-1]
B	Buoyancy parameter	[-]
B_c	Critical value of B where the flow is in the intermediate regime	[-]
B_t	Critical value of B where the flow is completely buoyancy dominated	[-]
b	Radius of a plume	[m]
b_1, b_2	Constants	[-]
C_{in}	Average in-canyon air pollution	[kg m-3]
C_{amb}	Average ambient air pollution	[kg m-3]
C_p	Specific heat of air	[J kg-1K-1]
D	A constant in Eq. 2.30	[-]
D_p	Diffusion coefficient	[-]
e	Emissivity of walls	[-]
ε	Turbulence dissipation rate	[J kg-1s-1]
F	Buoyancy Flux	[m4 s-3]
F_{vol}	Volume flux	[m2 s-1]
g	Gravity	[m s-2]
g'	Reduced gravity	[m s-2]
γ_1, γ_2, γ_3, γ_4	Constants	[-]
H	Height of the urban street canyon	[-]
h_f	Heat transfer coefficient	[W m-2K-1]
J_p	Mass diffusion flux	[kg s-1]
k	Turbulence kinetic energy	[J Kg-1]
k_{can}	Average in-canyon turbulence kinetic energy	[J kg-1]
κ	von Karman constant	[-]

L	Width of the urban street canyon	[m]
M	Mass flux	[kg s-1]
N	Momentum flux	[N s-1]
n	Number of canyons	[-]
η	Weight deficit	[-]
ρ	Air density	[kg m-3]
Q	Heat flux	[MW]
q_{in}	Total heat flux into the canyon	[W]
q_{west}	Heat flux from the west wall into the canyon	[W]
q_{east}	Heat flux from the east wall into the canyon	[W]
q_{out}	Total heat flux out of the canyon	[W]
Ra_H	Rayleigh number	[-]
Re	Reynolds number	[-]
Ri	Richardson number	[-]
r	Width of a rising plume near a wall	[m]
r_c	Radius of a circular area source	[m]
Sc_t	Schmidt number	[-]
σ_w	Surface shear stress	[Pa]
T_{amb}	Ambient air temperature	[K]
T_{can}	Average in-canyon air temperature	[K]
T_{walls}	Average walls surface temperature	[K]
T_{west}	West wall surface temperature	[K]
T_{east}	East wall surface temperature	[K]
T_{lee}	Leeward wall surface temperature	[K]
T_{wind}	Windward wall surface temperature	[K]
T_{uproof}	Upstream roof surface temperature	[K]
$T_{downroof}$	Downstream roof surface temperature	[K]
Γ_i	Source parameter	[-]
τ	Residence time	[s]

τ_p	Residence time estimated by plume method	[s]
τ_s	Residence time estimated by momentum flux method	[s]
τ_q	Residence time estimated by heat flux method	[s]
$\vec{U}$	Velocity vector	[s]
U_0	Free stream velocity above the street canyon	[m s-1]
u	Characteristic horizontal in-canyon air speed	[m s-1]
u_c	Mechanically forced circulation	[m s-1]
u_j	Velocity inside a horizontal jet	[m s-1]
u_m	Characteristic horizontal mechanically driven in-canyon air speed	[m/s]
u_t	Characteristic horizontal buoyancy driven in-canyon air speed	[m s-1]
u_e	Entrainment velocity	[m s-1]
u_*	Friction velocity	[m s-1]
μ_t	Turbulent viscosity	[m2 s-1]
V	Volume flux	[m3 s-1]
v_{max}	Maximum measured vertical in-canyon speed	[m s-1]
υ	Kinematic viscosity of air	[m2 s-1]
w	Vertical velocity	[m s-1]
w_a	Vertical velocity inside an area source plume	[m s-1]
w_m	Characteristic vertical mechanically driven in-canyon air speed	[m s-1]
w_t	Characteristic vertical buoyancy driven in-canyon air speed	[m s-1]
w_p	Vertical velocity inside a rising plume	[m s-1]
w_e	Exchange velocity	[m s-1]
$w_{e,p}$	Exchange velocity estimated from plume method	[m s-1]
$w_{e,s}$	Exchange velocity estimated from momentum flux method	[m s-1]
$w_{e,q}$	Exchange velocity estimated from heat flux method	[m s-1]
Y_p	Mass fraction of species p	[-]
z	Depth	[m]

z_0	Roughness length	[m]
z_i	Mixed layer height	[m]

Table of Figures

Chapter 1: Introduction and Motivation

Urbanization

More than half of the world's population lived in urban areas for first time at the end of the year 2008, and it is predicted that about 70% of the population will live in urban areas by 2050 (United Nations [1]). Human exposure to air pollutants and increased thermal stress are risk factors for public health in urban areas. No international standard definition exists of an urban area, so that the meaning of an urban area varies between nations. The 2011 United Nations Demographic Yearbook [2] gives the definitions of urban areas in various nations. These definitions consist of combinations of the following factors: the size of the population, population density, distance between built-up areas, predominant type of economic activity, conformity to legal or administrative status and urban characteristics such as specific services and facilities. In the United States of America, an urban area is defined as an agglomeration of 2,500 or more inhabitants, generally having a population density of 1,000 persons per square mile or more, while in the United Kingdom an urban area is defined as settlements where the population is 10,000 or above, and in Japan as a city having 50,000 or more inhabitants with 60% or more of the houses located in the main built-up areas and 60% or more of the population (including their dependents) engaged in manufacturing, trade or other urban type of business. This variation between the definitions of an urban area makes comparison on the development of urbanization between nations and continents difficult; nonetheless the trend towards increased urbanization is clear.

The growth rate of population in the larger urban areas (megacities) is increasing rapidly. A megacity is defined by the United Nations [1] as a metropolitan area with a total population of more than 10.0 million people. Tokyo and New York were the only world's megacities in 1970. By 2011, there were 23 the megacities in the world and it is predicted that by 2025 that 37 megacities will exist. Today, most of these megacities are located in the developing countries and 13 of them are located in Asia. The increased urbanization and existence of megacities have raised public health concerns due to increased human exposure to gaseous pollution and particulates. Generation of anthropogenic heat, CO_2 and other gaseous constituents and particulates from activities within cities is substantial and may influence both thermal stresses on the 'at risk' public at city scales, and furthermore, affect climate change on the regional and global scales. An evidence about this is risk is given in a study by Dockery et al. [3] where the mortality rate ratio is given as a function of fine particles (with a diameter less than 2.5 μm, PM2.5) in the air measured in six US cities. Burning of fossil fuels in vehicles and power plants are the main sources of fine particles in the built urban environments. The mortality rate ratio is the ratio of actual mortality to that expected from population with the same demographics and thus isolates extra mortality due to local conditions. It expresses the increase or decrease in mortality of a study sample with respect to the general population. The study shows how the mortality rate ratio increases linearly with fine particles. In a city with about 30 μg m-3 of fine particles in the air the mortality rate ratio is measured to be about 25% higher than in a city with about 10 μg m-3. The air

quality is thus a factor in determining both the quality of life of the urban populations and the longevity.

Beijing (20 million people) is an example of a megacity with a severe air quality problem. The rapid urbanization, the fast growing economy and the presence to industrial factories and coal power plants are the reasons given for the air quality problem in Beijing. In January 2013, the PM2.5 level was measured at 20 times (Blackest day [4]) higher than safe levels set by the World Health Organization (WHO). Beijing is an example of a city where some realistic actions need to be taken to increase the air quality for the population.

It is not only the concentration of particles that determines the quality of life in a densely populated area. The thermal condition within the area is also an important factor where too high thermal stress affects at-risk segments of the population. For example, in Russia during the summer of 2010 a heat wave killed about 15,000 people (LeComte [5]). Li and Bou-Zeid [6] show how an urban area increases and extend the effects of a heat wave, which leads to increased risk for the population.

The urban heat island (UHI) intensity is used to describe the temperature difference between an urban area and its rural environment. Urban areas are usually warmer due to more built structures and less soil and vegetation. A great amount of the urban areas are made of materials such as concrete and asphalt that convert and store more incoming radiation as sensible heat than their surrounding rural environments. Measurements show also that the maximum measured UHI effects often occur during nighttime (Kim and Biak [7], Papanastasiou and Kittas [8]) which can be explained by

the increased heat storage of the built urban environment compared to its ambient rural areas which cool down faster. The anthropogenic heat fluxes also lead to a higher air temperature within urban areas. The effects of urbanization as measured by the population density on the UHI intensity is discussed in Oke [9]. In a city of 100,000 people the maximum observed UHI intensity was 4 – 8°C, in a city of one million people the measured UHI intensity was 8–11°C, and in a European city of 10 million people the maximum observed UHI intensity was 10°C. With increasing numbers of megacities in warm regions, such as in South-Asia, the thermal stress on the population will thus continue to increase.

In a study by Kim et al. [10], a time-series analysis was conducted to estimate the acute effects of high air temperature in six South Korean cities and the data compared to the daily mortality in those cities. Clear patterns were found in four of these cities. For example in the capital city Seoul (population: 10.3 M) the increase in daily mortality for 1°C increase in air temperature (above the threshold temperature 27 – 29.7°C), above the threshold temperature, is about 16.3%. Studies on these impacts are thus important to understand the risk of thermal stress the population in urban areas.

Thesis Outline

Several environmental hazards emerge with increased urbanization, as has been discussed above. The studies show both mortality rate ratio increases, with increased fine particles in the atmosphere and by increased thermal stress. In the last few decades, simulations have been used to better understand the air, heat and constituents flows

within urban areas. The results and increased knowledge can be used to ensure better design and management in densely populated urban areas. City ventilation and dispersion of pollutants are thus important topics in the coming decades.

Pollutants dispersion and air quality in urban environments are affected by its unique thermal regime. This thesis focuses mostly on the effects of the buoyant force on the flow within the built urban environments. The buoyancy exists due to the fact that urban areas are often at a higher temperature than the ambient air as described by the UHI effects. Studies show (for example Allegrini et al. [11] and Li et al. [12]) how the buoyant force affects the air flow and constituents dispersion within the built urban environment. In this thesis the goal is to define under what mechanical (synoptic flow) and thermal conditions, the buoyant force plays a critical role in determining the air flow and thus the dispersion of pollutants out of the built urban environments. It is done by introducing the buoyancy parameter, B, which takes into account the ratio between mechanical and buoyancy forces. The results can guide scientists when to take into account the buoyancy the atmospheric dispersion models applied at built urban environments. In Chapter 2, analytical and semi-empirical solutions on buoyant plumes in an otherwise static environment are introduced and the thermal effects evaluated on a city scale. In that chapter the goal is to quantify the strength of the buoyant force in an otherwise static environment. Chapter 3 introduces a field experiment performed in an artificial urban street canyon in Singapore which dealt with the buoyancy effects on the flow field within the canyon. In Chapter 4, computational fluid dynamics (CFD) simulations on the experimental canyon are performed. Chapter 5 focuses on the

buoyancy effects on the residence time of an air parcel within a single urban street canyon and thus on human exposure to the air pollutants. Chapter 6 deals with the role of horizontal advection on air quality within the built urban environments. Finally, summary, conclusions and future research directions are found in Chapter 7.

Chapter 2: On Buoyant Plume above the Built Urban Environments

Abstract

This chapter of the thesis focuses on the effects of buoyancy driven plumes on the otherwise static ambient environment. It is a part of this thesis to better understand the buoyancy flow in a general way. The air flow inside the plume determines the exchange rate of air and thus human exposure to air pollutants. Human exposure to outdoor air pollutants has raised concern in recent decades due to the increased urbanization. Semi-empirical solutions are used to simulate buoyant plumes formed above urban areas (city scale) and to determine the effects of buoyancy on the movement of the ambient air. The mass-flux inside the plume gives an estimate on the rate of removal of pollutants from an urban area and on the air exchange between the ambient and in-plume air.

Introduction

As mentioned in the first chapter, increased urbanization has raised public health concerns. Human exposure to pollutants is a determining factor on the quality of life within the built urban environment. According to the United Nations Environment Programme (UNEP [13]) more than one billion people are exposed to outdoor air pollution every year and urban air pollution is responsible for up to one million premature deaths and one million pre-natal deaths annually. Two ways to reduce the human exposure to pollutants are to reduce the release of pollutants within and in the proximity of the urban areas and through an appropriate urban design to increase the dispersion of pollutants out of the built urban environment. Organizations such as the World Bank are

working on finding efficient strategies to reduce urban air pollution from vehicular and other sources. By appropriate urban design and planning, dispersion of pollutants can be increased by improving the air exchange between the ambient and in-canyon air. The combination of mechanical and buoyancy forces (mechanically-buoyancy driven flow) determines the amount of dispersion of pollutants out of the built urban environment. In this chapter the focus is set on the buoyancy flow and its effects on the otherwise static nearby environment and the creation of the convective mixed layer above an urban environment. It is the difference in density between the heated air and the ambient air that leads to buoyancy fluxes within and across the urban canopy layer (atmospheric instability). The reasons for the buoyancy difference in the urban environment are discussed and then known semi-empirical and analytical solutions on buoyant plumes are applied where both plumes originated in a steady point source and plumes originated in a steady area source are considered.

Background

Howard [14] was an early observer of the temperature difference between the built urban environment and its surrounding rural environment. The urban heat island (UHI) is a concept used to describe the temperature difference between the urban areas and their surrounding rural areas. The primary reason for this difference in temperature that the majority of the urban areas are made of concrete and asphalt, which store more heat and thus reach higher temperatures than their surrounding rural areas (Stull [15]). The anthropogenic heat fluxes within urban areas also enhance the UHI intensity. The urban

air is heated through heat fluxes from the hot urban surface during sunny days and through anthropogenic heat release. It is this temperature difference between near surface air and ambient air that leads to buoyancy fluxes that affect the flow in and above the urban canopy layer. Case studies have been made in several cities. Oke [9] investigated the relationship between the city size and the UHI intensity. The measured temperature difference was up to 12 K. Gaffin et al. [16] conducted a study in New York City which showed on average a 2.5 K air temperature difference between Central Park and rural areas near Manhattan. Results from UHI studies in (sub)tropical regions, Washington, DC, and Houston, TX, are found in Roth [17], Hicks et al. [18] and Streutker [19], which show similar trends.

The atmospheric boundary layer is the part of the troposphere that is directly influenced by the earth's surface. The built urban environment affects the creation of the atmospheric boundary layer because of increased drag within the built urban environment and also due to larger heat fluxes from the built urban environment. During a sunny day of low synoptic wind speeds a buoyancy dominant boundary layer can be formed and this is known as a convective mixed layer. A sketch of an idealized convective mixed layer is shown in Fig 2.1. The convective mixed layer forms a kind of a dome above the built urban area. The height of the convective mixed layer, z_i, is a critical factor in determining air quality, where it defines the volume in which the released pollutants are mixed into (Schäfer et al. [20], Srivastava et al. [21]). Measurements on the height of the convective mixed layer have been made in cities around the world. Simpson et al. [22] used the AERMET model to determine the height above Oklahoma City, OK, in July 2003. The

maximum estimated mixing height (usually during afternoon) is around 2,000 m. Bianco and Wilczak [23] used Doppler radar to measure the height of the urban boundary layer in Houston, TX. The measured height during the afternoon was about 1,500–2,000 m. Bidokhti et al. [24] used LIDAR observations to measure the boundary layer height in Zanjan in Iran. The typical midday mixed layer height above the city was found to be about 2,200 m. Steyn et al. [25] used LIDAR to measure the height in Vancouver, Canada. The typical measured height was about 400–600 m. Menut et al. [26] also used LIDAR to measure the height above the Paris area: the maximum measured height was about 1,000 m. This recitation on the mixed layer height in various cities around the world shows some difference in measured heights. This difference can for example be explained by dynamic and unequal local weather conditions, different buoyancy intensities, local geographies and configurations of the cities.

Methods

Turner [27] described plumes as a rise of fluid when buoyancy is supplied steadily into the environment. The rise of the fluid leads to a movement of the ambient fluid through an entrainment of ambient fluid into the rising plume. In this chapter the goal is to characterize buoyant plumes formed above a built urban environment. In order to understand the effects of a buoyant plume on the otherwise calm or static ambient environment, semi-empirical solutions for plumes originated from a point source and from an area source are used.

A dimensional analysis by the well-known Buckingham Pi Theorem (White [28]) gives the relationship between the variables determining the properties of a plume. The variables that describe the properties of a plume are the buoyancy flux, F (m4 s-3), the height above the heat source, z (m), the radius of the plume, b (m), the average vertical velocity inside the plume, w (m s-1), and the reduced gravity within the plume, g' (m s-2), which is defined as

$$g' = g\frac{\Delta\rho}{\rho}, \tag{2.1}$$

where ρ the density of an ambient fluid (kg m-3), $\Delta\rho$ the difference in density between the ambient fluid and the buoyant fluid (kg m-3). The buoyancy flux, F, is then defined as

$$F = b^2\pi w g'. \tag{2.2}$$

By dimensional analysis where b, w and g' are the dependent variables and F and z the independent variables:

$$b = f_3(F, z), \tag{2.3}$$

$$w = f_1(F, z), \tag{2.4}$$

$$g' = f_2(F, z), \tag{2.5}$$

the following relationship is obtained by applying the Buckingham Pi Theorem:

$$b = \pi_3 \cdot z, \tag{2.6}$$

$$w = \pi_1 \cdot \frac{F^{1/3}}{z^{1/3}}, \tag{2.7}$$

$$g' = \pi_2 \cdot \frac{F^{2/3}}{z^{5/3}}, \quad \textbf{2.8}$$

where π_1, π_2 and π_3 are constants.

Morton et al. [29] and Turner [27] derived solutions for buoyant plumes originated in a point source in a static uniform environment. In their solutions it is assumed that the plume is confined within an inverted cone, with sharp boundaries between the plume and the environment. The conservation equations for volume, momentum and buoyancy fluxes inside the plume are based on the entrainment assumption, where the volume of air inside the plume increases proportionally to the entrainment of air into the plume with height. The momentum flux increases by g' and the buoyancy flux is a constant in the uniform environment. The plume radius (inverted cone) and vertical velocity are functions of height z. The conservation of volume, momentum and buoyancy can be written as:

$$\frac{d(b^2 w)}{dz} = 2\alpha b w, \quad \textbf{2.9}$$

$$\frac{d(b^2 w^2)}{dz} = b^2 g', \quad \textbf{2.10}$$

$$\frac{d(b^2 w g')}{dz} = 0, \quad \textbf{2.11}$$

where α is the entrainment coefficient, defined in Turner [27] as

$$\alpha = \frac{u_e}{w}, \quad \textbf{2.12}$$

and u_e (m s-1) is the velocity of ambient fluid into the plume (entrainment velocity). Solving these conservation equations gives the following relationship

$$b = \frac{6}{5}\alpha z, \tag{2.13}$$

$$w = \frac{5}{6\alpha}\left(\frac{9}{10}\alpha F\right)^{1/3} z^{-1/3}, \tag{2.14}$$

$$g' = \frac{5F}{6\alpha}\left(\frac{9}{10}\alpha F\right)^{-1/3} z^{-5/3}. \tag{2.15}$$

These solutions give the same relationship between the variables as the dimensional analysis, as expected. The mass flux, *M* (kg s-1), and momentum flux, *N* (N s-1), of the plume are:

$$M = \rho \cdot w(z) \cdot \pi b^2(z), \tag{2.16}$$

$$N = \rho \cdot w^2(z) \cdot \pi b^2(z). \tag{2.17}$$

In Eq. 2.14 and Eq. 2.15 the solutions for w and g' fail near the steady point source. The reason is that the point source is infinitely small and to avoid this error the source needs to be of a finite and non-vanishing size.

Michaux and Vauquelin [30] derived an analytical solution for a plume originated from a steady circular area source in a calm environment of uniform density that is valid at all heights above the source. This solution is used to simulate a plume above an urban area originated in a steady circular source. They introduce the plume function, Γ, which gives the balance between volume, momentum and buoyancy fluxes in the plume. The source parameter is a form of the Richardson number ($Ri = 2\eta gb/w^2$). Papanicolaou and List [31] discovered that the Richardson number becomes constant ($16\alpha/5$) at a

certain height above the source. That constant is used to normalize the Richardson number and the source parameter is then obtained as:

$$\Gamma(z) = \frac{5g}{8\alpha}\frac{\eta b}{w^2}, \tag{2.18}$$

where η is the dimensionless density deficit. At the source, the plume function is called the source parameter initially introduced in Morton [32]

$$\Gamma_i = \frac{5V_i^2 F_i}{4\alpha N_i^{5/2}}, \tag{2.19}$$

where V_i, N_i and F_i are the volume, momentum and buoyancy fluxes at the source. The relationship between the radius of the plume and the velocity inside it is derived in Michaux and Vauquelin [30]

$$\frac{b}{b_i} = \left(\frac{\Gamma}{\Gamma_i}\right)^{1/2}\left(\frac{1-\Gamma_i}{1-\Gamma}\right)^{3/10}, \tag{2.20}$$

$$\frac{w}{w_i} = \left(\frac{\Gamma_i}{\Gamma}\right)^{1/2}\left(\frac{1-\Gamma}{1-\Gamma_i}\right)^{1/10}. \tag{2.21}$$

So far, known semi-empirical and analytical solutions in the literature have been introduced to calculate the properties of a rising plume above an urban area. Now, additional equations will be introduced as part of this thesis to characterize the circulation of the flow above the urban area. The rise of the heated air creates the convective mixed layer. At a certain height, which depends on the buoyancy intensity, the heated air loses its momentum. This is where the mixed layer height, z_i, is defined. At that height the air has the tendency to turn and circulation of air above the urban area occurs (see Fig 2.1). The mixed layer derives its name from this circulation where it leads to uniform distribution of the conserved variables. In order to characterize this circulation, a no-flux

boundary at the mixed layer height, z_i, is set and the plume is allowed to turn around a corner before it hits the no-flux boundary at z_i. The vertical plume velocity is thus converted to horizontal velocity. It is assumed that the energy is conserved (Bernoulli's equation for a streamline), so the vertical velocity and the horizontal velocity are the same at z_i. Fig 2.2 shows the geometry of the plume, where h is the necessary depth to conserve the flow of mass at z_i. The conservation of mass equation for the flow at the curve defines h:

$$\boldsymbol{\rho \cdot w(z_i) \cdot \pi b^2(z_i) = \int_{z_i-h}^{z_i} \rho \cdot w(z_i) \cdot S(z) \cdot dz,} \quad \textbf{2.22}$$

where $S(z)$ is the side surface area of the plume (m2)

$$\boldsymbol{S(z) = 2 \cdot \pi \cdot b(z),\ 0 < z \leq z_i,} \quad \textbf{2.23}$$

Inserting Eqs. 2.13 - 2.15 into Eq. 2.22 gives:

$$\boldsymbol{\rho \cdot \frac{5}{6\alpha}\left(\frac{9}{10}\alpha F\right)^{1/3} z_i^{-1/3} \cdot \pi \cdot \left(\frac{6}{5}\alpha z_i\right)^2} \quad \textbf{2.24}$$

$$\boldsymbol{= \int_{z_i-h}^{z_i} \rho \cdot \frac{5}{6\alpha}\left(\frac{9}{10}\alpha F\right)^{1/3} z_i^{-1/3} \cdot 2 \cdot \pi \cdot \left(\frac{6}{5}\alpha z\right) dz}$$

Integration gives the following second-order polynomial

$$\boldsymbol{h^2(r) + 2z_i h(r) - \frac{6}{5}\alpha z_i^2 = 0.} \quad \textbf{2.25}$$

Assuming entrainment of air into the horizontal jet, where α is now the entrainment coefficient between the horizontal jet and ambient air. Conservation of mass and momentum fluxes gives $h(r)$ and the average horizontal velocity $u_j(r)$ inside the horizontal jet

$$\frac{d}{dr}\left(2 \cdot \pi \cdot r \cdot h(r) \cdot u_j(r) \cdot \rho\right) = 2 \cdot \pi \cdot r \cdot \alpha \cdot u_j(r) \cdot \rho, \quad \textbf{2.26}$$

$$\frac{d}{dr}\left(2 \cdot \pi \cdot r \cdot h(r) \cdot u_j(r) \cdot \rho \cdot u_j(r)\right) = 0. \quad \textbf{2.27}$$

Integration on Eq. 2.27 gives

$$2 \cdot \pi \cdot r \cdot h(r) \cdot \rho \cdot u_j(r) = \frac{M_0}{u(r)}, \quad \textbf{2.28}$$

where M_0 is the momentum flux at z_i. Now by inserting Eq. 2.28 into Eq. 2.26 $u_j(r)$ and $h(r)$ are obtained:

$$\frac{d}{dr}\left(\frac{M_0}{u_j(r)}\right) = 2 \cdot \pi \cdot r \cdot \alpha \cdot u_j(r) \cdot \rho. \quad \textbf{2.29}$$

Applying separations of variables and integrate; u_j(r) is obtained as:

$$u_j(r) = \sqrt{\frac{M_0}{2}\left(\frac{1}{\pi \cdot r^2 \cdot \alpha \cdot \rho + D}\right)}. \quad \textbf{2.30}$$

where D is a constant. D is determined such that the mass flux inside the plume turning around the corner is conserved. Finally, $h(r)$ is obtained by inserting Eq. 2.30 into Eq. 2.28

$$h(r) = r \cdot \alpha + \frac{D}{\pi \cdot r \cdot \rho}. \quad \textbf{2.31}$$

In the next section, solutions will be introduced under these idealized situations.

Results and Discussion

First, a plume originated from a steady point source is considered where the ambient conditions correspond to a calm sunny day. This situation leads to a convective heat flux from the urban surface to the ambient air. The heated air rises and the plume is formed. It is assumed that the strength of the point source corresponds to the heat flux of

an urban area of 1 km2. Eq. 2.9–Eq. 2.11 supply the values that give the properties of the plume. The reference heat flux is set as 100 W m-2 (Stull [15]). The total heat flux from the steady point source is thus about Q = 100 MW. Calculations on the plume variables are also made for total heat fluxes of 60 MW and 140 MW. The relationship between the buoyancy flux and the heat flux Q is

$$F = \frac{g \cdot Q}{\rho \cdot C_p \cdot T}, \qquad \textbf{2.32}$$

where C_p is specific heat of air at a constant pressure (J Kg-1K-1) and T is the temperature of ambient air (K). The reference value of the entrainment coefficient α is set as 0.10, but calculations on the plume variables are also made for α = 0.08 and α = 0.12. These values are found in Turner [27] and are determined by experiments.

Velocity is a function of the height in the rising plume. The magnitude of w provides insight into the synoptic wind conditions necessary to account for the buoyancy flux. Fig 2.3 shows how w decreases with increased height. For Q = 100 MW, w(500) is about 6.5 m s-1 but has decreased to 4.2 m s-1 at 2,000 m height above the source. The figure also shows w for two other values of the source heat flux, Q = 60 MW and Q = 140 MW. If w at 2,000 m height is considered, for Q = 60 MW, w = 3.5 m s-1 is obtained, w = 4.2 m s-1 when Q = 100 MW and w = 4.7 m s-1 for Q = 140 MW. Knowing the right amount of the heat flux from the source, which in this case is an urban area, is important when estimating the buoyancy effects on the local air flow. The point source approach overestimates the velocity in the near-field of the source, where the velocity is infinite at the origin. Thus, later on the area source approach is used to calculate the velocity in the

plume near the source. The second value calculated is the reduced gravity, g', which gives information about the buoyancy intensity in the plume. Fig 2.4 shows how the scaled reduced gravity decreases with increased height. The reduced gravity drops by 90% between z = 500 m and z = 2,000 m. This provides an idea about the buoyancy fluxes in the atmosphere above an urban environment. To realize the size of the affected ambient area in the environment around the plume, the radius b of the plume is calculated. Fig 2.5 shows how the plume expands linearly by increased height for three values of α. Larger α means more entrainment of air into the plume from the surrounding environment. Again, working out the situation at z = 2,000 m, the radius of a plume for α = 0.08 is about 185 m, 240 m when α = 0.10 and 285 m when α = 0.12. In a broader sense the size of the plume can give information about expected air flow conditions above urban areas, for instance, this information about the upstream flow is important for pilots since it affects the local turbulence. Effects of different values of α on w and g' are also considered. Fig 2.6 and Fig 2.7 show the change in w and g' for three values of α. The value of w is lower for a larger value of α, so the mass flux inside the plume is conserved. At a height of 2,000 m above the source, w = 4.8 m s-1, 4.2 m s-1 and 3.6 m s-1 when α = 0.08, 0.10 and 0.12 and the values of g'/g at 2,000 m height are 0.0009, 0.001 and 0.001 when α = 0.08, 0.10 and 0.12. The amount of entrainment air into the plume affects the velocity of the rising air quite significantly but the magnitude of the reduced gravity is less sensitive.

Two more values of the plume are now being considered to better understand its properties, the mass flux, M, and the momentum flux, N. The mass flux inside the plume

is equal to the amount of air entrained into the plume at each height and the momentum flux gives a sense of the importance of the buoyancy flux in the case when synoptic wind exists. In Fig 2.8, the mass flux with height for three values of heat flux with $\alpha = 0.10$ is plotted. The mass flux increases with height and also increases with increased Q. M increases with z raised to the power of 5/3 and N increases with z raised to the power of 4/3. When z = 2,000 m the mass fluxes are $7.5 \cdot 10^5$ kg s-1, $9.0 \cdot 10^5$ kg s-1 and $1.0 \cdot 10^6$ kg s-1 for heat fluxes of 60 MW, 100 MW and 140 MW, and the momentum fluxes for the same heat flux values are $2.7 \cdot 10^6$ N s-1, $3.7 \cdot 10^6$ N s-1 and $4.6 \cdot 10^6$ N s-1 as can be seen in Fig 2.9. M increases with Q raised to the power of 1/3 and N increases with Q raised to the power of 2/3. The two fluxes for three values of α are plotted as before and shown in Fig 2.10 and Fig 2.11. When z = 2,000 m the mass flux values for $\alpha = 0.08$, 0.10 and 0.12 are $6.5 \cdot 10^5$ kg s-1, $9.0 \cdot 10^5$ kg s-1 and $1.1 \cdot 10^6$ kg s-1 and the momentum flux values are $3.2 \cdot 10^6$ N s-1, $3.7 \cdot 10^6$ N s-1 and $4.2 \cdot 10^6$ N s-1. As can be seen, the value of α has a large impact on the flux inside the plume. M increases with α raised to the power of 4/3 while N increases with α_e raised to the power of 2/3.

With these relatively simple calculations on a plume originated from a steady point source, the goal is to understand how w, g', b, M and N depend on z, Q and α. To further understand the formation of the convective circulation above an urban area, the buoyant plume is allowed to reach a prescribed convective mixed layer height. Heights of the convective mixed layers have been measured above urban areas around the world and the height has been found to depend on the location and density of the urban area as well as the time of day. We set z_i at 2,000 m, which is a realistic height during a calm sunny

day. The mixed layer height is defined as a no-flux boundary leading to a turn of the air flow around a corner so that a horizontal jet forms. The average horizontal velocity inside the jet is $u_j(r)$ and is given in Eq. 2.30 where r is the distance from the center of the buoyant plume. Fig 2.12 shows how $u_j(r)$ decreases with increased distance from the center of the plume where Q = 100 MW and α = 0.10. At a distance of 2,000 m from the center of the plume, $u_j(r)$ is 25% of the velocity at the center of the buoyant plume, and at a 10,000 m distance from the center of the plume $u_j(r)$ is 5% of the velocity at the center. This analysis demonstrates the spread and the strength of the jet under the given conditions. The height of the horizontal jet indicates the spread of the jet in horizontal and vertical directions. Eq. 2.31 gives $h(r)$ which is plotted with the buoyant plume in Fig 2.13. The figure shows an increase in depth of the horizontal jet with increased distance from the center of the plume, as expected. These idealized calculations give insight into the flow above an urban area. The rise of the buoyant plume leads to entrainment of ambient air into the plume and that, with the formation of the convective mixed layer which is like a cap above the urban area, leads to circulation of air above the urban area.

In the existing literature, such idealized buoyant plumes formed above an urban area originate from an infinitely small and steady point source. The shortcoming of such results is that they are invalid near the source of the plume where the velocity at the infinitely small point source is infinite. Thus a plume originated in a circular steady area source is now considered and the solution will give more realistic information on a plume above an urban area. To compare the solution to the previous calculations, the local heat flux is set as 100 W m-2 and the total heat flux thus, Q = 100 MW. The radius of the

circular area is thus r_c = 564 m. Eq. 2.20 gives the development of the radius of the rising plume while Eq. 2.21 gives its velocity. The velocity of the area source plume $w_a(z)$ is plotted with height and is compared with the point source plume velocity in Fig 2.14. At z = 0 m, w_a = 0, then w_a increases by z until it reaches its maximum velocity w_a = 3.2 m s-1 at z = 1,000 m. Above that the velocity slowly decreases. Compared with the point source plume velocity, the difference is largest near the source of the plumes but gradually with increased height the two methods give similar results. The shapes of the two plumes with the horizontal jets are finally shown in Fig 2.15. The radius of the circular area source is r = 564 m at z = 0 and it decreases to z = 300 m where it reaches its minimum radius r = 200 m. The reason for this shrinkage is that the velocity of the plume is low and the flow is laminar near the source, so the entrainment of ambient air into the plume does not occur. Above z = 300 m the radius of the plume increases gradually due to entrainment of ambient air into the plume. The point source plume and the area source plume give the same increase in both velocity and shape above z = 1,000 m, as expected.

Now consider the mass flux inside the plume with respect to removal of pollutants emission at the ground level. The U.S. Environmental Protection Agency defines carbon monoxide (CO) as one of the harmful pollutants to public health and the environment. CO is found in urban areas mostly due to burning of fossil fuels. During periods of low synoptic winds the pollution level is generally higher in urban areas. In this otherwise static environment it is the buoyant plume that removes air pollutants from the ground level. Now consider a simplified example in order to realize the effects of the buoyancy flow inside the plume on the removal of CO from the ground level. Fig 2.16 shows a

control volume of the plume near the area source with a source of CO inside it. The information about a plume originated in an area source is applied where it gives a valid result near the source as discussed earlier. The ground level is assumed to be the volume up to 10 m (a realistic height of buildings) above the area source; the CO is well mixed inside that area under the steady state conditions. At 10 m height the total mass flux inside the plume is $5.5 \cdot 10^5$ m3 s-1. If the mass flux of CO inside the control volume is known, the concentration inside it can be determined by the following equation:

$$[CO] = \frac{M_{CO}}{V}, \qquad \textbf{2.33}$$

where $[CO]$ is the concentration of CO (kg m-3), V the volume flux inside the plume (m3 s-1) and M_{CO} the mass flux of CO from the source at the ground level (kg s-1). It is assumed that vehicles are the only source of CO inside the plume where it gives a tangible quantity. According to EPA [33] the average emission rate of CO from an average passenger car is about 13 g km-1. Setting the average speed inside our idealized city as 50 km hr-1 the mass flux of the average passenger car is 650 g hr-1 (0.18 g s-1). In Los Angeles there are 5,600 cars km-2 [34], in New York 3,600 cars km-2 [34] and in Singapore about 1,400 cars km-2 [35], which gives 1.26 ppm, 0.8 ppm and 0.3 ppm. EPA sets average air quality standards for CO as 9 ppm (10.3 mg m-3) for an 8-hour period [36]. These simple calculations show that under purely buoyancy driven flow conditions, the air quality inside a typical city can still meet the EPA requirements on air quality.

Conclusions

In this chapter simple semi-empirical solutions on rising buoyant plumes (Turner [27], Morton et al. [29], Michaux and Vauquelin [30]) is introduced and applied to estimate the air flow above urban areas in an otherwise static and uniform environment. The rise of air is due the UHI effect and it affects the ambient air through entrainment of ambient air into the plume. Concentrating on the results for the buoyant plume originated in a circular steady area source, which gives more realistic solutions near the source, the velocity of the rising plume is about 3 m s-1. Considering the interplay between synoptic wind above an urban area and the buoyancy flux above the area, based on the calculations the synoptic wind should be dominant when it is larger than about 3 m s-1.

More realistic consideration on the air flow and removal of pollutants within urban areas is to consider the interplay between the mechanical and thermal forces and to take into the account the configuration of the buildings of the built urban environments. In the forthcoming chapters the concentration will be on determining the air flow at the street scale (up to 200 m) when both of those forces exist and to introduce both a field experiment in an idealized urban street canyon as well as computational fluid dynamics (CFD) simulations.

Figures

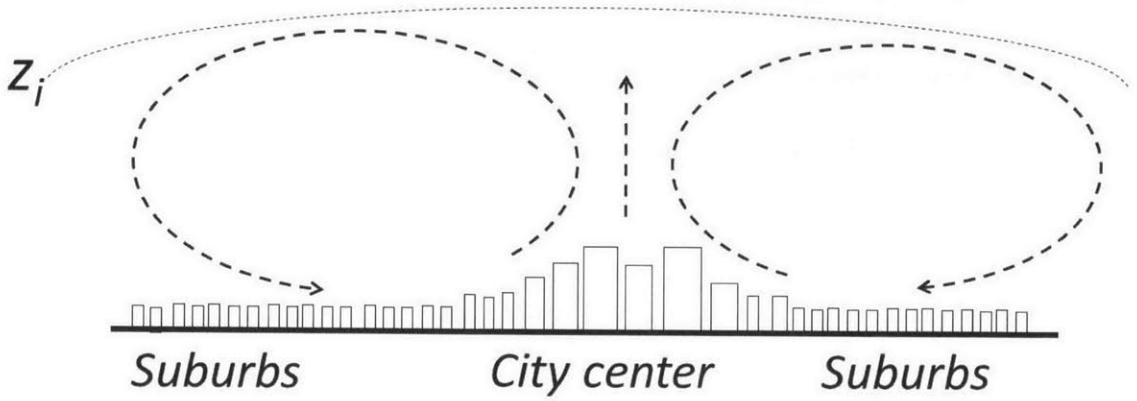

Fig 2.1 The formation of a convective mixed layer above an urban area. The height of the layer, z_i, determines the volume in which the pollutants are diluted.

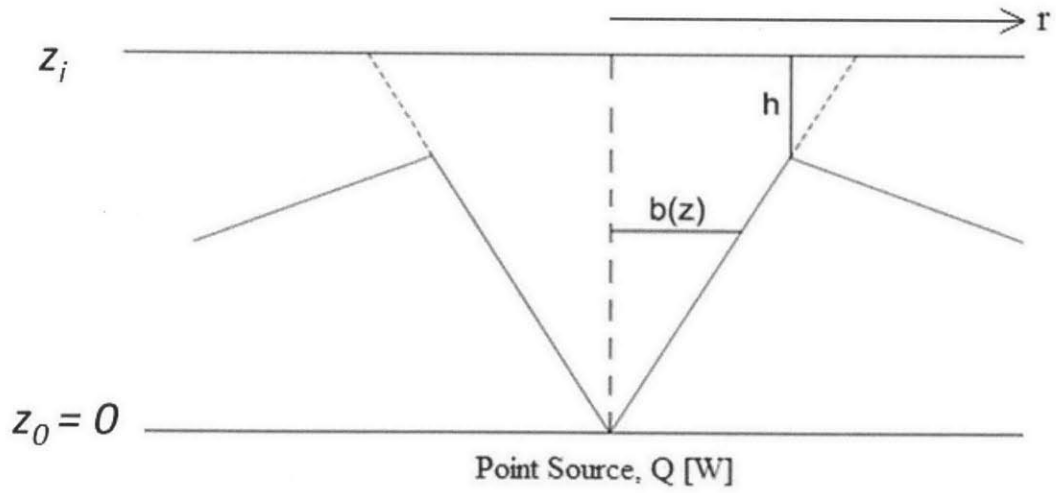

Fig 2.2 A rising plume originated at a point source and the no-flux boundary at a given mixed layer height, z_i.

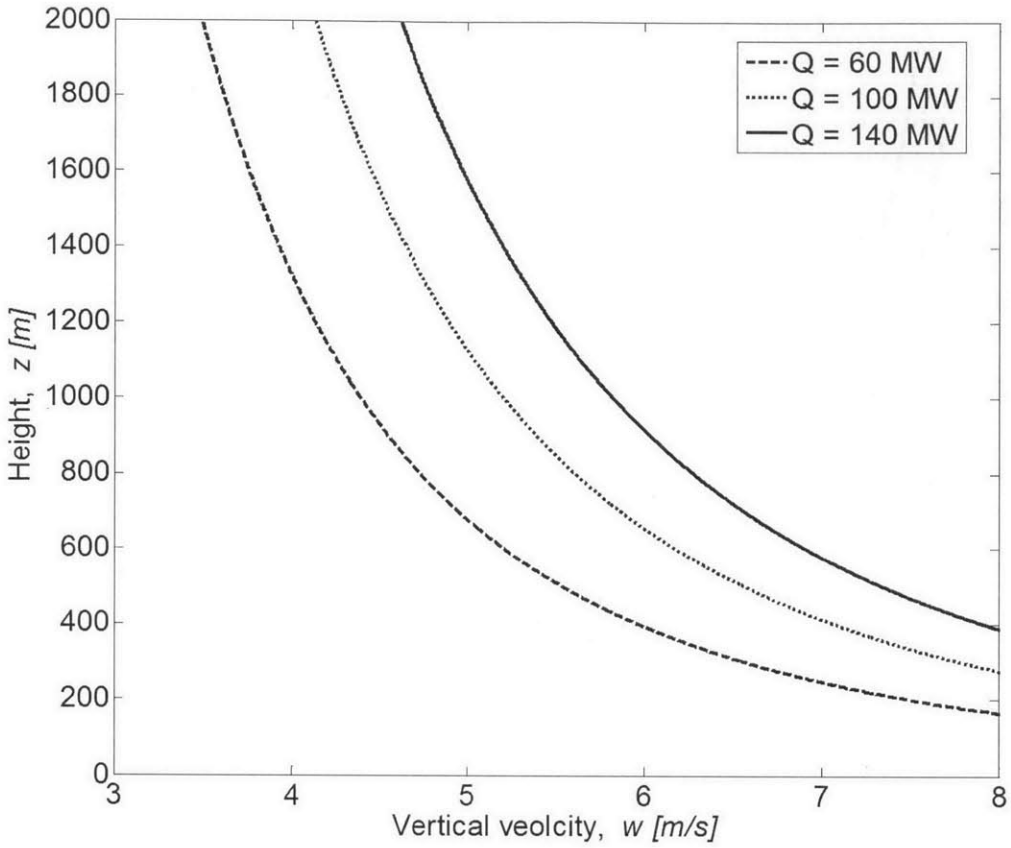

Fig 2.3 The average vertical velocity inside the plume decreases by the depth raised to the power of -1/3. For a plume originated in an infinitely small point source the velocity at the source itself is infinite. The solution is thus not valid near the source. The entrainment coefficient is set as a constant, $\alpha = 0.10$.

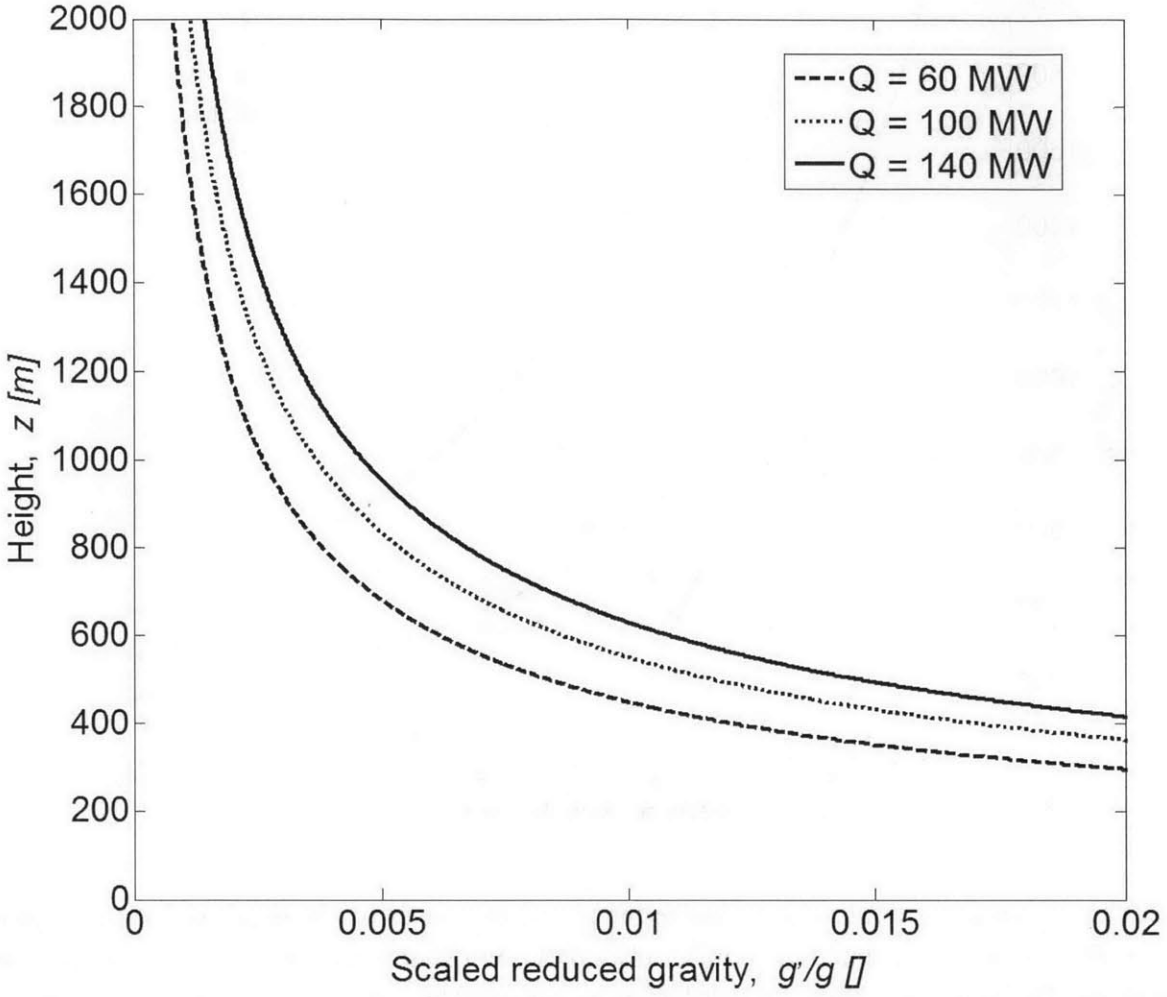

Fig 2.4 Scaled reduced gravity decreases with depth raised to the power -5/3. The entrainment coefficient is set as a constant, $\alpha = 0.10$.

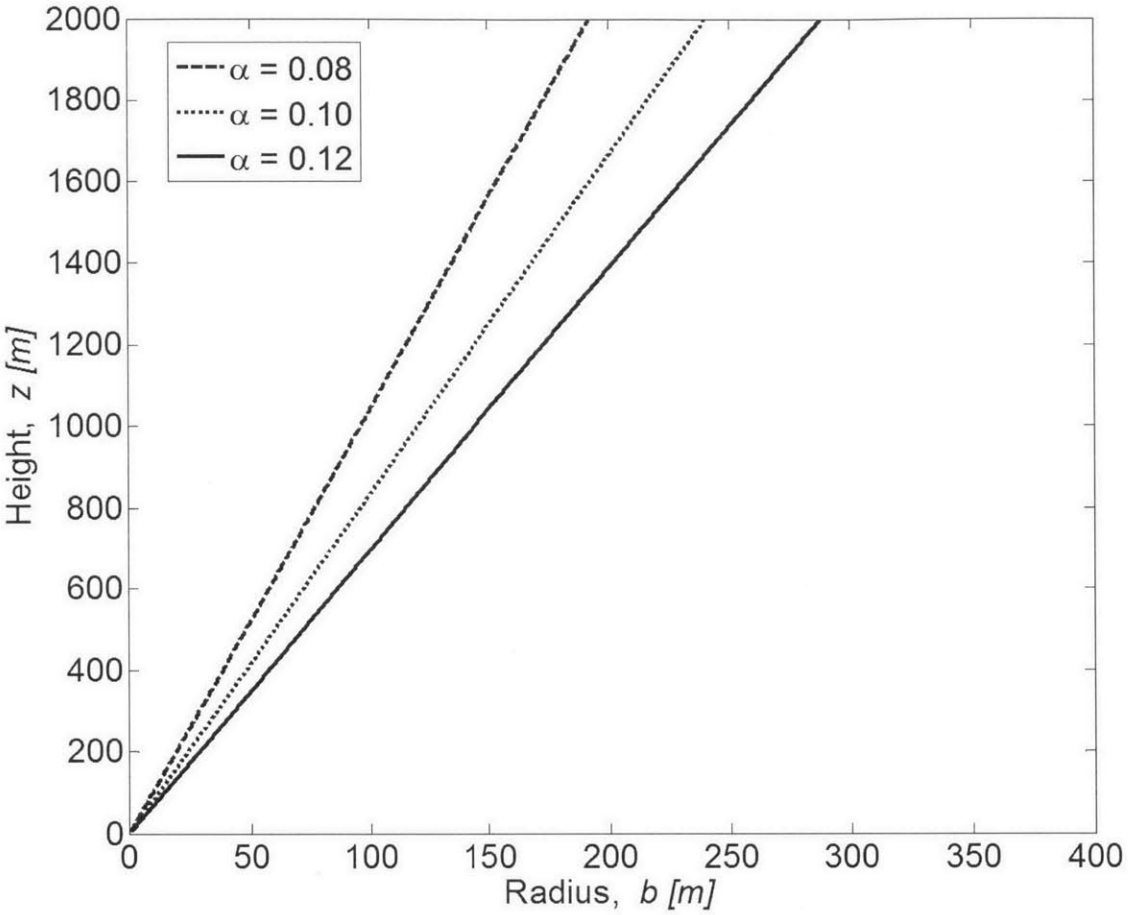

Fig 2.5 The radius of the plume increases linearly with the height above the point source. In this case the heat flux is Q = 100 MW and three different values are set for the entrainment coefficient, α.

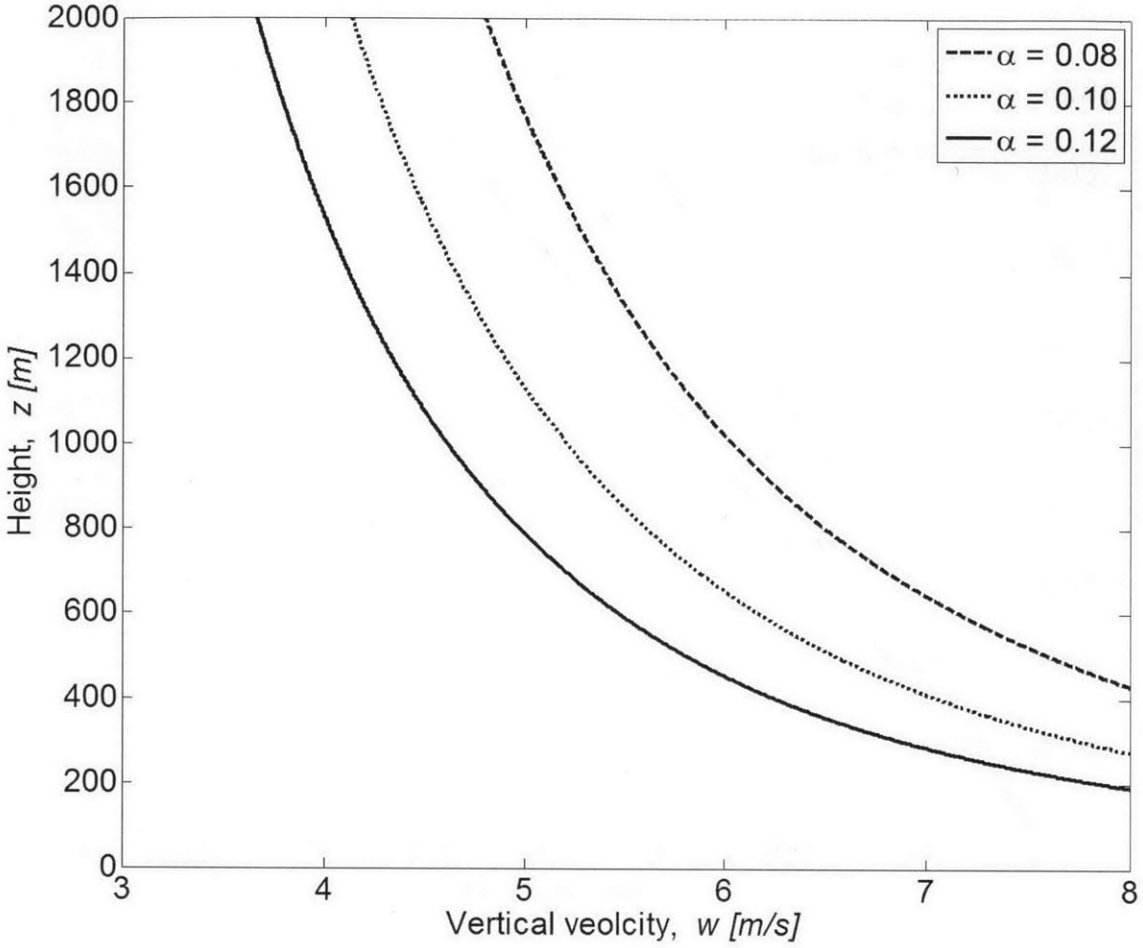

Fig 2.6 The vertical velocity as a function of height for three values of the entrainment coefficient. The heat flux, Q, is 100 MW.

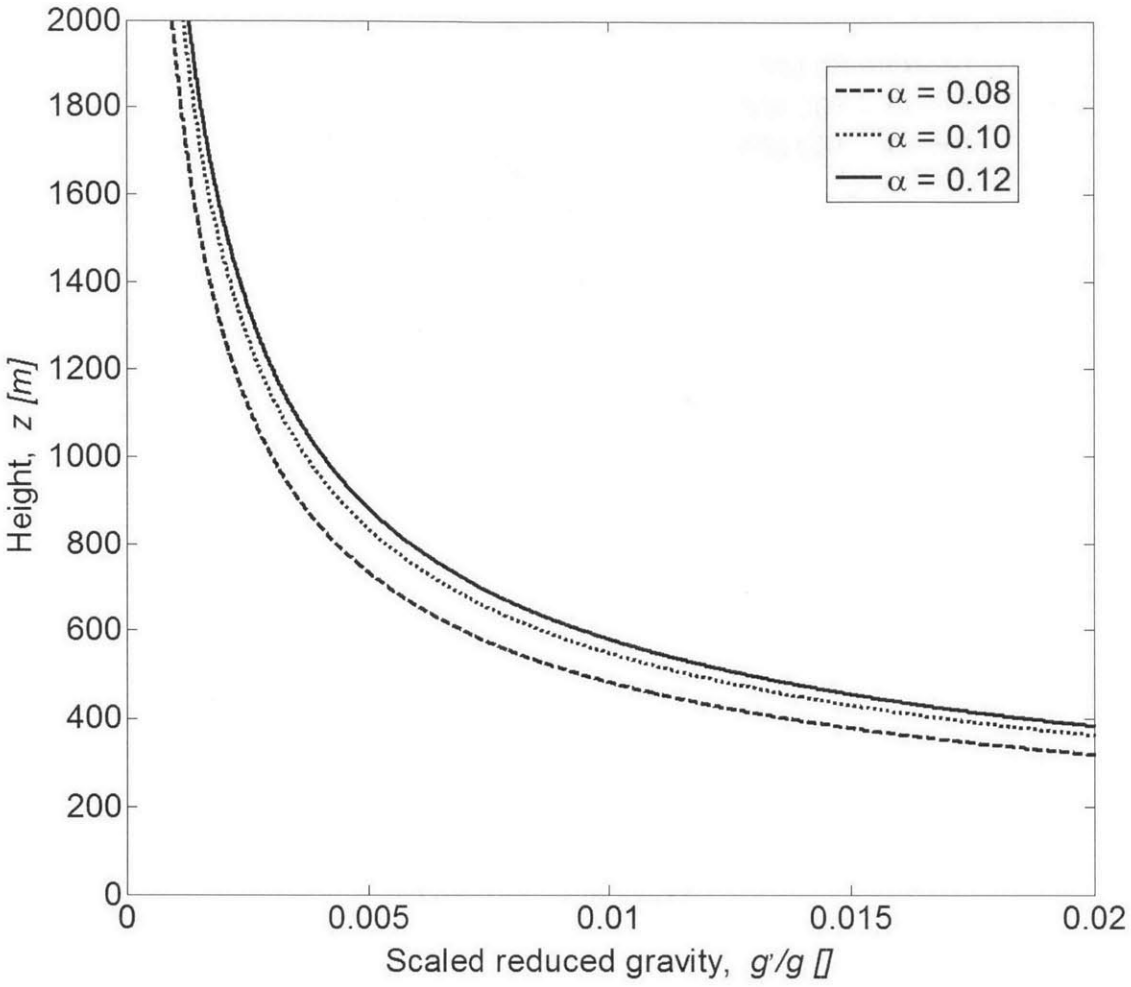

Fig 2.7 The scaled normalized reduced gravity plotted by height for three values of the entrainment coefficient. The heat flux, Q, is 100 MW.

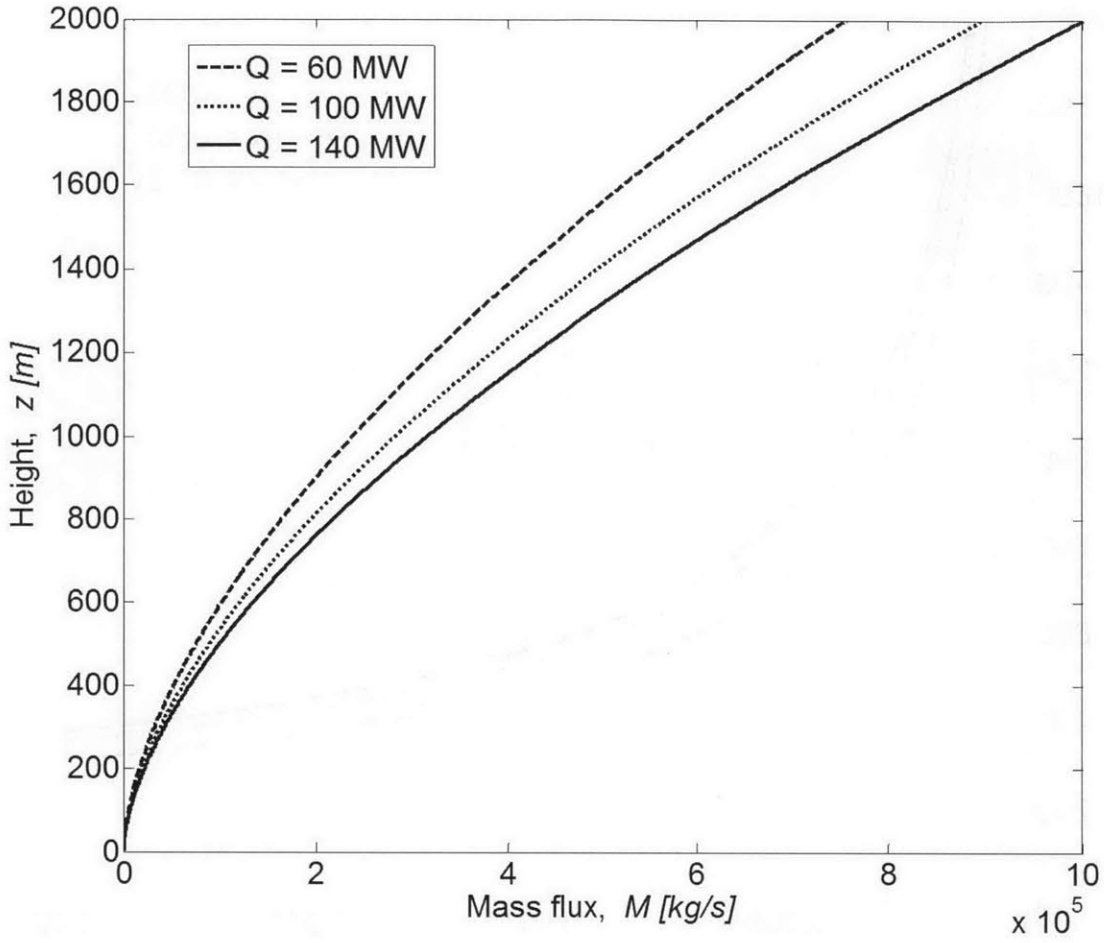

Fig 2.8 The increase in mass flux with increased height for three values of heat fluxes, Q.

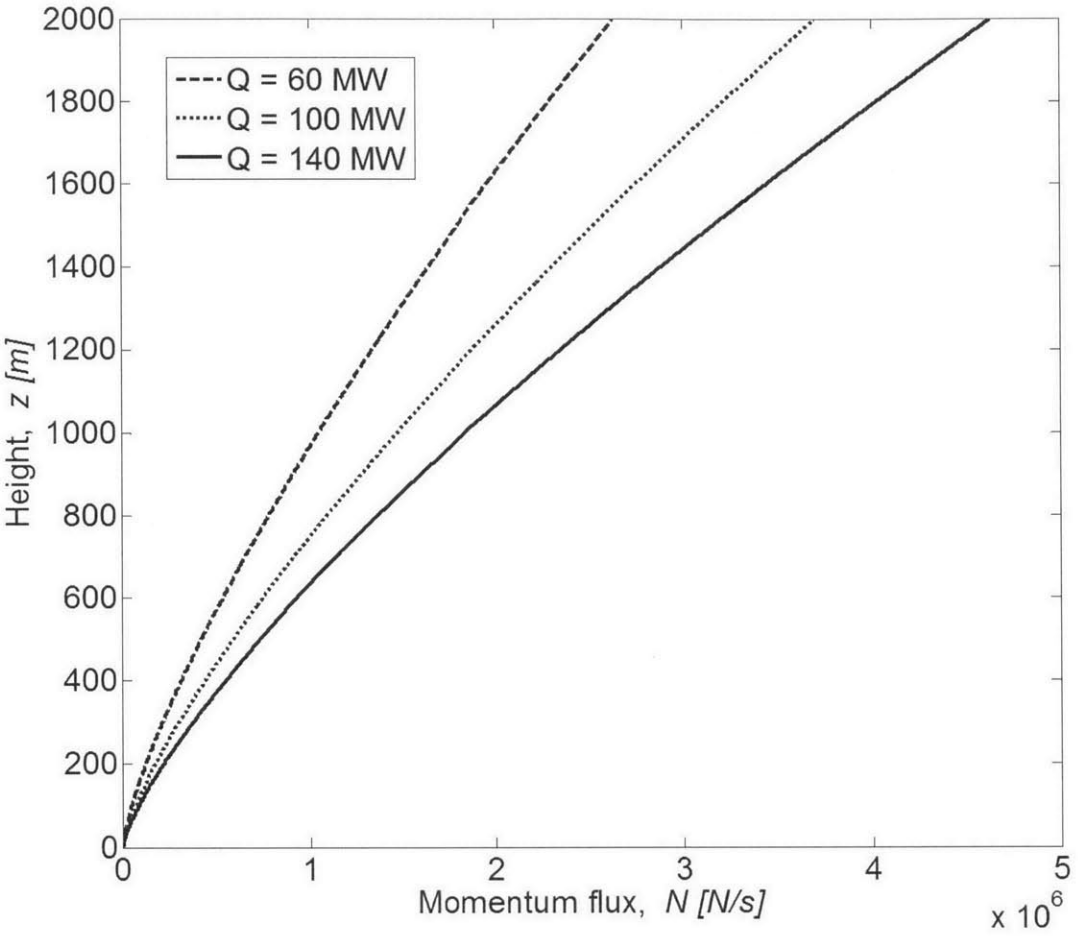

Fig 2.9 The momentum flux increases with height raised to the power of 4/3.

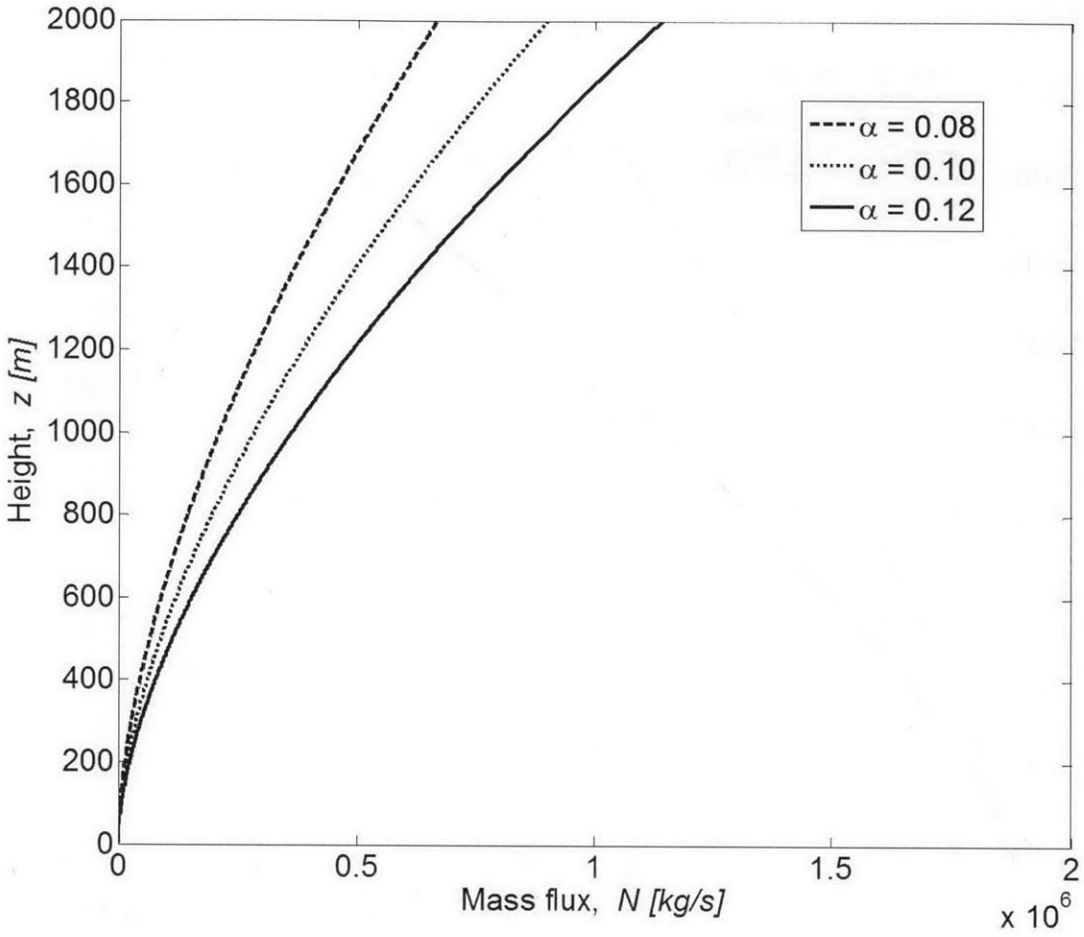

Fig 2.10 The increase in mass flux by height for three values of α and Q = 100 MW. The mass flux increases with height raised to the power of 5/3.

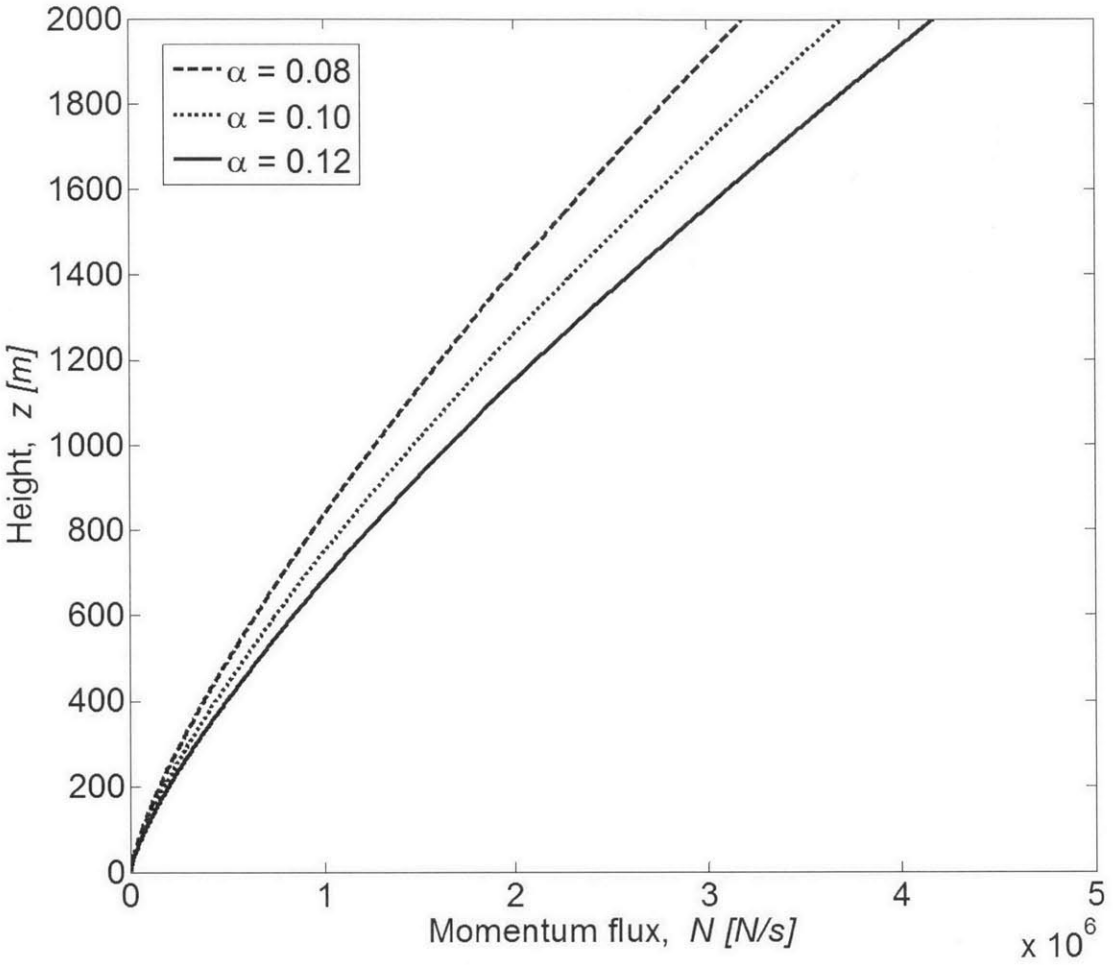

Fig 2.11 The increase in momentum flux by height for three values of α.

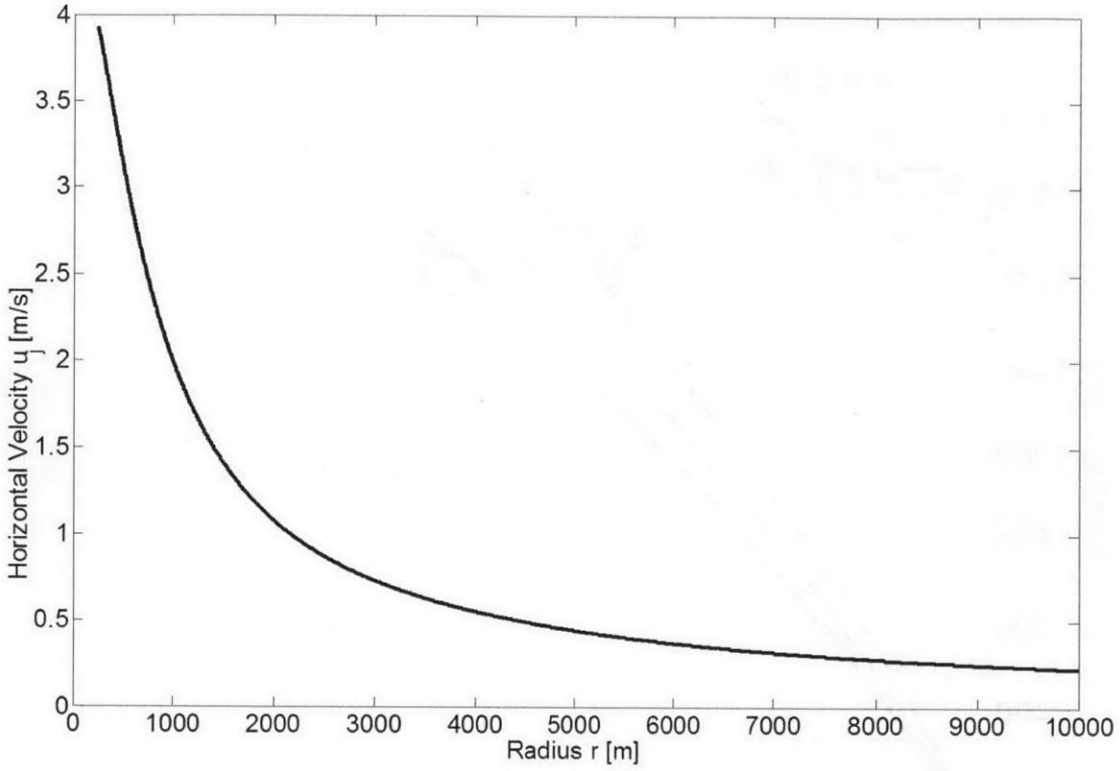

Fig 2.12 The drop in the horizontal velocity by the distance from the center of the rising buoyant plume. At a 10 km distance from the center the horizontal velocity has dropped to 5% of the velocity at the center of the plume.

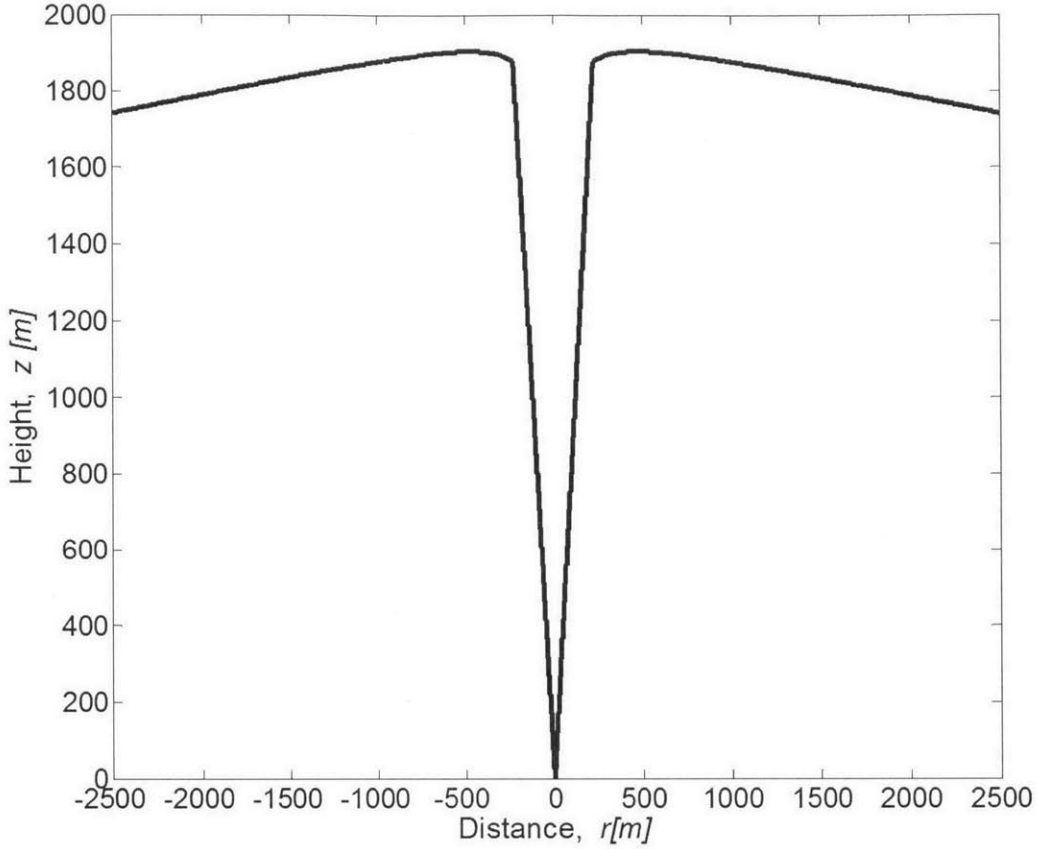

Fig 2.13 The size of the buoyant plume and the horizontal jet.

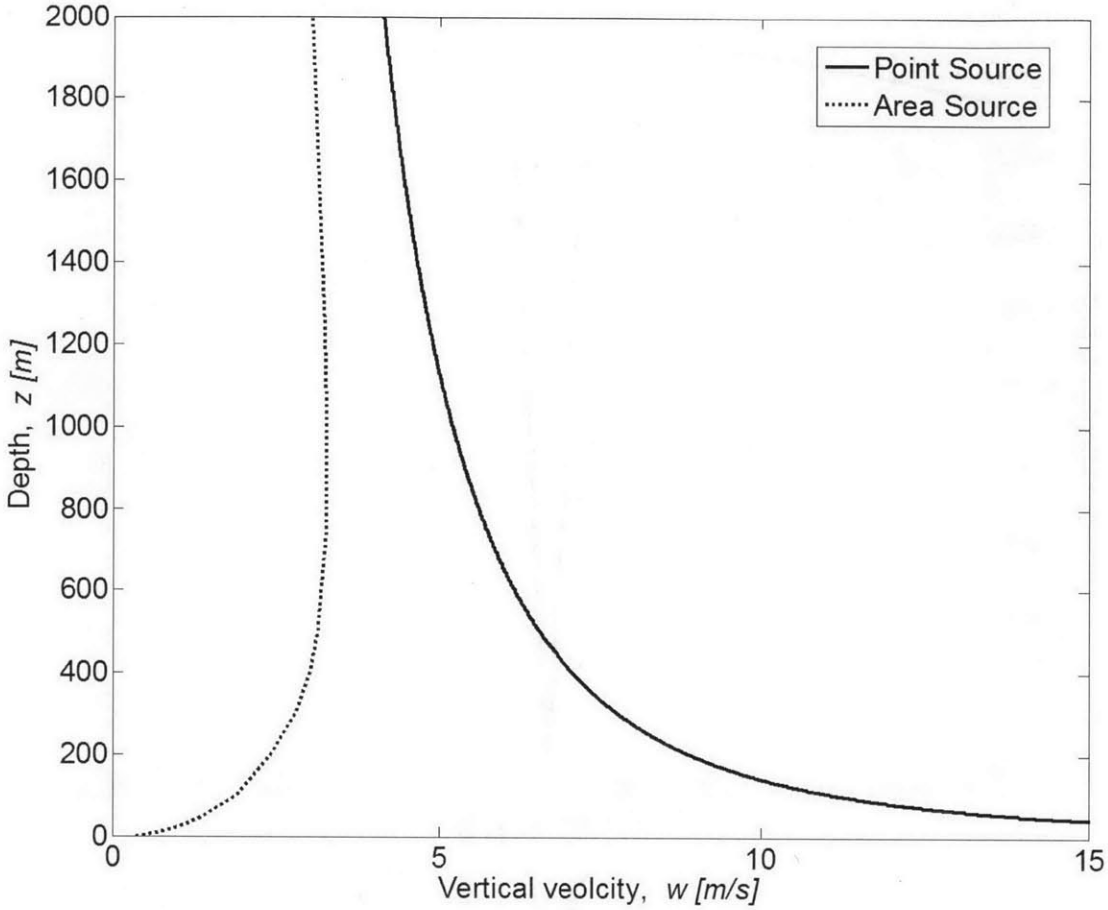

Fig 2.14 The vertical velocity inside the two plumes as a function of height.

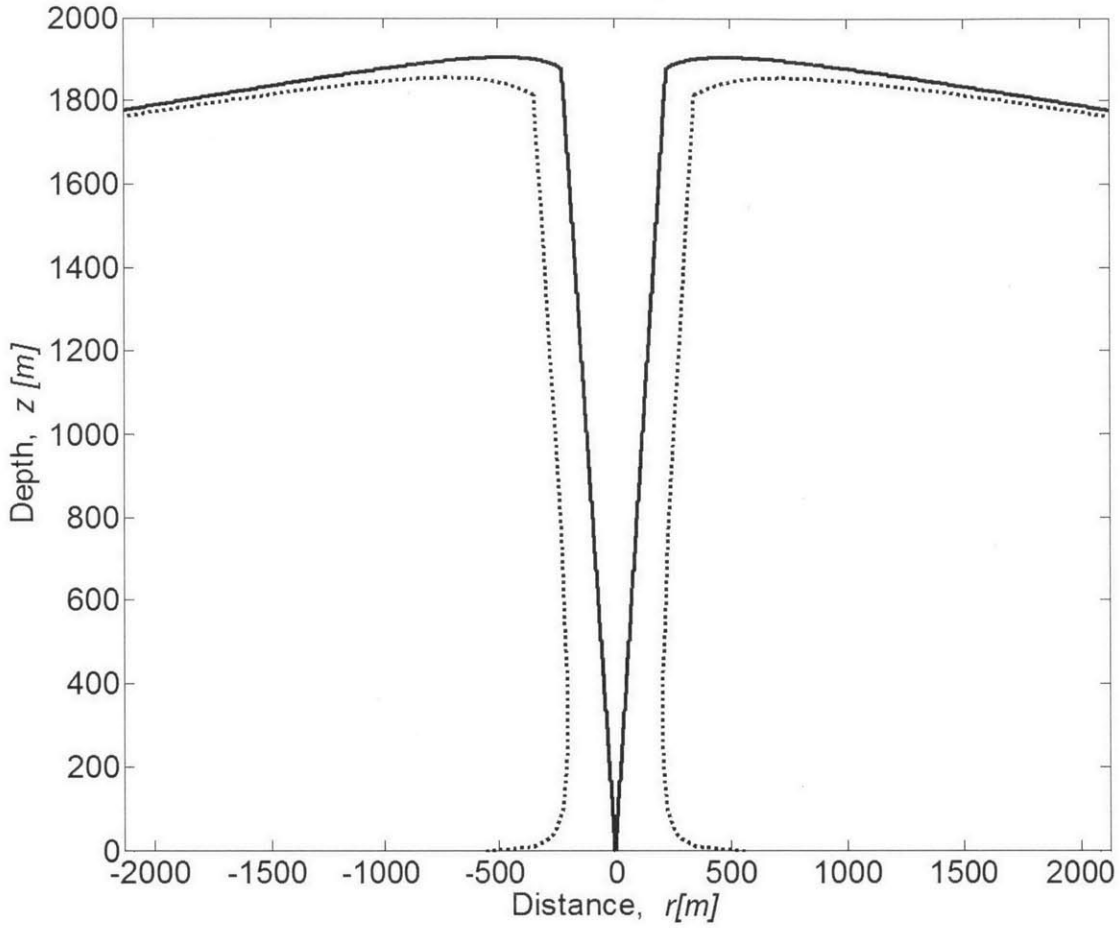

Fig 2.15 The shapes of the plumes originated in a point source and an area source.

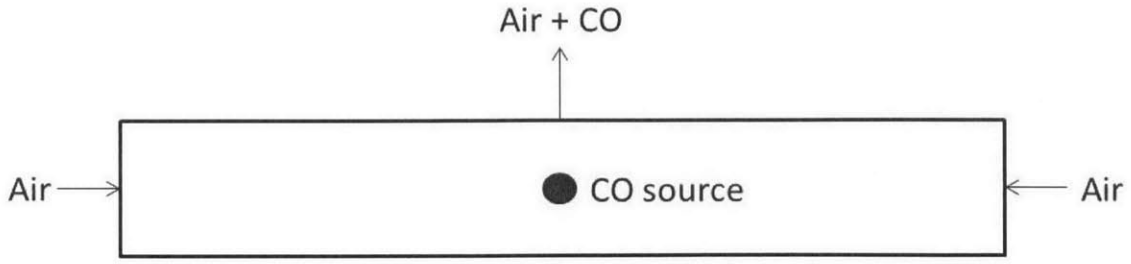

Fig 2.16 The control volume above the circular area source and the pollutant source of CO inside it.

Chapter 3: The Diurnal Conditions in an Idealized Urban Street Canyon located in the Tropical Region

Abstract

In this chapter results from a field experiment performed in an artificial urban street canyon in Singapore in June and July of 2012 are introduced. The field experiment was collaboration between MIT, University of Notre-Dame, Indiana and Nanyang Technological University, Singapore. It was funded through the Singapore-MIT Alliance for Research and Technology (SMART) project. The goal of the field experiment is to understand better the thermo fluid processes within a street canyon of a city in a tropical area in an idealized (controlled) urban street canyon. The experimental set-up, the flow visualization method, the collected data and a theoretical consideration on the air flow were first presented in Dallman et al. [37]. A buoyancy parameter, B, is introduced. It characterizes the balance between the mechanically driven air flow and the buoyancy driven air flow inside the canyon. In Chapter 4 computational fluid dynamics (CFD) simulations on the air flow within the idealized urban street canyon are performed where the buoyancy effects are extended beyond what is found in the literature and the results compared with the findings presented in this chapter.

Introduction

By the end of 2008, for the first time in the human history, more than 50% of the earth's population lived in urban areas, and this is expected to rise to 70% by 2050 [1]. It has long been known that urban air quality has an impact on public health, but with

increasing urbanization the control and mitigation of health impacts has raised awareness on related issues. A fundamental understanding on the air flow and dispersion of pollutants within the built urban environment is a necessary element in predicting levels of exposure to pollutants. The complex morphology of urban building structures and connective roads requires an understanding of turbulence within the resulting urban canyons. The use of dense and low porosity construction materials leads to rapid heating in response to direct solar exposure due to the large thermal mass. Hence, buoyancy effects may be as important as mechanically driven or shear-induced flows.

In a review paper by Britter and Hanna [38], pertinent research has been divided into flow on the street scale, the neighborhood scale, the city scale and the regional scale. Studies at each scale are described as: i) Street scale (less than 200 m) mainly deals with air quality issues, where emissions from vehicles are most often the source of pollutants; ii) the neighborhood scale is area 1–2 km in size, wherein detailed computational studies of turbulence are still feasible; iii) the city scale (20–30 km) is characterized by buildings that lead to a high drag force or reduced wind in the urban area as well as large thermal storage; and iv) regional scale (up to 200 km) is an area where large scale pressure gradients are prominent and synoptic flow prevails. In this study the focus is set on the air flow at the street scale.

The combination of mechanical and buoyancy effects characterizes the air flow within an urban canyon. The magnitude of mechanical forcing within an urban environment depends on the synoptic wind conditions and building configuration, while buoyancy forcing depends on the temperature differences between the urban surfaces and

the ambient air that drive sensible heat fluxes. Three heat exchange mechanisms exist, with different impacts on the stability of the near-surface urban air: first, a neutral condition with no divergence of sensible heat flux; second, an unstable condition with a heat flux from the surface to ambient air; and finally, a stable condition where there is a heat flux from air to the surface. In this study the focus is on the daytime conditions where solar radiation heats the buildings and road surfaces significantly. The study is therefore limited to unstable regimes but neutral conditions are included as a reference for the comparison of cases, including additional buoyancy forcing on the flow. The urban area is simplified into a two-dimensional urban street canyon, shown in Fig 3.1. The temperature difference between the near-surface air and the ambient and inner canyon fluids leads to buoyancy fluxes within and across the canyon.

Background

There have been limited foundational studies of buoyancy effects in urban canyons. In this section the major findings are reviewed and the launching point for this current study defined. The traditional way to quantify the interaction between the buoyancy and the mechanical forces is to use the Richardson number (*Ri*). Within the canyon, *Ri* is defined in Turner [27] and Li et al. [12]

$$Ri = -\left(\frac{g(T_{walls}-T_{amb})H}{T_{amb}U_0^2}\right), \qquad \textbf{3.1}$$

where g is the gravitational acceleration (m s-2), T_{walls} the average temperature of the canyon walls (K), T_{amb} the ambient air temperature (K), H the height of the canyon (m), and U_0 the free stream velocity above the canyon (m s-1).

In Fernando et al. [39] the aspect ratio of the canyon is taken into the definition of *Ri*. The thermal driving force in the canyon is considered to be the temperature difference between the walls and the air (T_{walls} - T_{amb}) and thus the buoyancy driven circulation characterized by $\left(\frac{g(T_{walls}-T_{amb})}{T_{amb}}\right)$. This buoyancy driven circulation competes with the mechanically forced circulation, u_c, inside the canyon driven by the overlying flow, U_0. From simple kinematics (mass balance), $\frac{\partial u}{\partial x} \sim \frac{\partial w}{\partial z}$, where u and w are the characteristic horizontal and vertical velocities of the flow. Thus, $\frac{U_0}{L} \sim \frac{w}{H}$ which leads to $w \sim u_c \sim U_0 \frac{H}{L}$. The balance between the buoyancy and mechanical effects is given by Richardson number for the canyon in Fernando et al. [39]

$$\boldsymbol{Ri_c = -\left(\frac{g(T_{walls}-T_{amb})H}{T_{amb}}\right)/u_c^2 = -\left(\frac{g(T_{walls}-T_{amb})H}{T_{amb}U_0^2}\right)\left(\frac{L}{H}\right)^2,} \qquad \textbf{3.2}$$

where L is the width of the canyon (m) and H/L the aspect ratio of the canyon. Fernando et al. [39] state that, according to numerical simulations performed by Sini et al. [40], the canyon flow is dominated by buoyancy when Ri_c is larger than 0.5–1.0.

The Experimental Setup and Installation

In the real urban environment it is not only the configuration of the buildings and the mechanical and buoyancy forces that determine the flow field. Human activities such as the traffic behavior also affect the flow field. Due to difficulties in getting permission to install experimental devices in a real urban street canyon in Singapore, an artificial street canyon was built. The advantage of performing the field experiment in such an

artificial street canyon is that the environmental conditions are as controlled as possible. The human activities are thus omitted thus less factors affecting the flow inside the canyon. The factors affecting the flow field in this artificial experimental street canyon are the near-field environment (trees, buildings, etc.), the synoptic wind strength, the wind direction and unsteadiness and the buoyancy intensity inside the canyon. Shipping containers have before been used to investigate the air flows within urban areas, for example, in Biltoft [41] and Zajic et al. [42].

Our experimental site was at the north-east part of the Nanyang Technological University (NTU) campus in Singapore. The site consists of a large grass field which is surrounded by trees in the east, north and west and a ten-story building in the south. Fig 3.1 shows two pictures of the site, one taken from the south and another one taken from the north. The pictures also show the artificial street canyon, constructed of four shipping containers, where two of them are aligned together parallel to the other two. The gap between the containers forms the experimental street canyon. The length of each container is 12 m and the width and height are 2.5 m. The gap (width) between the containers was chosen to be L = 3.75 m (aspect ratio of 2/3) to have the flow in transition from wake interference to skimming flow regime, according to the definition in Oke [43]. Our main goal was to estimate the thermal effects on the flow inside the canyon. The fact that the walls of the containers are made of steel with high solar absorptivity ensured that the thermal effects would be detectable. We considered the use of heaters to exaggerate the thermal effects but due to time constraints it was not done.

To collect the data needed, several measurement devices were installed both inside and above the canyon. The installation is shown in Fig 3.1. At the top of the containers three weather stations to measure the ambient wind speed and direction above the canyon as well as the ambient temperature were installed. The weather station device used was the Vaisala Weather Transmitter WXT 520 which measures barometric pressure, humidity, precipitation, temperature, and wind speed and direction in two dimensions. Each weather station has its own data logger and is powered by its own battery. The highest weather station was located 2.5 m or $1H$ above the canyon. The goal was to measure the vortex formed inside the canyon when the ambient air flow (synoptic wind) is near perpendicular to the axis of the canyon and the measurement devices were thus located inside the canyon with that in mind. Four three-dimensional sonic anemometers were installed inside the canyon to measure the three-dimensional flow and turbulence statistics. The sonic anemometers used were RM Young 81000, which measures the wind speed and direction, the speed of sound and sonic temperature. The sonic anemometers were connected to Campbell Scientific CR5000 data loggers and are powered by batteries. Two of the sonic anemometers were located near the west wall to estimate the thermal effects of the heated wall on the flow field inside the canyon. The other two were located such that the vortex or the circulation inside the canyon could be measured. Two additional weather stations were located inside the canyon the measure the air temperature within the canyon and to further support our measurements on the flow inside the canyon. Four thermocouples were installed at the walls of the canyon. The

thermocouples used were Campbell Scientific CS220-L Surface-Mount Type-E Thermocouple Sensors.

Flow Visualization

One of the goals of the experiment was to devise and implement flow visualization technique in order to better characterize the flow structure inside the canyon. Flow visualization also clearly shows the unsteadiness of the flow inside the canyon. A few flow visualization techniques were considered for use, such as releasing bubbles by a bubble machine, releasing smoke by a smoke machine, releasing CO and, finally, releasing fog from a fog machine. All of the techniques have advantages and disadvantages. Releasing CO makes it possible to use carbon monoxide detectors, which measure the concentration of CO in the air, to quantify and estimate its residence time inside the canyon but it has negative impacts on the environment and is not visible. Smoke is clearly visible but we would have needed permission to release it and it is also semi-quantitative. Bubble machines also give the opportunity to quantify and estimate the residence time and even show the turbulence at the roof level by using a high frequency video camera, but it can be hard to see the bubbles on sunny days so that method was considered to be more suitable inside and in laboratories. After considering these possibilities it was decided to release fog to visualize the flow inside the canyon. Fog can be generated either by a dry ice machine or a fog machine where ice cubes are used instead of dry ice. This technique also has its advantages and disadvantages. It is relatively inexpensive and simple to install and it clearly shows the flow inside the

canyon even on bright and sunny days. There is no need to use an expensive high frequency camera as the dense fog is clearly visible. Its main disadvantage is that the fog quickly evaporates even before it is dispersed out of the canyon.

The fog machine used was a low fog machine, Antari Z Series (1500 W) shown in Fig 3.2. The device vaporizes 'fog juice' (glycerin-based fluid). The vapor is then released through a space with the ice cubes, forming a fog which is dispersed horizontally out of the machine where it becomes visible. The machine was adjusted such that it released fog for a period of one minute. One of the disadvantages of this machine is that it demands a lot of ice cubes. The air temperature was about 30°C on the day and the experimental site was located far away from a freezer, consequently not as many release experiments were performed as planned. A Canon PowerShot S100 12.1 MP digital camera was used to record the movement of the fog and to analyze it later on.

Fig 3.3 shows four pictures under four different weather situations of the air flow inside the experimental canyon. Picture (a) is taken during the morning before sunrise with near zero wind flow. The fog stays near the ground and the residence time of the fog inside the canyon is very high. Picture (b) is taken during the day when the wind is blowing perpendicular to the axis of the canyon. The picture clearly shows how a vortex is formed inside the canyon. Picture (c) shows a shift in wind direction. A vortex was formed when the flow was perpendicular to the axis of the canyon, but it is dispersed out of the canyon where the flow is now parallel to the axis of the canyon. Finally, picture (d) shows the fog when the flow is parallel to the canyon. From picture (c) the unsteadiness of the flow can be seen. The fog was released for a period of about 30 seconds and

according to the pictures the air flow is perpendicular to the axis of the canyon and parallel to it during that time span. To further estimate the unsteadiness of the air flow inside the canyon and its effects on the flow structure a one-minute-long video shot is analyzed into details. In Fig 3.4 we can see four consecutive snapshots of the flow inside the canyon. For the first five seconds a counter-clockwise rotating vortex is formed. After five seconds the synoptic wind direction swifts leading to the formation of a clockwise vortex which exists for about 25 seconds. After 30 seconds the synoptic wind direction shifts again and the fog is dispersed out of the canyon parallel to its axis. During a 30-second period flow in three directions inside the canyon is obtained, which make this problem obviously rather unsteady.

The Collected Data

Measurements on the flow and the temperature field inside and above the experimental canyon were performed over 10 days, from June 30th through July 10th, 2012. During that period the southwest monsoon season is dominant in Singapore. As the goal was to estimate the thermal effects on the air flow inside the canyon, clear sunny days during the experimental period were optimal.

Fig 3.5–Fig 3.11 show examples of five-minute average data measured during the 10 days are displayed. Fig 3.5 shows the diurnal ambient air temperature measured by the weather station located 2.5 m ($1H$) above the west container. On July 1st, 6th and 8th there is a clear diurnal cycle in the air temperature. The air temperature peaks at around 2 pm – 3 pm and it reaches about 30°C at that time, compared with about 23°C during the

night. During the other seven days the temperature drops and then rises occasionally during the day. These drops are due to patchy rain in the monsoon climate in Singapore. The rainfall clearly affected the field experiment by decreasing the time periods when the thermal forces played a role in determining the flow field inside the canyon. Despite that, enough data to work with were collected. In Fig 3.6, the five-minute average in-canyon air temperature data measured by the weather station located near the middle of the canyon are displayed. Similar trends in air temperature as for the ambient air temperature can be seen, as expected. Fig 3.7 presents the diurnal temperature difference between the ambient and in-canyon air temperatures. During the three clear sunny days the average in-canyon day temperature is about 0.5–1.0°C higher than the ambient air temperature, which can be explained by the existence and the proximity of the heated walls of the canyon. The surface temperatures of the walls are shown in Fig 3.8 and Fig 3.9. The west wall of the canyon warms up during the mornings and the temperature peaks around noon. The maximum west wall temperature is about 50°C. During the night the surface temperature is about 23°C or the same as the in-canyon air temperature. Because of the low heat capacity of the steel, the surface temperature warms up and cools down quickly as can be seen in the figures. The east wall temperature follows the in-canyon air temperature during the morning but during the afternoon, when the sun shines on the wall, it heats up quickly and peaks at about 4pm. The maximum east wall temperature measured was about 60°C. The temperature difference between the two walls affects the formation of vortices inside the canyon. Fig 3.10 plots the diurnal temperature difference between the two walls. The maximum difference was measured at midday on July 8th

and turns out to be 12°C. This is also the temperature difference between the walls and the air that affects the flow field inside the canyon through creation of buoyancy. Fig 3.11 shows the difference between the warmer wall at each time and the in-canyon air temperature. The maximum temperature difference is measured 30°C at 4pm on July 8th. As will be seen it is the balance between the buoyancy forces and the mechanical force due to the synoptic wind that determines the flow inside the real urban environment. In Fig 3.12–Fig 3.20, the measurements on the air flow speed and the direction inside and above the canyon are introduced.

First, the free stream velocity or the synoptic wind velocity, U_0, above the canyon, is considered and is plotted over the ten days period in Fig 3.12. This figure shows how U_0 is near zero during the night until about 5am (except on July 2nd). At 5am U_0 begins to increase and at average fluctuates about 1–2 m s-1 during the day. The maximum U_0 was measured on July 1st when it reached 3.5 m s-1. The in-canyon velocity, u, is then shown in Fig 3.13, which shows a similar trend, as expected. Fig 3.14 shows the ratio between U_0 and the measured in-canopy velocity, u. On average U_0 is about 1.5–2.0 times larger than u. In the simple artificial urban street canyon the main factor determining the ratio between U_0 and u is the direction from which U_0 is flowing towards the axis of the canyon. In Fig 3.15 and Fig 3.16 the measured diurnal flow direction (north 0°; east 90°; south 180°; and west 270°) inside and above the canyon is displayed. The figures show how the wind fluctuates but, at some times, like during the day of July 1st, the flow is more constant with respect to direction. Concentrating on the day of July 1st, then the ambient flow was roughly from east-south-east (120°), meanwhile the in-

canyon flow was from the west-south-west (240°). Remembering that the axis of the canyon is in a south-north direction, this fact indicates a circulating flow inside the canyon (vortex).

The main goal of the field experiment is to investigate the thermal effects on the creation of a vortex inside the canyon when the ambient flow is near perpendicular to the axis of the canyon. Due to the unsteadiness in the flow, in Dallman et al. [37] the concentration is set on the special case when the flow is near perpendicular (defined +/- 15°) to the axis of the canyon and the leeward wall is at a higher temperature than the windward wall, i.e., the buoyancy force and the mechanical force are both creating a vortex in the same direction (assisting flow). In the next part of this chapter the main assumptions and results made in Dallman et al. [37] are introduced. Then in Chapter 4 computational fluid dynamics (CFD) simulations on this special case are performed.

Considerations on Heat Fluxes

From the measurements a rough estimate on the diurnal heat flux into the canyon from the walls is

$$q_{west} = h_f(T_{west} - T_{can})A_{wall} + e\sigma(T_{west}^4 - T_{can}^4)A_{wall}, \quad 3.3$$

where q_{west} is the heat flux from the wall into the canyon (W), h_f the heat transfer coefficient (W m-2K-1), A_{wall} the surface area of the wall (m2), T_{west} the average temperature of the west wall (K), T_{amb} the in-canyon air temperature (K), e the emissivity of the wall and σ the Stefan-Boltzmann Constant. Same equation is applied to

calculate the heat flux from the east wall. The total heat flux from the wall into the domain is then

$$q_{in} = q_{west} + q_{east}. \quad \textbf{3.4}$$

The heat transfer due to the mean motion of the air out of the canyon can be estimated by the following equation

$$q_{out} = \rho C_p (T_{can} - T_{amb}) \overrightarrow{u_{out}} A_{out}, \quad \textbf{3.5}$$

where q_{out} is the heat flux out of the canyon (W), ρ density of air (kg m-3), C_p specific heat capacity (J kg-1K-1), T_{amb} ambient air temperature (K), $\overrightarrow{u_{out}}$ the velocity out of the canyon (m s-1) and A_{out} the area (m2) out of the canyon perpendicular to $\overrightarrow{u_{out}}$. The goal is to estimate h_f by assuming q_{in} is equal to q_{out}. The estimated value on h_f will then be compared to the value we obtain by CFD simulations (Chapter 4) and to other experiments on h_f.

The average 5-minute heat flux in the experimental canyon is calculated on July 8th where that day there was no rainfall, so a clear diurnal cycle is obtained. The experimental canyon and the heat fluxes are shown in Fig 3.17 in two dimensions. The heat flux out of the canyon, q_{out}, is also in the horizontal direction. The direction of the velocity is known from the measurements inside the canyon and A_{out} is estimated from the direction at each time. The heat flux out of the canyon during the day of July 8th is shown in Fig 3.18. The figure shows a clear diurnal cycle where the heat flux is largest during the middle of the day but is near zero during the morning and the evening.

Knowing q_{out} an estimate on the average h_f during the day is performed, by solving for h_f from Eq. 3.3. From those equations, the average h_f during the diurnal cycle is about 4.8 W m-2K-1. The total heat flux from the walls is then plotted in Fig 3.19.

In Chapter 4 the CFD simulations on the flow and heat fluxes inside a two-dimensional urban street canyon are introduced. Those simulations give an estimate of the average h_f as 7.8 W m-2K-1, which is of the same order and the calculations on h_f obtained from the field experiment. In Mills [44] an estimate on h_f is given based on experimental data on a heated wall. For natural convection in air h_f is estimated to be between 3 – 25 W m-2K-1. These simple calculations on h_f are thus within that given range.

Special Case

When the leeward wall is at a higher temperature than the windward wall the buoyancy and the mechanical forces assist each other in creating a vortex inside the canyon. This scenario is displayed in Fig 3.20 where the upper panel shows a purely mechanically driven vortex and the lower panel a buoyancy driven vortex. When the forces exist at the same time, as occurs in the real environment, the two scenarios can be superposed. In this part the theoretical considerations and the experimental results for this case are introduced. The theoretical consideration and the results were originally published in Dallman et al. [37]. The CFD simulations performed and introduced in the next chapter will be compared with the results.

The experimental data show the unsteadiness and the fluctuation in the flow in the real environment. To eliminate or minimize these effects when evaluating the effects of the heated leeward wall on the in-canyon air flow when the ambient flow is perpendicular to the axis of the canyon, time series where the ambient flow is for some minimum time perpendicular to the axis of the canyon are considered. In Dallman et al. [37] the minimum time is set to be 30 seconds but during that time an air parcel completes about three circles in the canyon, which can be estimated, for example, from the flow visualization videos already introduced.

In Dallman et al. [37], theoretical considerations on the flow inside a two-dimensional urban street canyon when the synoptic flow is perpendicular to the axis of the canyon are introduced and the leeward wall is at a higher temperature than the windward wall. To evaluate the buoyancy effects on the flow a dimensionless buoyancy parameter, *B*, is defined. The deduction on *B*, performed in Dallman et al. [37], is shown in Appendix 1. The main difference between *B* and the classical Richardson number used to evaluate the buoyancy effects on the flow is that it takes into account the aspect ratio of the canyon and also considers the temperature difference between the two walls instead of the difference between the walls (average surface temperature) and the air in the canyon. The *B* parameter is defined as

$$\boldsymbol{B} = \left(\frac{g\Delta T_{walls} H}{T_{amb} U_0^2 [1+(H/L)^2]}\right), \qquad \textbf{3.6}$$

where $\Delta T_{walls} = T_{lee} - T_{wind}$ is the temperature difference between the canyon walls (K), H the height of the canyon (m), T_{amb} the ambient air temperature (K), and U_0 the free stream velocity above the canyon (m s-1). The difference between the classical Richardson number and the buoyancy parameter is that B takes into the account the wall temperature difference between the two walls forming the street canyon while the Richardson number considers the temperature difference between the surface of the canyon and the ambient air.

The B parameter evaluates the balance between the mechanical and buoyancy forces exerted on the canyon. The B parameter does not distinguish which wall inside the canyon is at a larger temperature. When the leeward wall is heated, buoyancy-driven flow occurs in the same direction as the mechanically-induced flow inside the canyon (assisting flow), but when the windward wall is heated the buoyancy flow is in the opposite direction to the mechanically-induced flow. In this study, the focus is on the case when only the leeward wall is heated. By calculating the B parameter of the flow, a classification on the air flow into a purely mechanically driven regime and a purely buoyancy driven regime with an intermediate regime in-between can thus made. In Dallman et al. [37] the relationship between B and u in the skimming regime is deduced and is shown in Appendix 1. Dallman et al. [37] use vorticity generation to show that the buoyancy driven velocity inside the canyon is a function of the buoyancy level raised to the power of 0.5 and also assume that the mechanically driven flow inside the canyon is linearly proportional to free stream flow above the canyon, i.e.,

$$\frac{u}{U_0} \sim \begin{cases} u_m/U_0 \approx \gamma_1 & B < B_c \\ u_t/U_0 \approx \gamma_2 B^{1/2} & B > B_t \end{cases} \quad \textbf{3.7}$$

where u is the characteristic horizontal velocity inside the canyon, U_0 the free stream flow velocity above the canyon as before, u_m the characteristic mechanically driven horizontal velocity inside the canyon (Fig 3.20), u_t the characteristic buoyancy driven velocity inside the canyon (Fig 3.20), γ_1 and γ_2 are constants, B_c the critical buoyancy parameter where the flow is no longer purely mechanically driven and B_t a critical value of B where the flow is completely buoyancy dominated. Between the two limiting regimes, an intermediate regime is expected ($B_c < B < B_t$), where the flow depends on the free stream velocity and differential heating. Simple linear superposition gives a parameterization for the velocity in the intermediate regime,

$$\frac{u}{u_0} \approx \gamma_3 + \gamma_4 B^{1/2}, \quad \textbf{3.8}$$

where γ_3 and γ_4 are constants.

One of the goals of the field experiment was to investigate if these flow regimes exist in the real environment and then evaluate the values of B_c and B_t. In Fig 3.21 the results for the characteristic in-canyon velocity measured by the weather station located near the middle of the canyon are displayed, first published in Dallman et al. [37]. The figure shows how u is near constant for B values less than 0.05, and how u begins to increase when B is about 0.05. Thus, $B_c \approx 0.05$. The best fit on Eq. 3.8 gives the following equation, $\frac{u}{U_0} \approx 0.40 + 0.60B^{1/2}$. It is not believed that the purely dominant regime is reached which is why CFD simulations are introduced in Chapter 4.

Conclusions

Experimental work requires interpretation and simplifications on collected data. In this part of the thesis a field experiment within a real built environment was introduced. The goal was to investigate the buoyancy effects on the circulation inside a street canyon when the ambient flow is roughly perpendicular to the street canyon and the leeward wall is at a higher temperature than the windward wall (assisting flow). The air flow inside the canyon begins to increase when the buoyancy parameter, B, is about 0.05 – 0.1 (Dallman et al.). The fact that only nine points met the criteria set for the independent variables (ambient velocity and thermal situations), CFD simulations will be performed in the next chapters where the buoyancy effects are extended beyond the conditions in the experimental street canyon and beyond what is found in the literature.

Figures

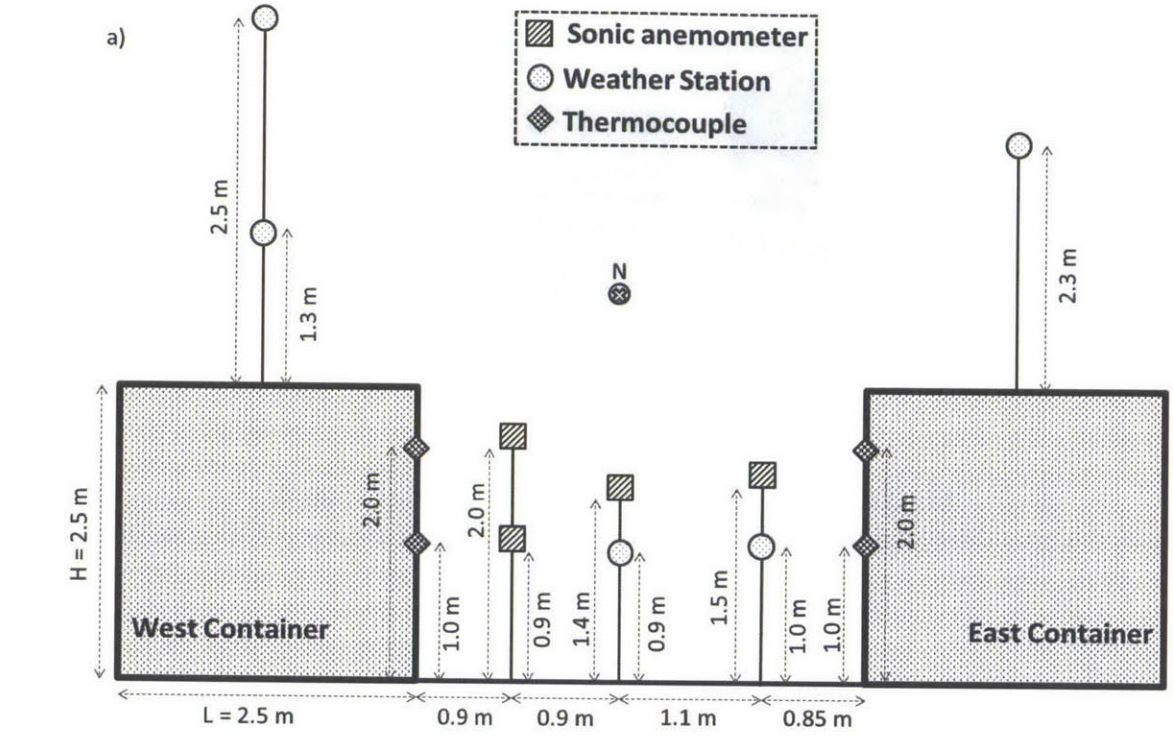

b)

c)

Fig 3.1 (a) The field experimental instrumental set-up from south. (b) The experimental site from south. (c) The experimental site from north.

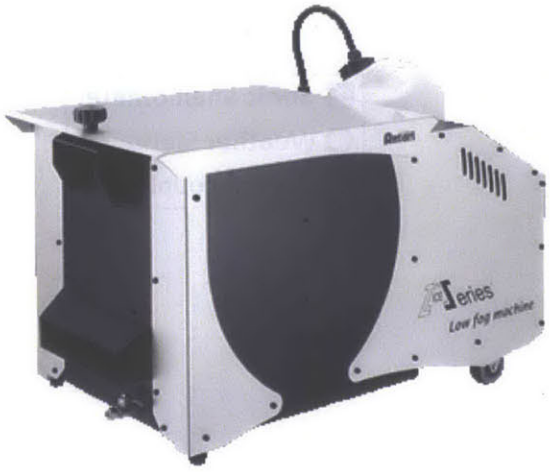

Fig 3.2 The low fog machine Antari Z series 1500 W. (http://concertaudiovisual.com.au/hire/image/cache/data/ICE%20Low%20Fog%20Machine-800x800.gif)

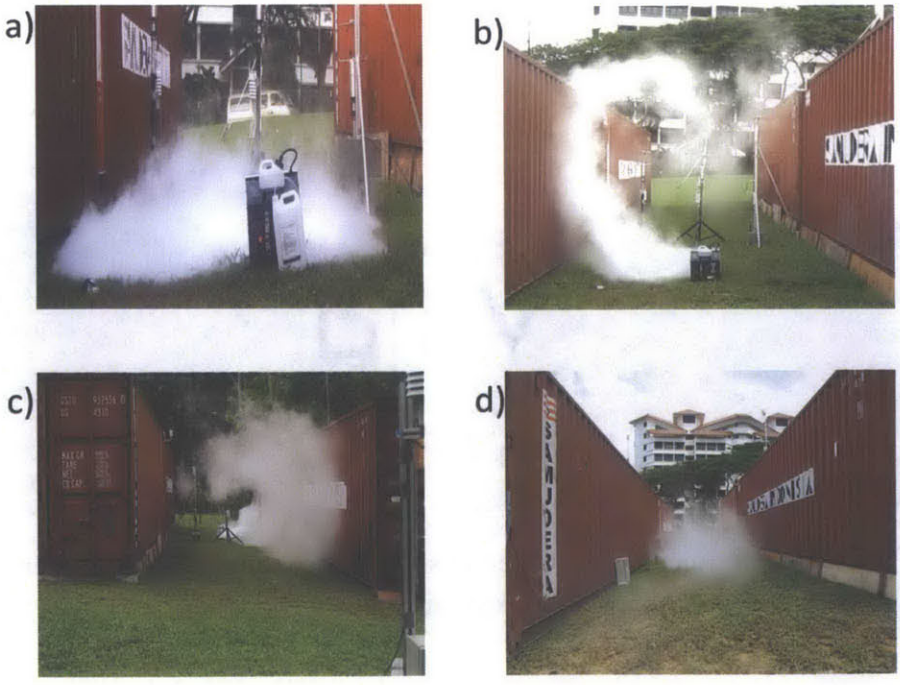

Fig 3.3 Flow visualization. (a) Early morning – no wind – no buoyancy effects. (b) The synoptic flow perpendicular to the canyon – formation of a vortex. (c) Shift from perpendicular flow toward flow parallel to the canyon. (d) Flow parallel to the canyon.

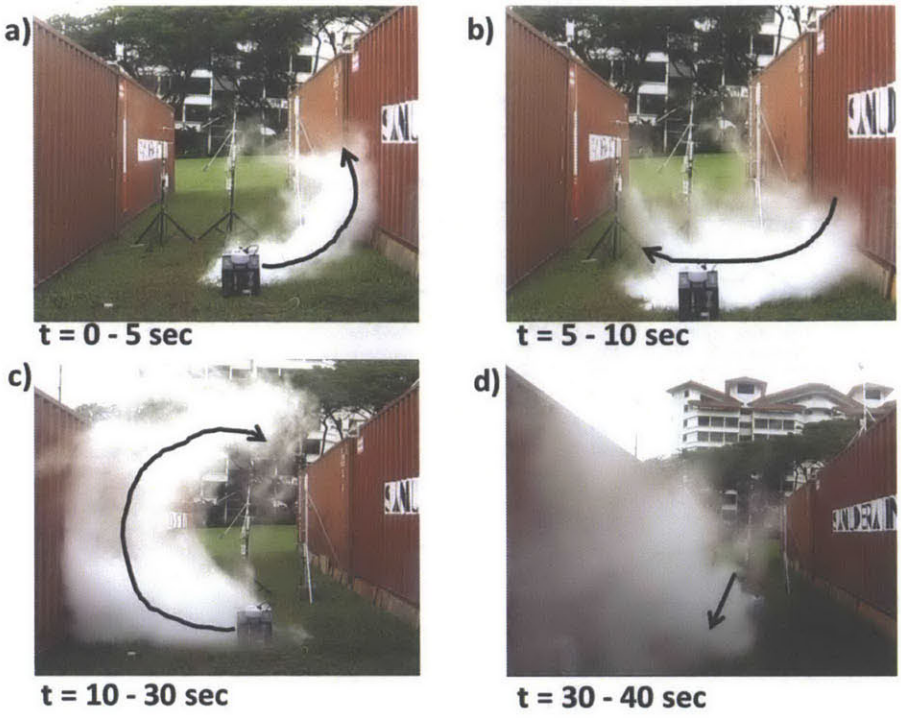

Fig 3.4 Four snapshots of the flow during a 40-second period.

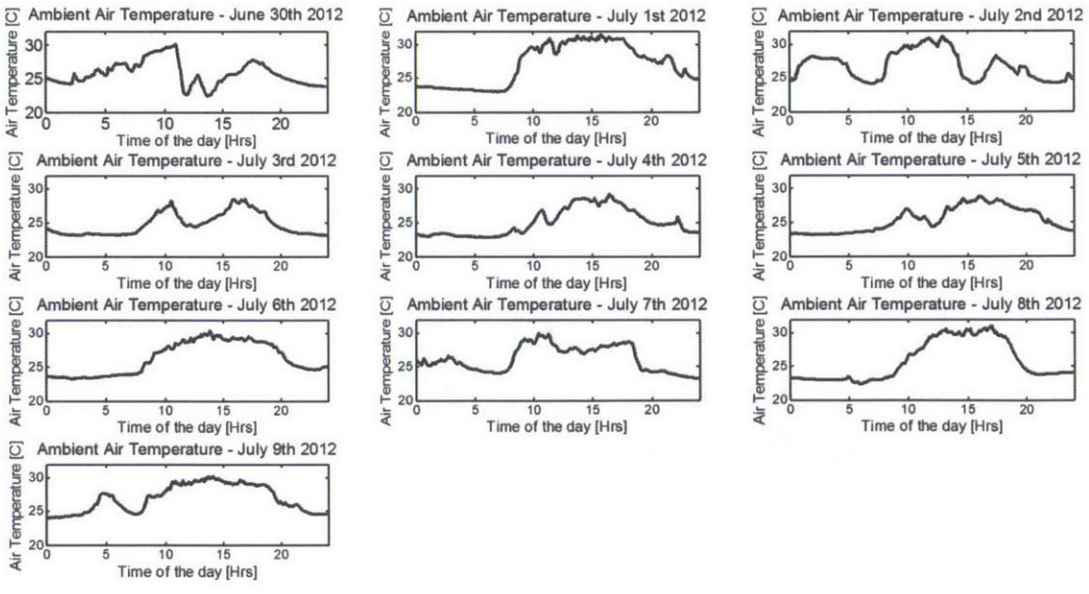

Fig 3.5 The diurnal ambient air temperature measured with the weather station 2.5 m above the west container.

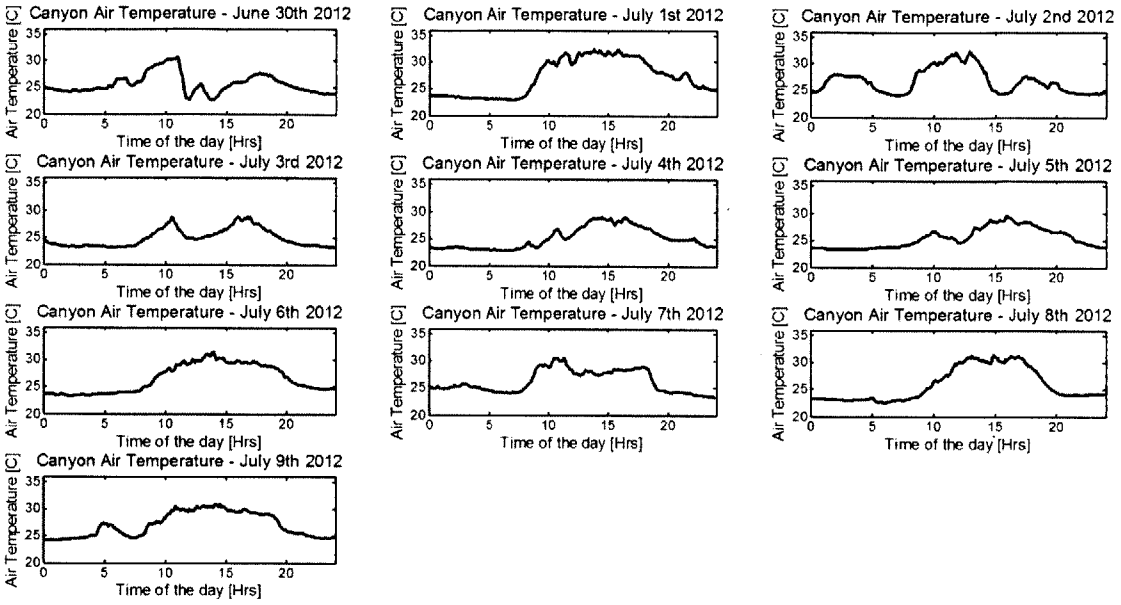

Fig 3.6 The diurnal in-canyon air temperature measured with the weather station located near the middle of the canyon.

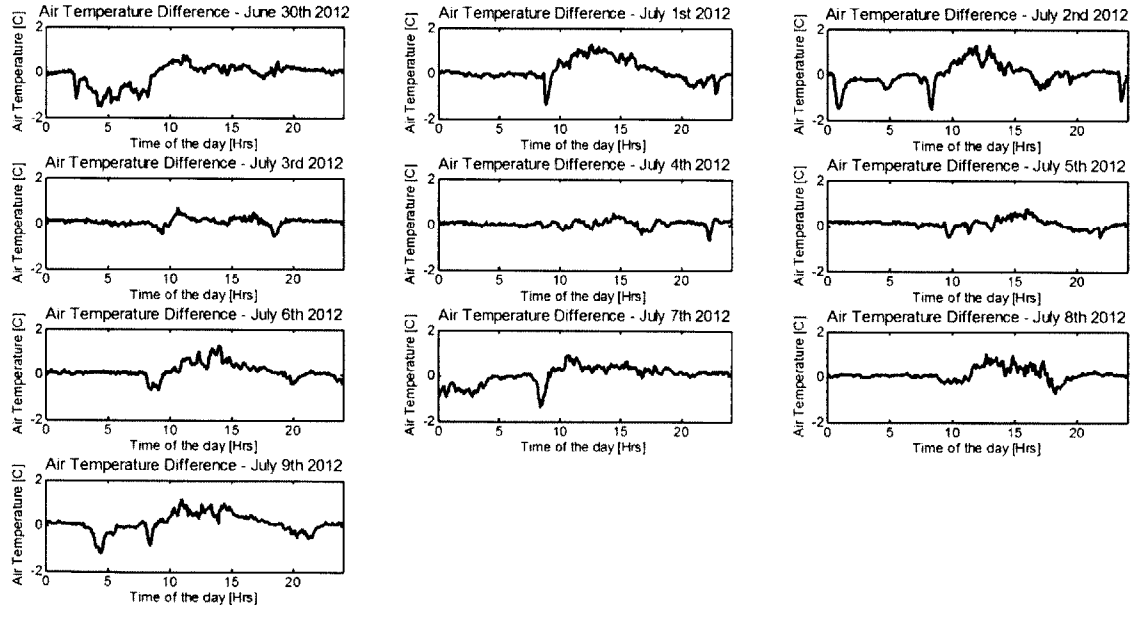

Fig 3.7 The calculated air temperature difference between ambient air temperature and the in-canyon air temperature.

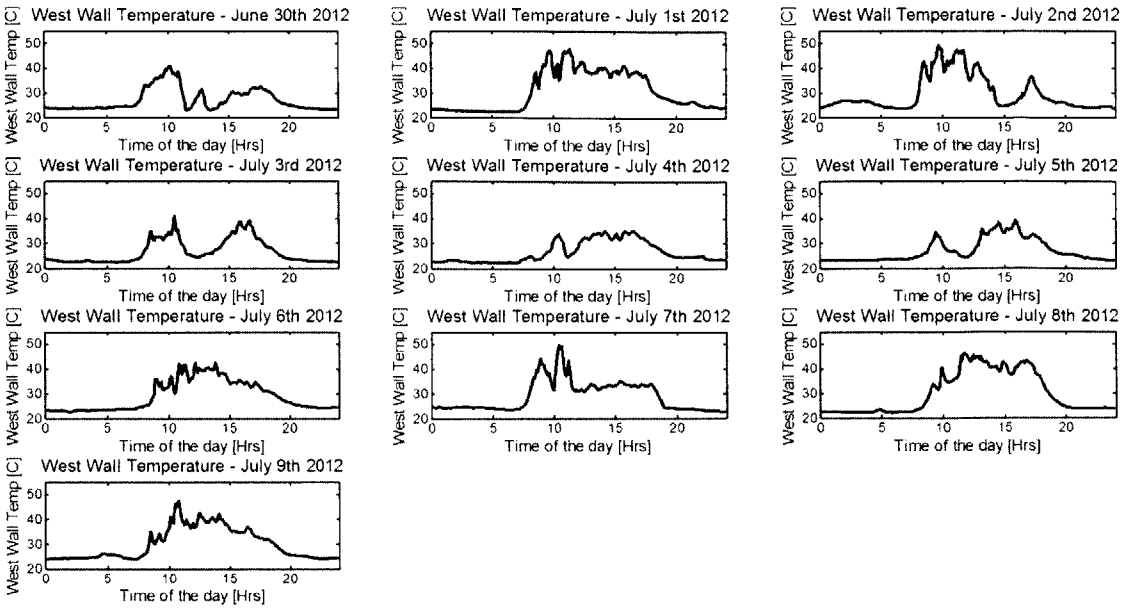

Fig 3.8 The diurnal west wall surface temperature measured by the two thermocouples attached to the west wall.

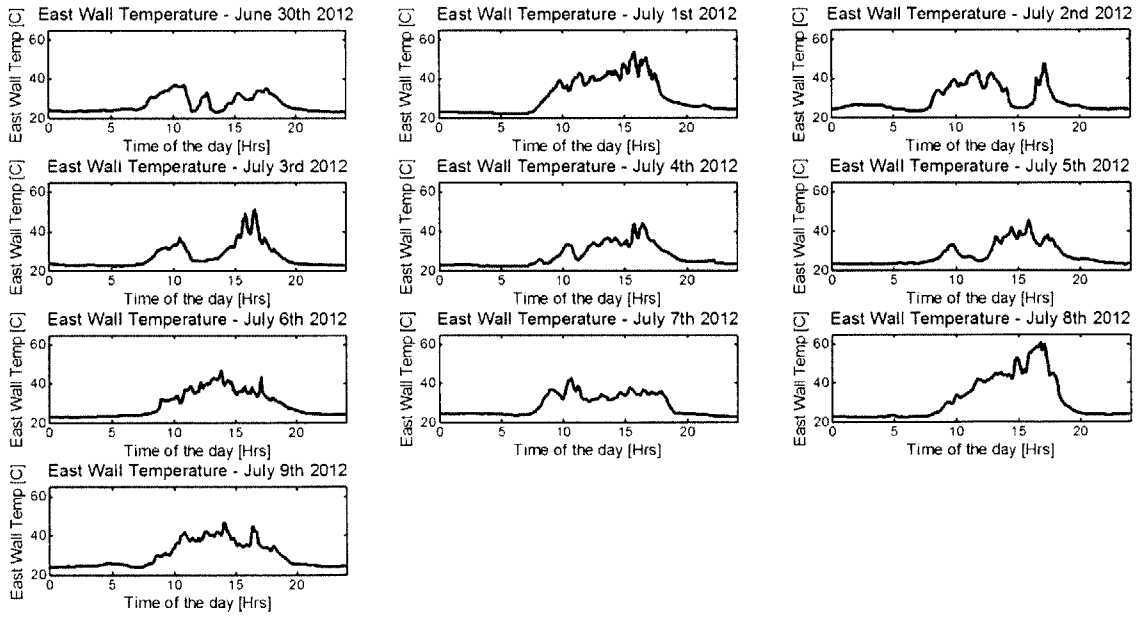

Fig 3.9 The diurnal east wall surface temperature measured by the two thermocouples attached to the east wall.

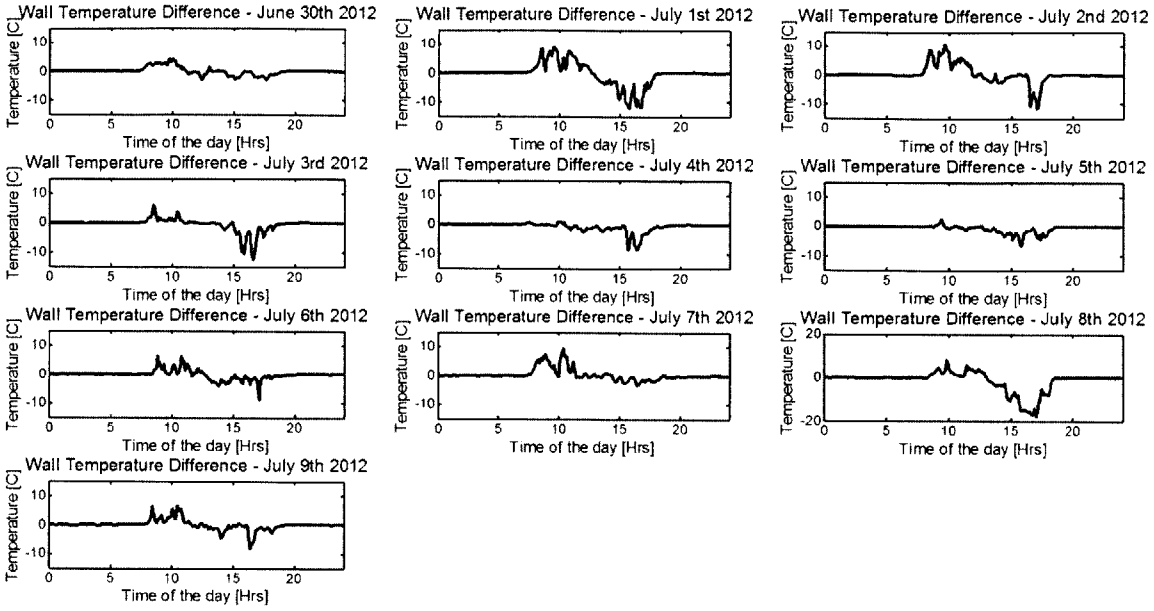

Fig 3.10 The calculated temperature difference between the two walls of the canyon. This difference drives the thermal circulation inside the canyon.

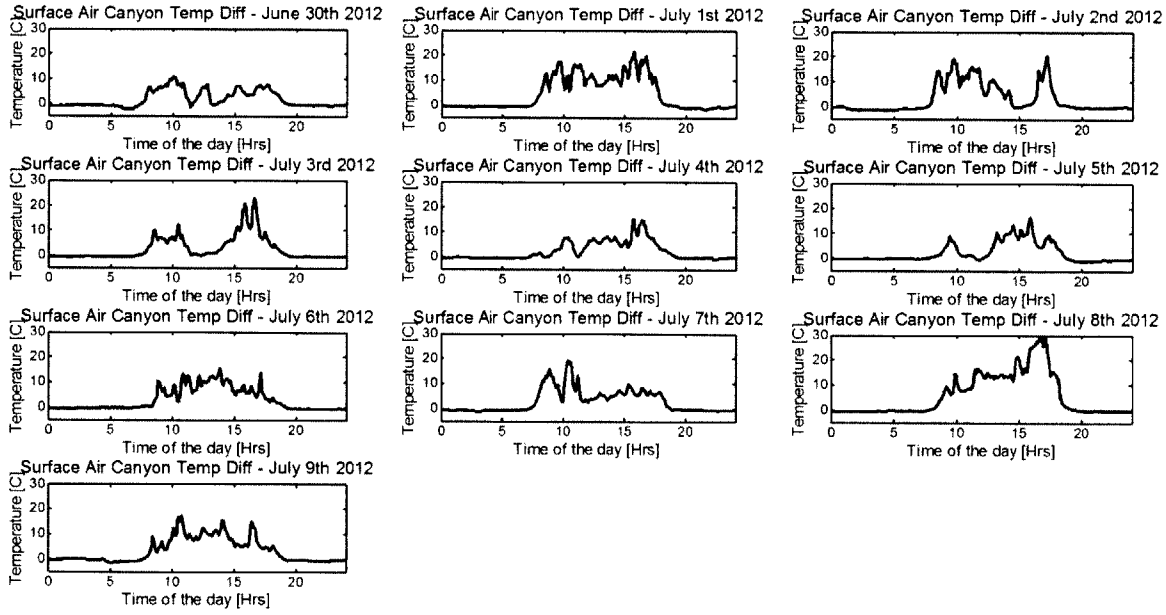

Fig 3.11 The calculated temperature difference between the in-canyon air and the wall which is at higher temperature at each time.

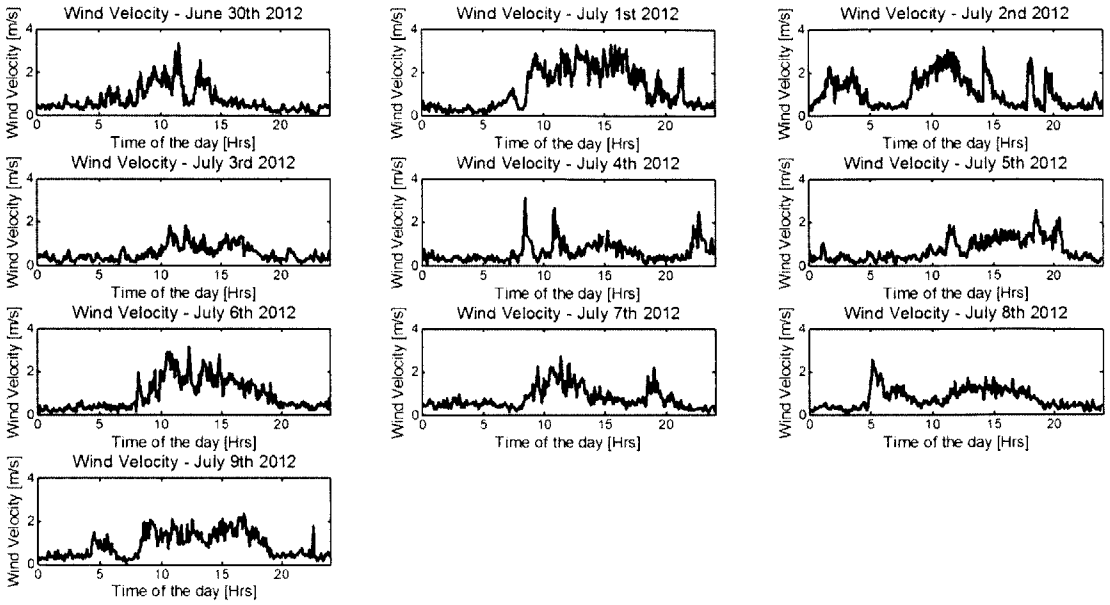

Fig 3.12 The synoptic wind speed above the canyon measured by the weather station located 2.5 m above the west container.

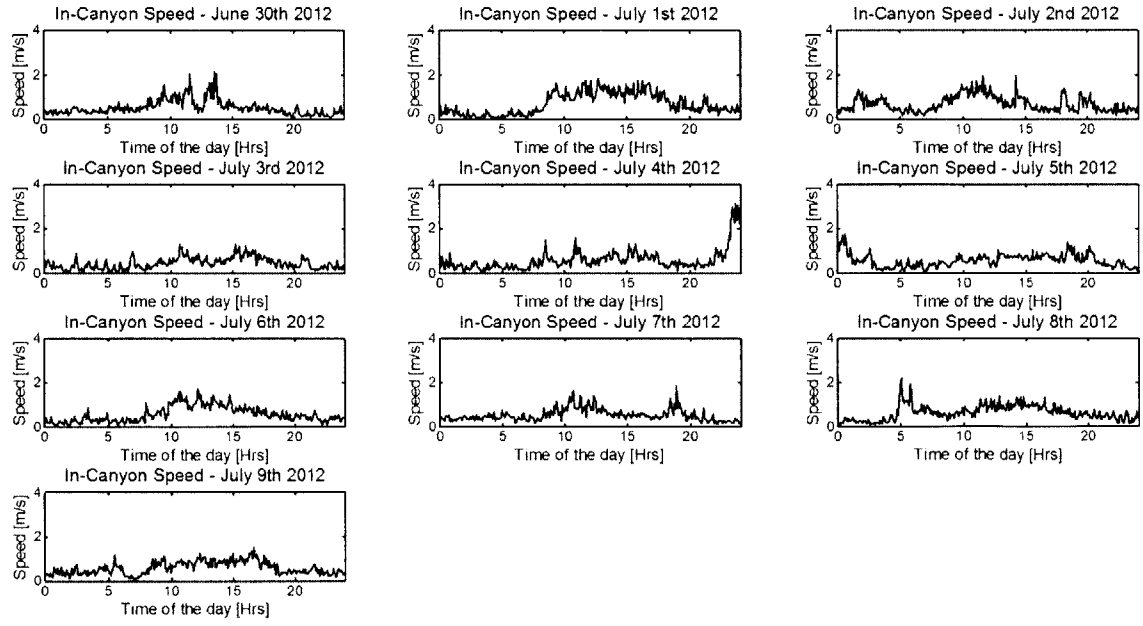

Fig 3.13 The in-canyon speed measured by the weather station located near the center of the canyon.

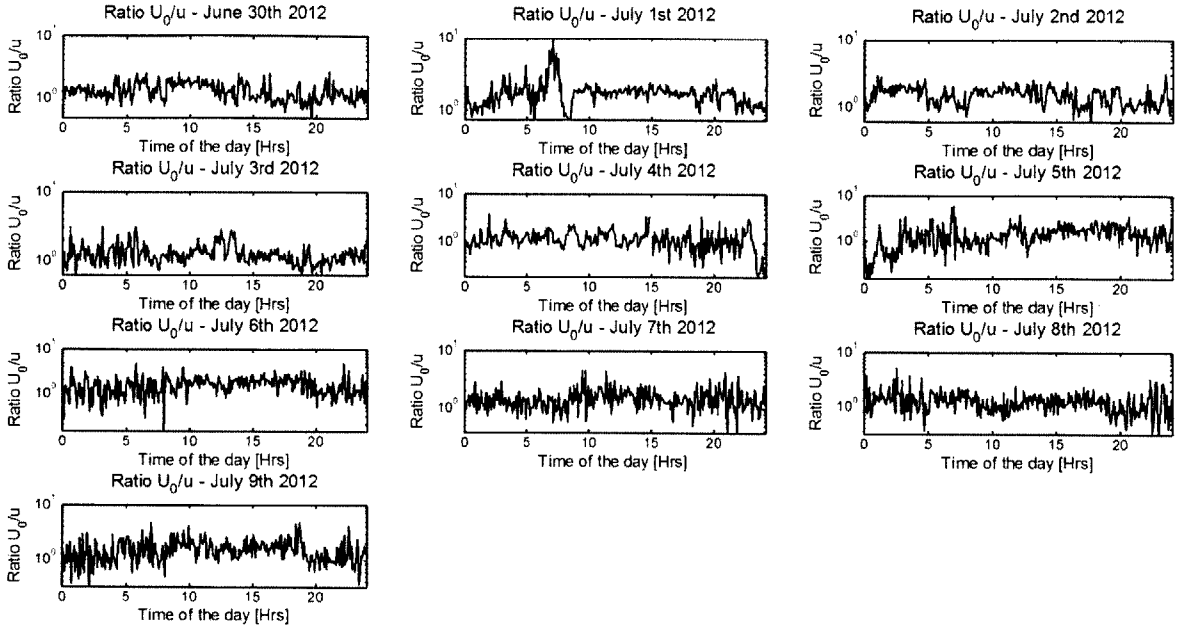

Fig 3.14 The ratio between the ambient speed, U_0, and the in-canyon speed, u.

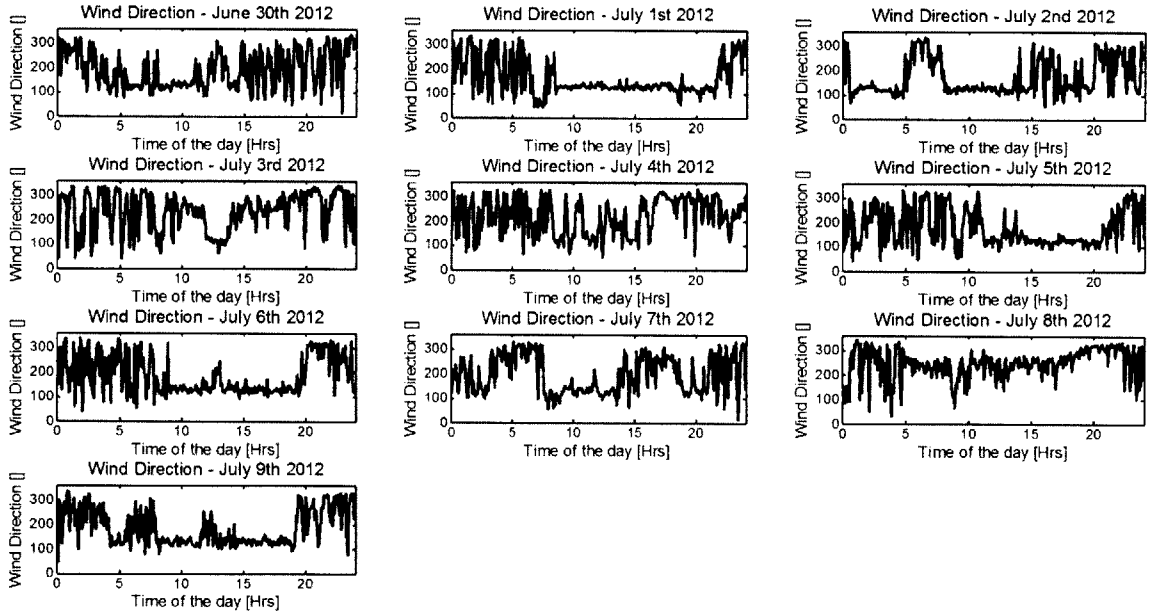

Fig 3.15 The synoptic wind direction measured by the weather station 2.5 m above the west container.

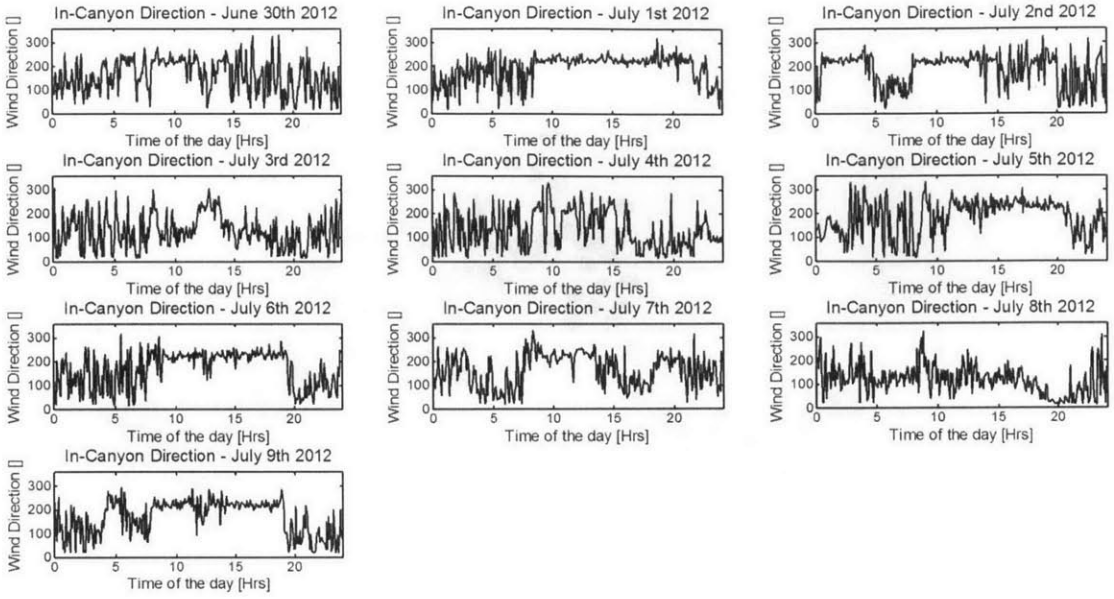

Fig 3.16 The flow direction inside the canyon measured by the weather station near the center of the canyon.

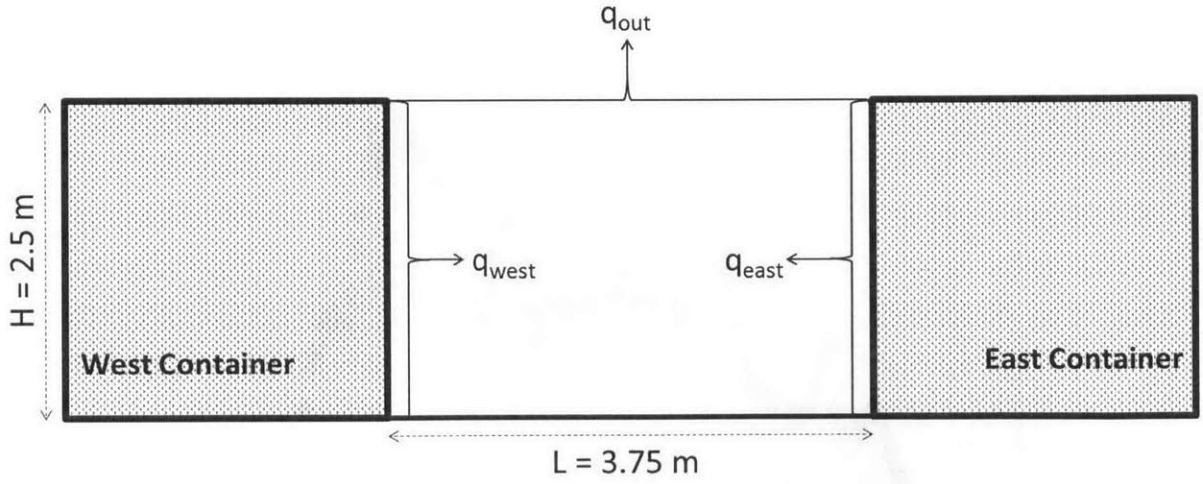

Fig 3.17 The heat fluxes under consideration. q_{out} is also in the horizontal direction (3-D).

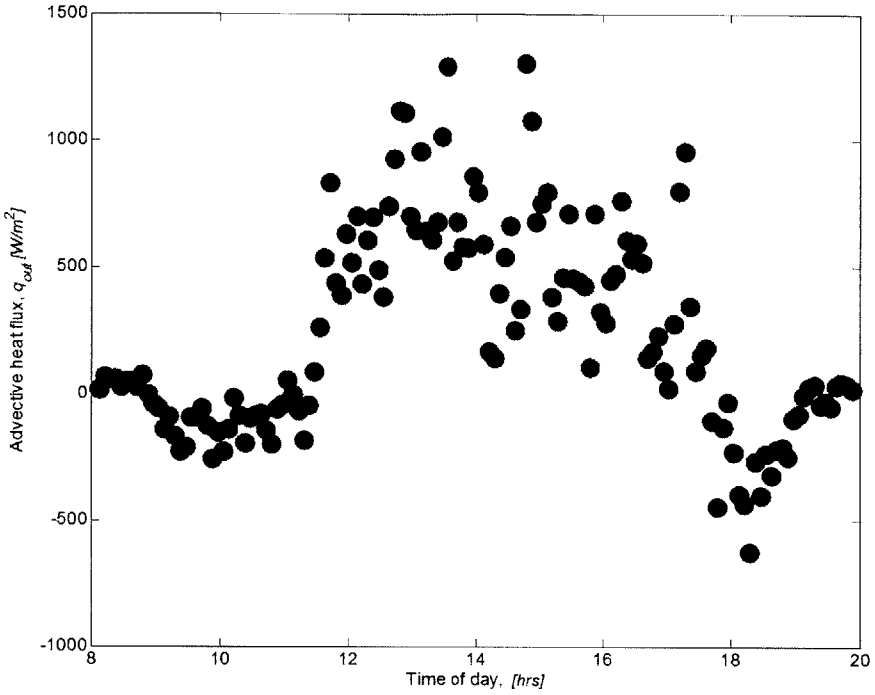

Fig 3.18 The calculated heat flux out of the canyon calculated by Eq. 3.5.

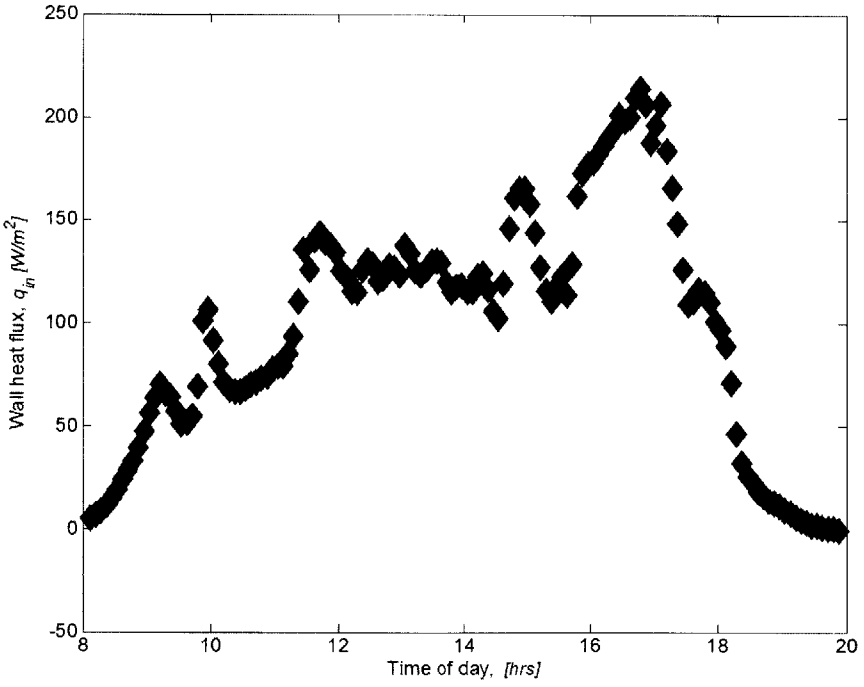

Fig 3.19 The heat flux into the canyon calculated with Eq. 3.3 and Eq. 3.4.

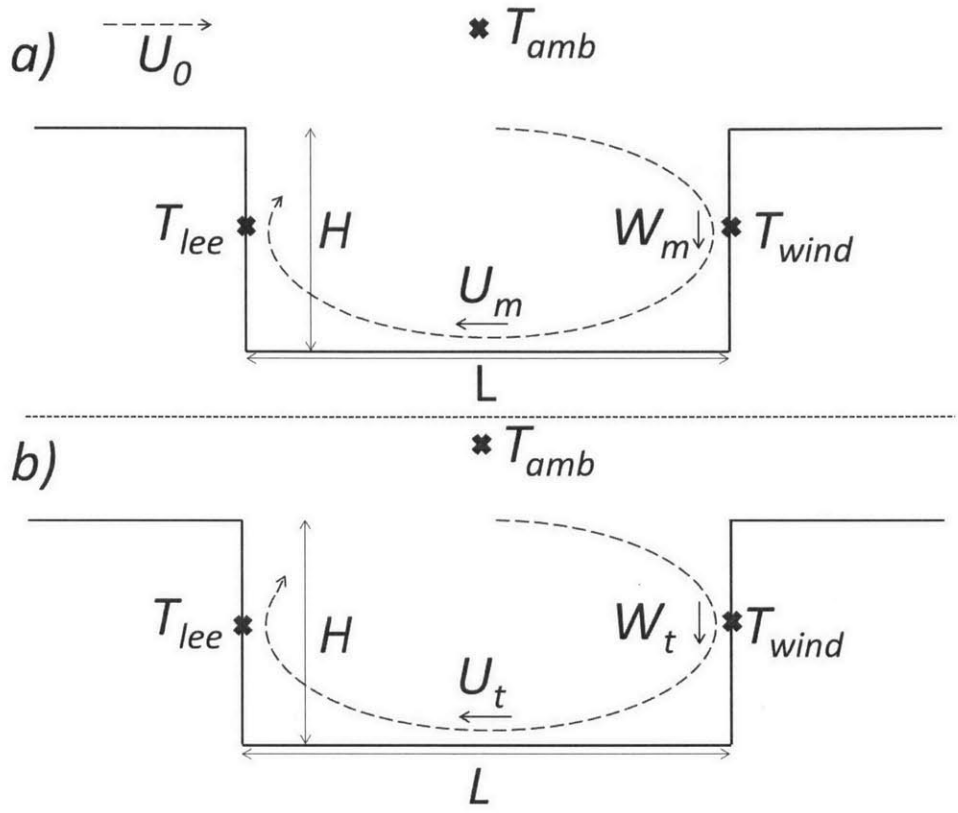

Fig 3.20 (a) Predicted flow inside the urban street canyon when the windward wall, the leeward wall and the ambient air are at an identical temperature (isothermal). (b) No free stream flow exists, and the temperature of the leeward wall is at a higher temperature than the windward wall, which is at the same temperature as the ambient air above the canyon. If the buoyancy case is added to the isothermal case, the thermal conditions assist the mechanically driven flow where two vortices are rotating in the same direction, leading to larger air speeds inside the canyon.

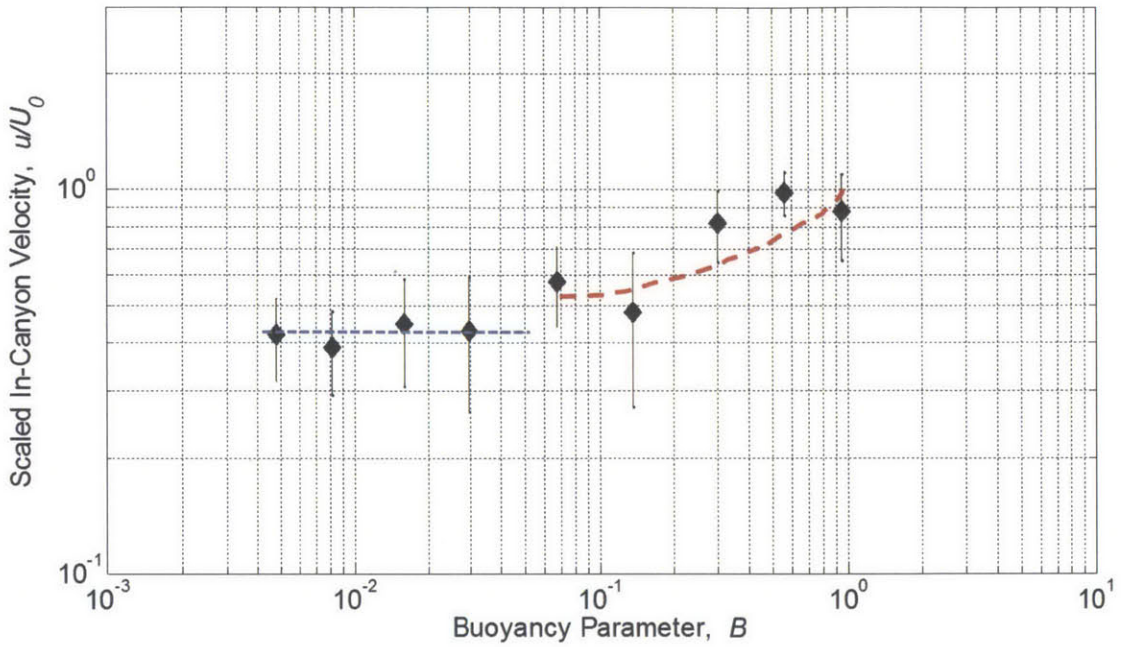

Fig 3.21 The scaled in-canyon velocity, u, as function of B. The plot was originally published in Dallman et al. [37].

Chapter 4: On Buoyancy Forced Flows in Urban Street Canyons

Abstract

During sunny days with periods of low synoptic wind, buoyancy forces can play a critical role in the air flow, and thus on the dispersion of pollutants in the built urban environments. Earlier studies (Allegrini et al. [11], Dallman et al. [37], Kim and Baik [45], Park et al. [46]) provide evidence that when one surface in an urban street canyon is at a higher temperature than local ambient air, buoyancy forces can modify the mechanically-induced circulation within the canyon (i.e., gaps between buildings). The aspect ratio of the urban canyon is a critical factor in the manifestation of the buoyancy parameter. In this chapter, computational fluid dynamics (CFD) simulations are performed on urban street canyons with six different aspect ratios, focusing on the special case where the leeward wall is at a higher temperature than local ambient air. Under these circumstances the mechanical forced circulation and the buoyancy force circulation are acting in the same direction (assisting flow). A non-dimensional measure of the influence of buoyancy is used to predict demarcations between the flow regimes. Simulations are performed under a range of buoyancy conditions, going beyond those of previous studies (Allegrini et al. [11], Dallman et al. [37], Kim and Baik [45], Park et al. [46]). Observations from a field experiment and a wind tunnel experiment are used to validate the results. The results were originally published in Magnusson et al. [47].

Introduction

In the current study it is shown how the in-canyon air flows are affected by the heating of the leeward wall. The CFD simulations are performed for urban street canyons of six aspect ratios, and these cover all three flow categories identified by Oke [43]: isolated roughness flow, wake interfernce flow and skimming flow.

Sini et al. [40] developed and implemented the numerical model CHENSI to simulate air flow in an urban street canyon as well as vertical exchange of pollutants between the canyon and the ambient air. The model shows that the differential heating of the walls influences the air exchange at the roof level and, consequently, air quality within the street canyon. In addition, the model predicts various flow structures, depending on the wall temperatures. In this early study the absolute value of Ri is low ($<$ 10.0) compared with values explored in this study and Chapter 4. Later, Kim and Biak [45] investigated the thermal effects on air flow and pollutant dispersion in street canyons for various aspect ratios. The simulations were performed for lower Ri than considered in this study. The effects of temperature differences between the street and the ambient air, the windward wall and the ambient air, and the leeward wall and ambient air were investigated. When the leeward wall was heated, only one vortex formed inside the canyon, regardless of the aspect ratio and thermal conditions. When the windward wall was heated, two vortices could be formed, depending on the aspect ratio. Li et al. [29, 33] performed large-eddy simulations of flow in an urban street canyon, with heating of the street surface. They found that street heating significantly enhanced the mean flux,

turbulence and turbulent fluxes inside the canyon. The modulus of Ri for their simulations was limited to 2.4.

The effects of the buoyancy flux due to heated walls in an urban street canyon were investigated in a real urban street canyon in Nantes, France, by Louka et al. [34, 35]. They found that the effects of wall heating were only important for the near wall flow. CFD simulations were also performed by Louka et al. [50], but these simulations overestimated the effects of the heating of the windward wall. In complementary wind tunnel measurements by Allegrini et al. [11], an urban street canyon with a differential wall heating was considered for three different Reynolds numbers (Re). For the windward heated case, when Re is 9,000, two main counter-rotating vortices were formed, in agreement with CFD simulations of Louka et al. [50]. The leeward wall heating leads to accelerated rotation of the vortex.

Solazzo and Britter [51] performed CFD simulations on a two-dimensional urban street canyon with heating of all three canyon surfaces, for $-0.1 < Ri < 0$. Air temperature within the canyon was uniformly distributed except near the heated wall, and thus the contribution of the heated wall to the flow as a whole was minimal. On the other hand, Fernando et al. [39] presented three-dimensional CFD simulations on the thermal effects of a downtown area in Phoenix, Arizona. The results showed significant buoyancy effects all the way to the middle of the canyon at tens of meters above the ground. The mismatch can be partially explained by higher buildings in the downtown area which leads to higher calculated Ri. Also, in a complex geometry, as in the downtown area of Phoenix,

low wins 'dead zones' in the wakes behind the taller buildings are affected by buoyancy fluxes.

Cai [52] performed large eddy simulations under differential wall heating conditions, where $|Ri|$ was limited to 2.14. The vortex rotation was accelerated when the leeward wall was heated and was suppressed by the heating of the windward wall.

Similar LES studies of Park et al. [46] showed that heating of the leeward wall and the street leads to increased air speeds in the canyon, while heating of the windward wall leads to a smaller mechanically driven vortex and an extra thermally driven vortex near the windward wall, rotating in a different direction compared to the mechanically driven vortex. The Ri was small compared with the simulations presented in Chapter 4. It is showed how the in-canyon flows are affected by the leeward wall heating. The CFD simulations are performed for urban street canyons of six aspect ratios, and these cover all three flow categories proposed by Oke [43]: isolated roughness flow, wake interference flow and skimming flow.

For further validation, one of the street canyons simulated has the same aspect ratio as the canyon considered in the field experiment of Dallman et al. [37]. For this aspect ratio the flow is in transition from wake interference to the skimming flow regimes. The observed ranges of heating and buoyancy are included, but the simulations extend the buoyancy effects beyond what is found in the literature to explore a wider range of conditions than observed in the short-duration field experiment. The special case of $U_0 = 0$ was also investigated.

The goal is to classify the flow into mechanically and buoyancy driven flows, with an intermediate (transition) regime in-between. The conditions where buoyancy effects are larger than in previous studies are explored. The flow regimes and transitions between them are shown to be captured by a dimensionless number that includes the degree of mechanical forcing, thermal contrasts and canyon geometry. Finally, an estimate on the buoyancy effects on the eddy viscosity (v) inside the canyon is considered, which is useful for gaining basic insights into the effects of buoyancy on pollutants and human exposure to particulates in urban canyon settings.

The goal is to classify the flow into mechanically and buoyancy driven flows, with an intermediate (transition) regime there in-between. Conditions where buoyancy effects are larger than in previous studies are explored. The flow regimes and transitions between them are shown to be captured by a dimensionless number that includes the degree of mechanical forcing, thermal contrasts and canyon geometry. Finally, the buoyancy effects on the turbulence viscosity (v) inside the canyon are estimated, which is useful for gaining basic insights into the effects of the buoyancy intensity on air quality and human exposure to air pollutants in the built urban environment. In the next chapter, the focus is on the buoyancy effects on the residense time, exchange rate and human exposure inside a simulated urban street canyon.

The CFD Simulations

The computational domain is shown in Fig 4.1. The free stream velocity above the canyon is characterized by horizontal velocity U_0, which is defined to be perpendicular to

the urban street canyon (normal to its axis). The buoyancy flow is driven by the difference in temperature between the two walls and ambient air. The temperatures of the walls are T_{lee} and T_{wind}, and the ambient air above the canyon temperature is T_{amb}. The street temperature is denoted by T_{street}. The CFD model is integrated until steady-state conditions are achieved. The air flow is considered to be steady when the fluid parcel has made several complete circuits inside the canyon, i.e., the time scale is larger than H/u. In the field experiment, the problem is dynamic and more complex. The field experimental data (Dallman et al. [37]) used for comparison are considered to be steady or near steady when the flow is normal to the canyon axis (+/- 15°) for at least 30 seconds (approximately three circulations of a fluid parcel).

The finite volume (Appendix 2) CFD code ANSYS FLUENT 13.0 is used in this study. The standard k-ε turbulence closure is used to solve the Reynolds-averaged Navier-Stokes equations of the fluid flow. The k-ε model is a two equation model. The transport equations for the turbulence kinetic energy, k, and the rate of dissipation, ε, can be found in the ANSYS Theory Guide [53]. The main assumption is that the turbulence viscosity is isotropic, which means that the ratio between the Reynolds stress and rate of deformation is equal in all directions, while in such models as large-eddy simulation (LES) that magnitude depends on directions. The wide use of the k-ε model and how well it has been tested makes it more appropriate to simulate the flow dealt with in this chapter. Full buoyancy effects are used in the standard k-ε turbulence model, so buoyancy effects are included in the equations for k and the dissipation rate, ε. The density of air is calculated using the Boussinesq approximation. The simulations are performed to achieve

steady-state conditions, which should be sufficient for the problems of interest. In the real environment, the problem is dynamic and more complex. Hence, the field experimental data (Dallman et al. [37]) used for comparisons are steady or near steady and the flow is normal to the canyon axis (+/-15°) for at least 30 seconds. The temperature difference between the walls is considered to be constant during this period and thus the flow is quasi-steady. The CFD simulations were considered converged when the scaled simulated residuals were less than 10^{-6}.

The canyon is simulated as a smooth wall cavity with height H and width L (H is 2.5 m and L varies between the simulations in order to produce different canyon aspect ratios). CFD simulations that extend the buoyancy effects beyond the experimental setting of Dallman et al. [37] are performed. The purpose is to investigate the physical effects of the different wall heating configurations on the air flow inside the canyon. Specifically we investigate the development of varying flow regimes for different values of the B parameter. In the field experiment in Dallman et al. [37], two obstacles (containers) rise above the ground which leads to separation of the flow at the edge of the upstream obstacle. Because of the complex landscape around the experimental site (trees, buildings, an industrial site and fences) and lack of information on the oncoming velocity profile, the cavity approach is considered to be better suited for the purpose of this study. The effect of the B parameter on the air flow is thus isolated from flow separation above the canyon. The experimental results indicate that the flow is reattached at the roof of the upstream building which makes the cavity approach relevant. Also the laboratory experiment performed by Allegrini et al. [11] is closer to the setting of the CFD

simulations (cavity approach). The height of the canyon is H and its width is L. The height of the domain above the canyon is $7H$, and its upstream and downstream extents are $5H$. ANSYS Inc. recommends that the height, the upstream length and the downstream length of a computational domain (Fig 4.1) are not less than five times the height or the diameter of the obstacle.

The mechanical boundary conditions are the following at the inlet: the wind velocity, turbulent kinetic energy and turbulent dissipation rate profiles are defined as in Richards and Hoxey [54]

$$U(z) = \frac{u_*}{\kappa} ln\left(\frac{z+z_0}{z_0}\right), \quad \textbf{4.1}$$

$$k = \frac{u_*^2}{\sqrt{C_\mu}}, \quad \textbf{4.2}$$

$$\varepsilon(z) = \frac{u_*^3}{\kappa(z+z_0)}, \quad \textbf{4.3}$$

where z is the height above the ground (m), u_* is the friction velocity (m s-1), κ the von Karman constant (0.40), z_0 the roughness length of the urban terrain, meant to reflect the effects of the roughness of the surface (in this case the buildings) on the wind flow. For an area of few buildings and many trees as the experimental site in Dallman et al. [37] z_0 is set as 0.25 m, following Stull [15]. C_μ a constant in the standard k-ε model. The outlet has a zero gauge pressure which means that the pressure difference across the boundary is zero and the air flow thus horizontal at this vertical boundary. The top boundary is defined as a wall with no shear stress. The upstream and downstream roofs, the street and

the two walls are defined as smooth walls with no slip shear conditions. In the special case when U_0 is set to zero, the inlet is defined as a pressure outlet with a zero gauge pressure.

The thermal boundary conditions are the following: the temperatures of inflow air at the inlet boundary and backflow air at the outlet are set as T_{amb} (300 K). The temperatures of the street (T_{street}), windward wall (T_{wind}), upstream (T_{uproof}) and downstream ($T_{downroof}$) roofs and the top (T_{top}) boundaries are all set to the same temperature as the ambient air. The temperature of the leeward wall (T_{lee}) is kept constant and the gravity vector is changed using successive steady state steps. *Re* of the flow is about 40,000, so the flow is *Re* independent; according to Castro and Robins [55], a flow around a surface-mounted cube becomes *Re* independent for $Re > 30{,}000$.

The ANSYS FLUENT Workbench mesh generator is used to configure the CFD model. The cells are quadrilateral and smaller grid sizes are defined near the surfaces of the computational domain. Larger grid sizes are permitted at distances away from the surfaces (Ansys [53]). The mesh resolution for the computational domain expands from $0.025H$ to $0.1H$ with an expansion factor of 1.05. The standard wall function is applied which is the default setting in Fluent. Sensitivity experiments were performed to ensure that the computational domain and the mesh resolution do not bias the results.

Fig 4.2 is an illustration of the flow inside the urban street canyon under two conditions. The upper panel shows a vortex formed under mechanical forcing. The lower panel illustrates a bouyancy driven case, with no background winds. The temperature difference between the two walls leads to the formation of a vortex inside the canyon. If

the temperature difference from the lower panel is added to the mechanical case, it is believed that the buoyancy driven flow assists the formation of a vortex.

Results and Discussion

A goal of the CFD simulations is to investigate the relationship between a characteristic velocity (u) inside a canyon and the B parameter introduced in Dallman et al. [37] and shown in Eq. 3.6 and Eq. 3.7. Thus we introduce the following equations to compare the constants from each method:

$$\frac{u}{U_0} = \begin{cases} a_1 & B \leq B_c \\ a_2 + a_3 B^{b_1} & B_c \leq B \leq B_t \\ a_4 B^{b_2} & B \geq B_t \end{cases} \qquad \textbf{4.4}$$

where a_1, a_2, a_3, a_4, b_1 and b_2 are constants, B_c the critical buoyancy parameter B for buoyancy effects to set in and B_t the critical B for the flow to become completely buoyancy dominated. The in-canyon velocity, u, is measured as the average horizontal velocity inside a box from $0.1H$ above the street up to $0.4H$ above the street canyon, and $0.35L$ from the leeward wall up to $0.65L$, (the box is shown in Fig 4.3). The velocity at this position in the canyon is considered to be characteristic of the strength of the vortex (bulk flow) and to be consistent with u in Allegerini et al. [11], Dallman et al. [37] and Park et al. [46] which was measured in the lower part of the canyon.

Simulations with $U_0 \neq 0$, and a heated leeward wall have a combination of mechanical and buoyancy flows. The CFD simulations are performed for the buoyancy parameter between 0 and 500. This extends the physically realizable range and thus

includes extreme cases. Fig 4.3 shows the velocity vectors inside and just above a canyon of aspect ratio 1.0. The left panel shows the vector field inside the canyon for the mechanically driven flow (B = 0) and the right panel shows the vector field inside the canyon when the flow is buoyancy dominated (B = 400). The buoyancy flux at the leeward wall causes the vortex to extend above the canyon. The buoyant air near the wall rises and the resulting mixing causes entrainment of air towards the wall. This increases the air speeds within the canyon. To clarify distinctly the effects of the heated wall we performed simulations where U_0 = 0, the velocity vector field is shown in Fig 4.4. The heated left wall leads to natural convection from the wall. In a thin boundary layer ($\sim 0.05H$) next to the wall a thermally driven plume is formed that rises up above the canyon. Air is entrained into the plume from both sides. The entrainment of air into the plume inside the canyon leads to the formation of a thermally driven vortex as the figure shows. Thus in the case with a heated leeward wall, the mechanical and the buoyancy flow support each other.

The CFD simulations are validated against field data (Dallman et al. [37]), wind tunnel data (Allegrini et al. [11]) and large eddy simulation (Park et al. [46]) and the results for u/U_0 as a function of B displayed in Fig 4.5. The field experiment data encompasses $B \leq 1$. When B is about 0.05–0.1, the value of u starts increasing, indicating that B_c is about 0.05–0.1. The flow is not believed to reach the buoyancy dominant regime for the field data. The wind tunnel data have B values between 0 and 10. The data show an obvious increase of u with increased B. The CFD results show the same trend as the wind tunnel and field data. The flow is considered mechanically driven until B is

larger than 0.1 (B_c = *0.1*). When B is between 0.1 and 50 the flow is considered to be in the intermediate regime (B_t = *50*) and thus completely buoyancy driven when $B \geq 50$. Owing to weather conditions in the real environment and operational difficulties in wind tunnels, it is unlikely that the buoyancy dominant flow regime would be reached. Thus the wind tunnel data and the experimental results show only the mechanically driven and intermediate regimes, and the CFD has the advantage of extending the B range and crossing into the purely buoyancy driven regime.

The aspect ratio is a critical factor that affects the vortex formation and the relative role of mechanical and thermal forcing. CFD simulations were performed on canyons with seven aspect ratios and the results are shown in Fig 4.6. It shows some consistency in the development of u/U_0 by B for canyons with aspect ratios 0.3 – 1.2 but for the canyon with an aspect ratio of 2.5, u/U_0 is relatively lower in the mechanical and transitional regimes but increases more rapidly once the buoyancy dominant regime is reached at B = 50. To show how the aspect ratio of the canyons affects the thermal exponent, b_2, introduced in Eq. 4.4 and theoretically predicted to be 0.5, b_2 is plotted as a function of aspect ratio in Fig 4.7. As seen in the figure, for canyons of aspect ratios between 0.67 and 1.0, u/U_0 increases as a function of the B parameter raised to the power of about 0.5, which is consistent with the theoretical considerations. For canyons of lower aspect ratios, u/U_0 increases with B raised to the power of about 0.37 and for canyons of aspect ratios larger than 1.0, the exponent on the B parameter is larger than predicted in the theoretical considerations. The theoretical derivation on the relationship between u/U_0 and the B parameter was done for canyons in the skimming flow regime with one rotating

vortex centered in the middle of the canyon. The flow structure inside the canyons is shown in Fig 4.8 and Fig 4.9 for canyons with aspect ratios 0.3 and 2.5. A canyon with an aspect ratio 0.3 is in the isolated roughness flow regime (Oke [43]) with the center of the vortex near the windward wall and a canyon with an aspect ratio 2.5 has two vortices, stacked upon each other. The lower vortex is formed because of increased frictional resistance to the flow inside the deep canyon. When the leeward wall of the deep canyon is heated the weak lower vortex disappears and only one vortex is formed where the buoyancy flow overcomes the increased friction inside the canyon. The characteristic velocity used in this study accounts for the lower weaker vortex when the flow is purely mechanically driven, but when the buoyancy is taken into the account by heating the leeward wall, only one vortex develops and thus u is consistent and comparable with the canyons with the other aspect ratios. Fig 4.9 shows how the lower vortex disappears when the B parameter is increased. The relationship between u and B in Dallman et al. [37] is for canyons where only one vortex is formed inside the canyon. For a flow structure in a canyon with an aspect ratio near 1 (Fig 4.2), the vortex formed is centered in the middle of the canyon. The thermal effects are larger for canyons with larger aspect ratios, because of larger areas over which buoyancy can influence and increase the flow. Figures Fig 4.2 and Fig 4.9 show the domain where averaging of u is performed as dashed-line boxes.

Compared with the flow structure in a canyon with an aspect ratio near 1 (Fig 4.3), the vortex formed is centered in the middle of the canyon. The thermal effects are

more for canyons with larger aspect ratios, because of larger areas over which friction can influence and reduce the flow.

Human exposure to air pollutants is an important factor in determining quality of life in urban areas. The magnitude of turbulence (eddy) viscosity inside the canyon, v_{can}, indicates the amount of mixing between in-canyon air and ambient air above it and thus the efficiency of the pollutant removal from the canyon. The normalized average v_{can} inside the canyons is shown in Fig 4.10. The results show how v_{can}/U_0H increases with increasing B parameter. For a canyon with an aspect ratio of 1.0 v_{can}/U_0H increases with B nearly linearly. The buoyancy effects on the turbulence viscosity also increase with increased aspect ratio. The increase in v_{can}/U_0H between the mechanical case and the largest B is tenfold. This shows the importance of including thermal situations when simulating for air quality in urban areas.

Conclusions

Mechanically driven vortices can be developed in urban canyons when there is strong advection of ambient air above the city. In addition, solar and thermal radiation can heat the buildings' exterior walls far above the ambient air temperature. The heat flux near the walls can generate significant amounts of buoyancy. In this study we examined a purely thermally driven flow inside a street canyon and the influence of the leeward wall heating on the mechanically driven vortex inside urban canyons by performing CFD simulations over a wide parameter range. The differential wall heating leads to a buoyancy-driven flow that affects the flow field inside the urban street canyon. A

dimensionless buoyancy parameter B is used to characterize the changes in the flow regime under different amounts of wall heating. The B parameter also incorporates the effects of canyon geometry and advection strength above the city, for a particular type of (single-cell) flow structure. Steady-state simulations with a CFD code show that buoyancy can have significant effects on vortices formed inside urban canyons. The magnitude of this effect is dependent on the B parameter, which was varied between 0 and about 500 in this study. The CFD simulations were compared with theoretical considerations, and these match for canyons with aspect ratios of 0.67–1.0. The simulations show that the geometry of the canyon affects the in-canyon velocity magnitude as B varies. This occurs despite the fact that B includes the aspect ratio of the canyon.

A typical urban area geometry can consist of 3-4 floor story buildings, reaching at least 10 m height and an aspect ratio of about unity. For mild synoptic wind speeds of about 1.0 m s-1 and the wall temperature difference of about 10 K, B is on the order of 1.0 to 10. Lower synoptic wind speeds increase the magnitude of B and enhance the relative importance of buoyancy. For the geometry and temperature difference considered, the urban air flow is purely mechanically driven when U0 is larger than 4.0 m s-1, purely buoyancy driven when the flow is less than 0.2 m s-1 and thus in the intermediate regime there between. In warm regimes, such as Southeast Asia and the Middle East the buoyancy force inside the urban environment can clearly play a critical role in determining the air flow and dispersion of pollutants out of the urban environment and thus on human exposure to air pollutants. In a separate chapter, the effects of the

buoyancy force on the air exchange between the in-canyon and ambient air will be considered. It is an important factor in determining the air quality within the built urban environments and thus in determining the human exposure to air pollutants.

The increase of v_{can}/U_0H with increased B suggests that buoyancy plays a critical role in the removal of pollutants from urban street canyons during calm and sunny days. The turbulent kinetic energy increase is higher in deep canyons than in shallow canyons. Thus, when modeling for pollutant removal and distribution, it is necessary to account for the buoyancy force.

Future studies should also consider simulations that model the unsteadiness of ambient free stream wind under conditions where the buoyancy driven flow is dominant. Does the unsteadiness of flow direction and magnitude predominantly overcome the buoyant effects?

Figures

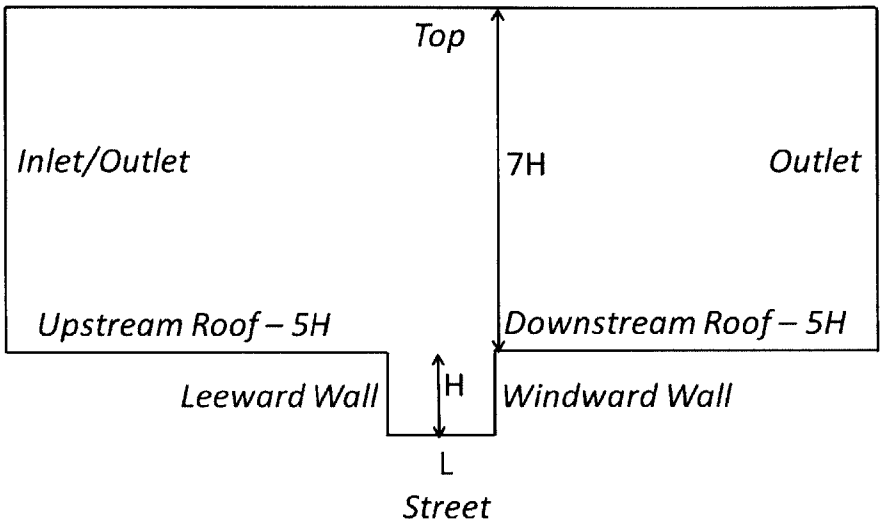

Fig 4.1 The computational domain for the urban street canyon is defined as a cavity in a smooth wall.

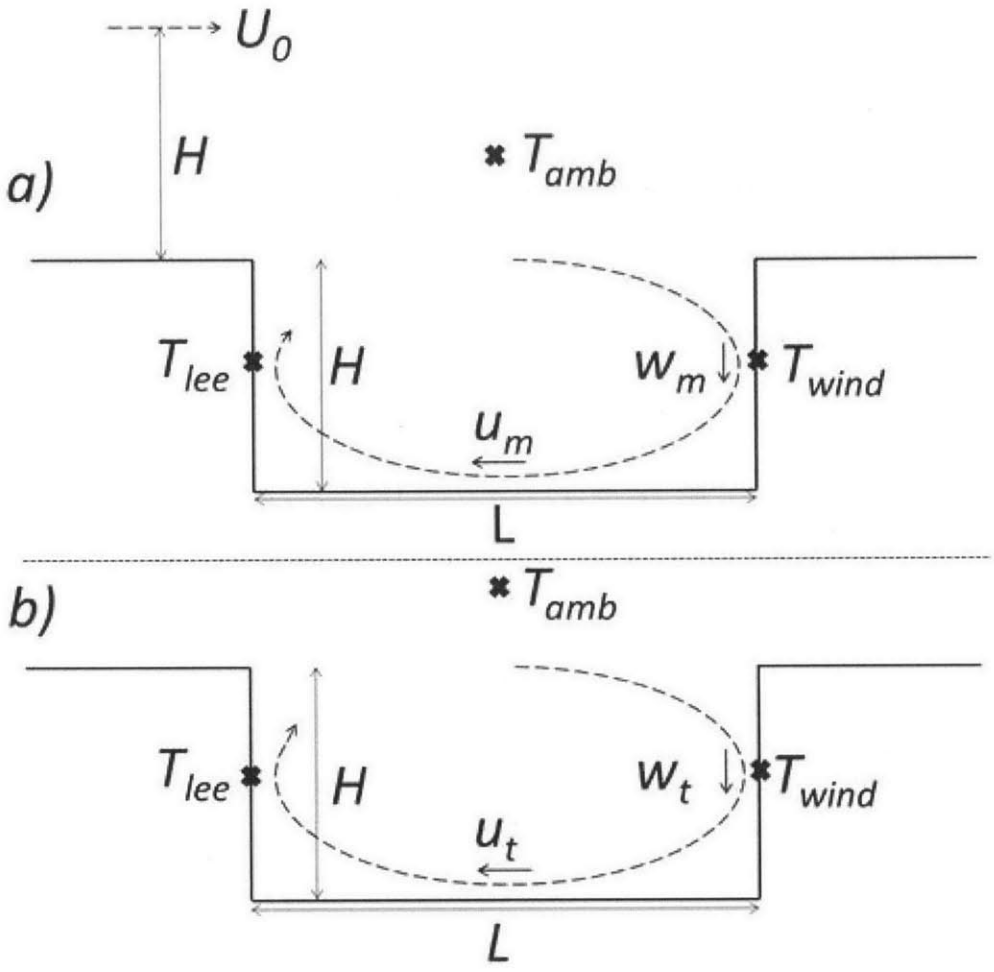

Fig 4.2 (a) Predicted flow inside the urban street canyon when the windward wall, the leeward wall and the ambient air are at an identical temperature (isothermal). (b) No free stream flow exists, and the temperature of the leeward wall is at a higher temperature than the windward wall, which is at the same temperature as the ambient air above the canyon. If the buoyancy case is added to the isothermal case, the thermal conditions assist the mechanically driven flow where two vortices are rotating in the same direction, leading to faster air speeds inside the canyon.

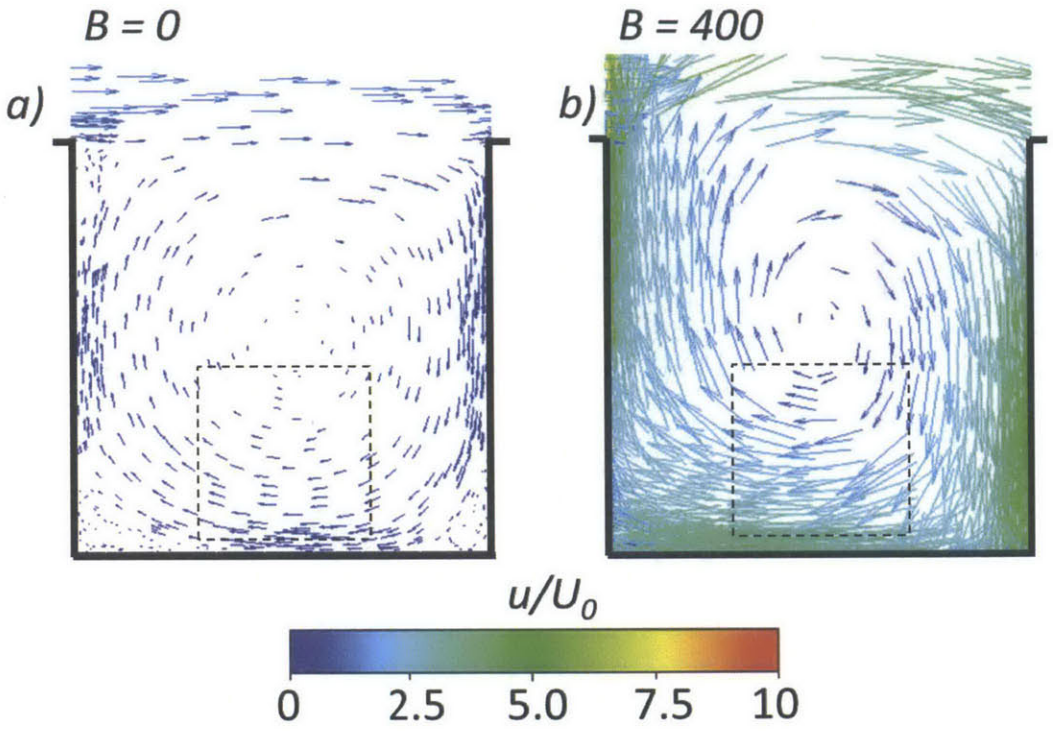

Fig 4.3 The vector field for two values of the B parameter, with the leeward wall heated in a canyon with aspect ratio 1. The region of the strong upward velocity at the heated leeward side is very thin, approximately $0.01H$. The boxes show where u is measured, from $0.1H$ up to $0.4H$ (vertically) and between $0.35L$ and $0.65L$ (horizontally).

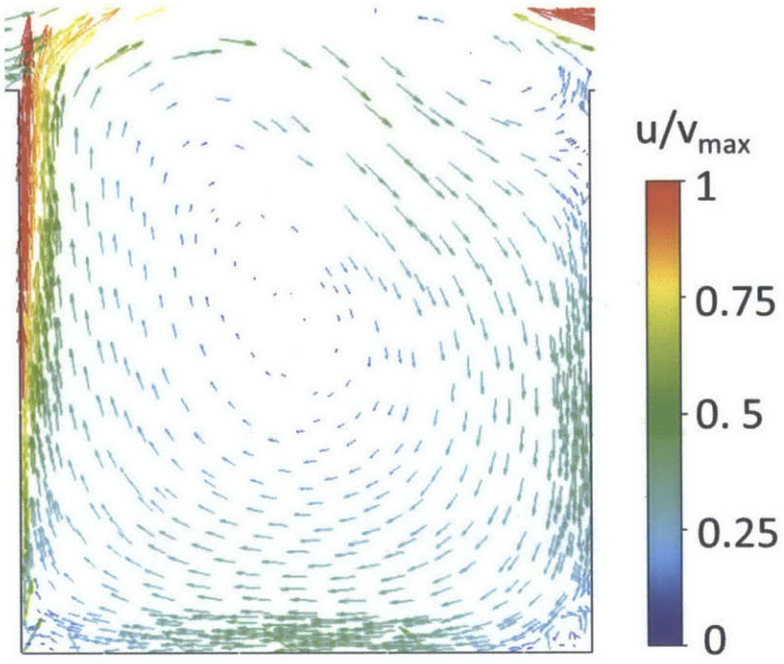

Fig 4.4 The heated left wall creates a thermally driven vortex inside the canyon of aspect ratio 1.0. v_{max} is the maximum measured velocity inside the canyon.

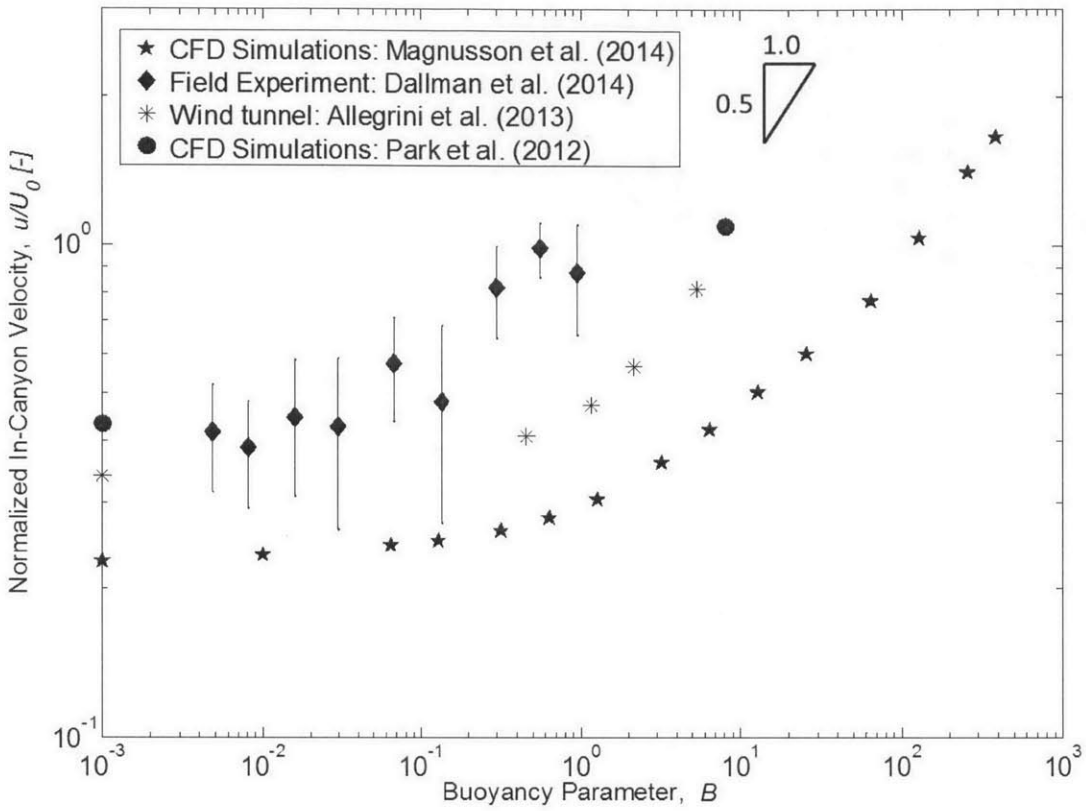

Fig 4.5 Comparison of current CFD simulations with wind tunnel data Allegrini et al. [11], field data Dallman et al. [37] and large eddy simulations results Park et al. [46]. The fit shows the $B^{1/2}$ behavior.

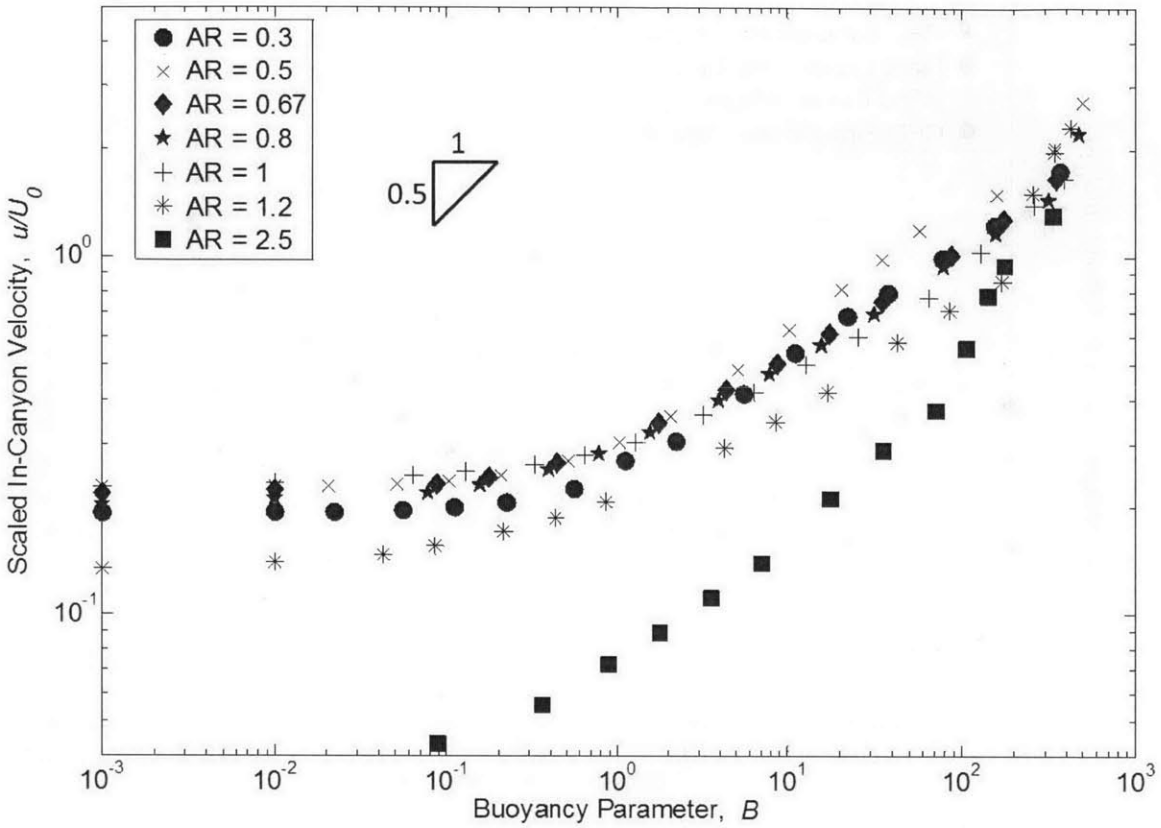

Fig 4.6 Normalized u as a function of *B* for canyons with seven different aspect ratios.

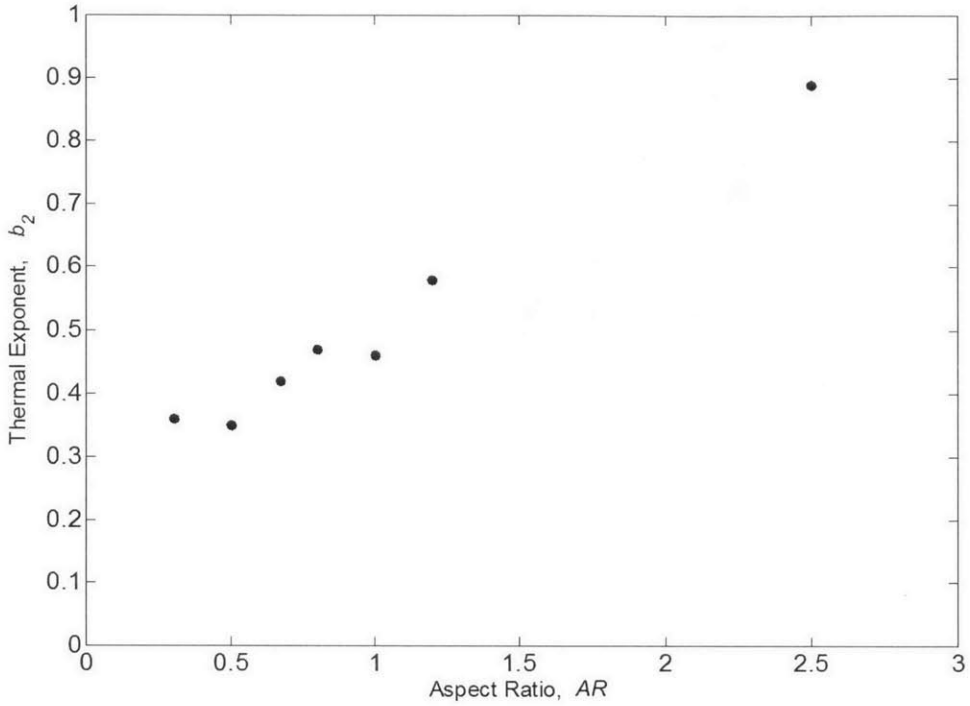

Fig 4.7 The thermal exponent b_2 from Eq. 4.4 varies with the aspect ratios of the canyons. The theoretical considerations in Dallman et al. [37] seem to hold for canyons with aspect ratios of 0.67–1.0.

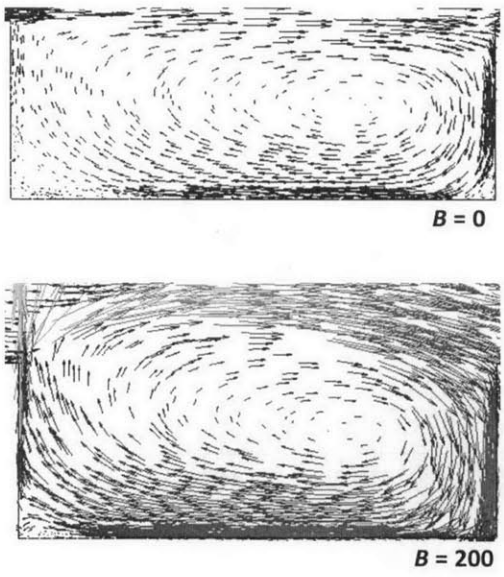

Fig 4.8 The flow structure in a canyon with an aspect ratio of 0.3.

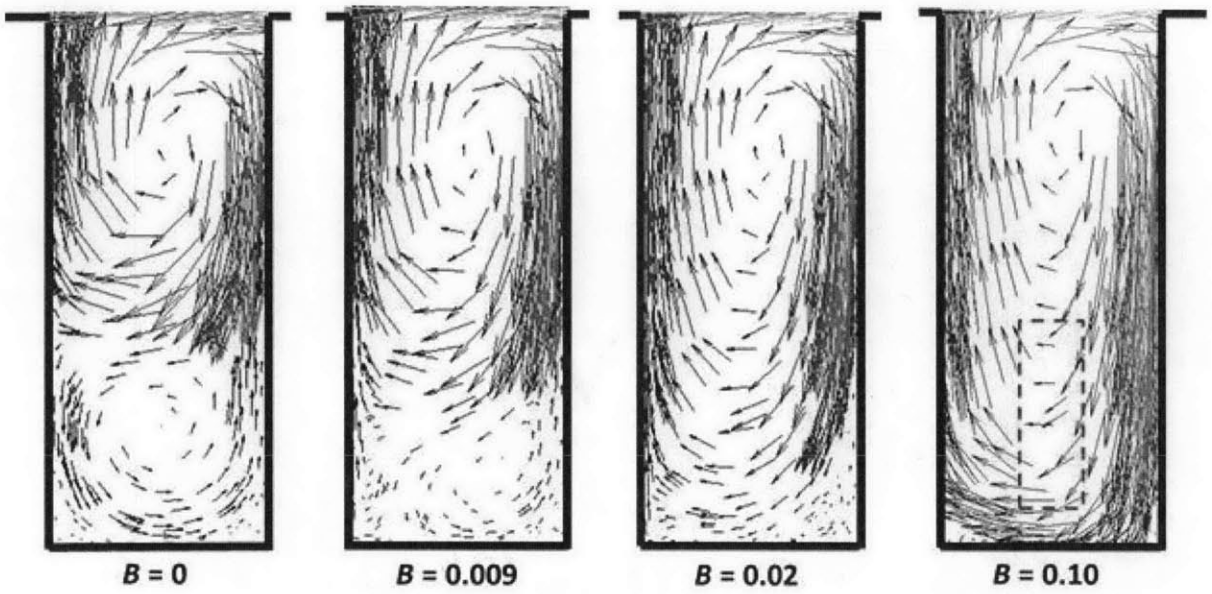

Fig 4.9 The flow structure in a canyon with an aspect ratio of 2.5.

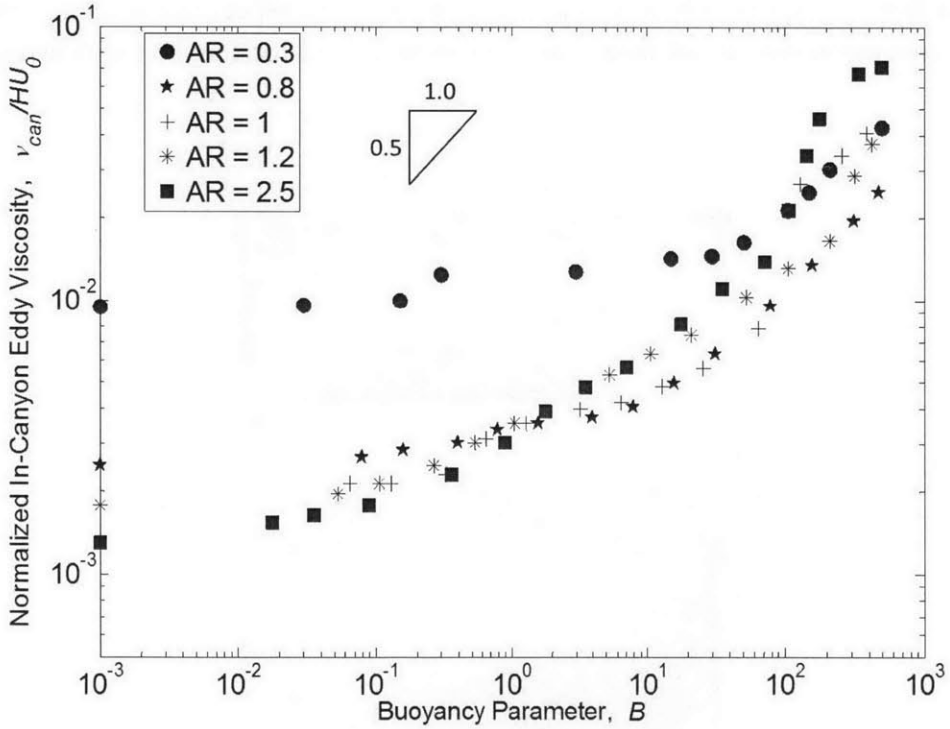

Fig 4.10 Development of the normalized v_{can} with B. The buoyancy effects are more important in determining v_{can} in deeper canyons (larger aspect ratios).

Chapter 5: Effects of Buoyant Plumes within Built Urban Environments on Human Exposure to Air Pollutants

Abstract

Local and synoptic weather conditions influence the air quality in the built urban environments. The mixing of air between the urban canopy layer and the above ambient air determines the local air quality and thus human exposure to toxic air pollutants. Human exposure to air pollutants is a factor of emission rate, population, location and time. Road vehicles and industrial facilities are the main sources for air pollution within the urban canopy layer. In this chapter the buoyancy effects on the air exchange between a single two-dimensional street canyon and the ambient air at the top interface (roof level) are considered. Exerting a buoyancy force on the urban street canyon increases the exchange of air through the entrainment phenomena described in Chapter 2. Release of a tracer within the urban canopy is added to the CFD simulations introduced in Chapter 4 and the CFD (mass balance), momentum exchange, and heat balance methods are used and compared to calculate the exchange velocity at the top interface. The base case considered in this chapter is a purely mechanically driven flow. The buoyancy parameter, B, is then used to estimate the importance of the buoyancy on the rate of air exchange between the two layers. Because human exposure to air pollutants is of an interest in this thesis, the relationship between the average residence time of an air parcel inside the canyon is found.

Introduction

The mixing of air at the roof level is a key factor in determining the air quality of the built urban environment and thus the human exposure to air pollutants. The turbulent mixing of air is a result of the fact that the average in-canyon velocity, u, is smaller (due to drag caused by the buildings) than the ambient velocity above the canyon. A shear layer is thus formed at the roof level where the mixing occurs. In this chapter the focus is set on determining the thermal effects on the air exchange rate between the ambient and in-canyon air at the roof level (top interface). The buoyancy parameter, B, (see Chapter 3) is used to classify the flow into mechanically driven, intermediate and buoyancy driven regimes and the exchange velocity, w_e, is calculated to determine the urban canyon air residence time, τ, of air inside the canyon. The motivation behind studies on the residence time of an air parcel in the built urban environment is epidemiological. Increased residence time means longer human exposure to the urban air pollutants. According to the World Health Organization (WHO [56]) 1.3 M annual deaths can be related to outdoor air pollution, which is a similar amount of deaths as that caused by road traffic accidents (1.24 M, WHO [56]). It is known that air pollution is a risk factor in, for example, lung cancer, other lung diseases and cardiovascular diseases (Vena [57], Pope et al. [58]). Pope et al. [58] show how each 10 μg m-3 increase of fine particles in the urban air lead to a 6% increased risk on cardiopulmonary and an 8% increased risk of lung cancer mortality. In a report made by The Committee on the Medical Effects of Air Pollutants (COMEAP [59]) in the UK, the mortality effects of long-term exposure to particulate air pollution in the UK were investigated. They consider the extreme case that if all

anthropogenic particulate air pollution were removed, more than 36.5 M life years would be saved over the next 106 years in the UK population alone. The current UK population is 63.2 M. Yim and Barrett [60] use the relationship between epidemiological evidence and PM2.5 concentration and conclude that approximately 13,000 premature deaths in UK are caused by UK combustion emissions and approximately 6,000 other deaths in UK are caused by non-UK European Union combustion emissions. Kumar et al. [61] show (based on Kumar et al. [62] and Gurjar et al. [63]) preliminary estimates that 1900 deaths in Delhi in 2010 can be related to exposure to traffic pollutants, which scales to about 0.31 M deaths in the Asian megacities.

Transportation of toxic materials, such as crude oil, liquefied natural gas (LNG) and other flammable and explosive liquids and compressed gases, with tank trucks, trailers and trains within urban areas has increased tremendously in the U.S. last decades because of increased production of oil and gas in the U.S. According to an Associated Press review of U.S. and Canadian accident records, at least 10 times since 2008 trains transporting oil have caused oil spills in the U.S., and most of them lead to fire explosions ([64]). During those accidents or even terrorist attacks, a vapor cloud formed by a spill of those materials can be distributed around populated urban areas. Understanding on the air flow and the rate of exchange within those areas is thus critical with respect to risk management and evacuation control.

Background

Complicated physical and chemical processes determine the air quality in the built urban environments. The emission rate of pollutants is one of the key factors determining the pollutant concentration within an urban area. The density of particles or gas compared to the density of the ambient air determines the settling rate and the concentration within the environment. Coagulation is the process whereby dispersed particles stick to each other, leading to formation of larger particles, which again leads to higher settling rate of the particles (Seinfeld and Pandis [65]). The goal of this study is only to investigate the physical and turbulence processes within the urban canopy layer and at the top interface; therefore, a passive tracer is released inside the urban canopy layer and the complex chemical processes are omitted. Detailed coverage about the chemical atmospheric processes is found in Seinfeld and Pandis [65].

Field measurements of the residence time of an air parcel in the urban environment were first performed about six decades ago (Chamberlain [66], Esmen and Corn [67], Slinn [68]). First, the goal of the experiments was to calculate the residence time at some specific location within the built environment, often the crowded downtown areas. Later, the approach became more general. Humphries and Vincent [69] performed a laboratory experiment to derive the relationship between the residence time of air trapped in the wake behind a flat plate and the characteristic variables of the flow. The deduced relationship is given by these six independent dimensionless groups:

$$\frac{U_0\tau}{H} = f\left(\frac{HU_0}{\nu}, \frac{l}{H}, \frac{k^{0.5}}{U_0}, \frac{fH}{U_0}, \frac{D_B}{\nu}\right), \quad \textbf{5.1}$$

where U_0 is the free stream velocity above the canyon (m s-1), τ the residence time (s), ν the kinematic viscosity (m2 s-1), l the eddy length scale (m), H the height of the flat plate (m), f the vortex shedding frequency (s-1) and D_B the Brownian diffusion coefficient (m2 s-1). Fackerell [70] determined with a wind-tunnel experiment on flow around two cubes that τ decreased with decreased distance between the cubes. Thus the aspect ratio can be added to Eq. 5.1

$$\frac{U_0\tau}{H} = f\left(\frac{HU_0}{\nu}, \frac{l}{H}, \frac{k^{0.5}}{U_0}, \frac{fH}{U_0}, \frac{D_B}{\nu}, \frac{H}{L}\right), \quad \textbf{5.2}$$

where L is the width between the two cubes (m). More recently, numerical simulations have been used to confirm the effects of the aspect ratio on the residence time of air (Cheng et al. [71], Simoëns et al. [72]). Richmond-Bryant et al. [73] used data from a field experiment in Oklahoma City, OK (Allwine and Flaherty [74]) to examine the relationship between the residence time and the urban boundary layer winds and urban topography. Their results support the relationship given in Eq. 5.2. In the studies mentioned above, the buoyancy force was not considered. The goal of this current study is to investigate the buoyancy effects on the mixing of air at the roof level and thus on the residence time of air in the urban street canyon.

It was shown in Chapter 4 how the air flow inside the canyon is influenced inside the canyon by performing a number of steady state CFD simulations for different B parameters of the flow. As mentioned above, the goal of this study is to investigate the

thermal effects on the exchange velocity and thus on residence time inside the urban canopy layer. The focus is set on the differential wall heating inside a two-dimensional urban street canyon.

Cheng et al. [75] performed CFD simulations on the thermal effects on the air and pollutant exchange rates in two-dimensional urban street canyons. All of the three surfaces inside the canyon were heated and the Richardson number was used to quantify the thermal effects. The results show that the air and pollutant exchanges increase with increased buoyancy intensity (larger B parameter). Kwak and Baik [76] considered the diurnal exchange of NO_x and ozone at the top interface of a two-dimensional urban street canyon. The study shows clear diurnal cycle effects on the removal of the pollutants. Photochemistry and dry deposition were included for the reactive pollutants. The turbulent fluxes at the top interface were found to be the dominant factor in removing the pollutants in the great majority of the time.

In this current study the focus will be on investigating the effects of the buoyancy force on the mixing of air at the roof level (the top interface) due only to different wall heating, which makes classification on the flow field by the B parameter straightforward. A passive scalar (tracer) is released inside the street canyon and any reactions are omitted, where the main goal is to investigate the turbulence mixing (physical process) of air in the shear layer at the top interface. The current study includes also larger buoyancy forces at the heated facades.

Methods

The goal of this chapter is to estimate the residence time of an air parcel inside an urban street canyon under differential wall heating. It is the heating of the walls that is driving the buoyancy flux inside the canyon and thus affecting the mechanical flow driven by the ambient air flow. The differential heating leads to formation of a wall plume near the heated wall. This plume rises above the top interface of the canyon, thus dispersing pollutants released inside the canyon. CFD simulations on the flow inside a single urban street canyon are performed based on the simulations from Chapter 4. In addition, a pollutant source is added inside the canyon. A tracer is released from the pollutant source at steady rate (steady mass flux). The tracer is of the same density and the ambient air. The mass flux is set such that the flow doesn't affect the flow field and the turbulence around the source. The concentration of the tracer inside the canyon is then used to calculate the exchange velocity at the top interface by applying Eq. 5.3.

Three methods have been developed and can be applied to estimate the residence time within the urban environment. The classical way to estimate the exchange velocity at the top interface of the canopy layer is to measure the mass flux and the average concentration within the urban environment and assume spatially uniformly distribution across the canyon. From the mass balance (CFD method), the following equation is obtained:

$$M = w_e(C_{can} - C_{out})L, \qquad 5.3$$

where M is the mass flux of the tracer inside the canyon (kg s-1 m-1), w_e is the exchange velocity at the roof-level (m s-1), C_{can} and C_{out} the concentration of the tracer inside the canyon and in the above ambient air respectively (kg m-3) and L the width of the canyon (m). Then the average residence time of an air parcel within the urban canyon can be calculated by the following equation:

$$\tau = \frac{(H/2)L}{Lw_e} = \frac{H/2}{w_e}. \quad \textbf{5.4}$$

where H and L are the height and width of the canyon respectively. The residence time is of an interest because it can be directly linked to human exposure to air pollutants.

For a well-mixed canyon, i.e., a uniform distribution of the scalar of interest, the air exchange rate at the top interface can be estimated using heat exchange considerations, as shown in Solazzo and Britter [51]. Assuming, that the only heat sources inside the canyon are the heated walls, i.e., omitting heat released from vehicles, occupants, etc. Under steady state conditions, the total heat flux from the walls equals the heat flux across the top of the canyon:

$$\sum q_{walls} = \rho C_p w_e (T_{can} - T_{amb}) L, \quad \textbf{5.5}$$

where $\sum q_{walls}$ is the total heat flux from the walls of the canyon (W m-1) obtained from the simulations, ρ the density of air (kg m-3), C_p the specific heat of air (J kg-1K-1), T_{can} is the in-canyon air temperature (K), T_{amb} the above-canyon ambient air temperature, L the width of the canyon (m) and w_e the exchange velocity of air in and out of the canyon (m s-1). Thus the heat flux based vertical exchange rate is:

$$w_e = \sum q_{walls} / \rho C_p (T_{can} - T_{amb}) L. \quad \textbf{5.6}$$

Bentham and Britter [77] deduced the relationship between the exchange velocity, w_e, the ambient free stream velocity, U_0, the in-canyon velocity, u, and the friction velocity, u_*, by considering the forces acting on a control volume of the fluid within the urban canopy layer. The morphology and density of the urban area are taken into the account through u and u_*. On average it is assumed that the force exerted by the surface (streets and facades) of the urban canopy layer is balanced by the momentum flux at the roof level (momentum exchange), i.e.,

$$\sigma_w A_c = \rho A_c w_e (U_0 - u), \quad \textbf{5.7}$$

where σ_w is the surface shear stress (Pa) and A_c the surface area of the canyon (m). The shear stress can be substituted by the friction velocity, $u_* = \sqrt{\sigma_w / \rho}$. Then an equation for w_e as a function of u_*, u and U_0 is obtained as:

$$w_e = \frac{(u_*)^2}{(U_0 - u)}. \quad \textbf{5.8}$$

In order to estimate the effects of the differential wall heating the following approach is used. Simulations are performed on a base case, with $U_0 > 0$ and $B = 0$ (mechanically driven flow). The differential wall heating is then taken into account by increasing a wall temperature and thus increasing the B parameter.

Results

Case A: $U_0 > 0$ and $B = 0$

The first case considered is when the flow is purely mechanically driven. A vortex is formed inside the street canyon which is driven by the free stream ambient flow of magnitude U_0. The vortex is shown in Fig 5.1. The in-canyon velocity, u, is at a lower magnitude than U_0, which leads to the formation of a turbulent shear layer at the top interface of the canyon where the turbulence mixing of in-canyon and ambient air occurs. For larger U_0, the exchange velocity of air increases and thus the residence time inside the canyon decreases. The CFD simulations show that the tracer is nearly spatially uniformly distributed inside the canyon. Thus, Eq. 5.3 and Eq. 5.4 are used to calculate the exchange velocity and the residence time of the released tracer inside the canyon. The residence time of a released tracer inside the street canyon as a function of U_0 is shown in Fig 5.2 (CFD method). U_0 increases by a factor of 30. Over this interval τ decreases by a factor of 30 and τ decreases linearly with U_0. Eq. 5.8 considers the exchange velocity as a function of u_*, u and U_0 (momentum exchange method). From the log wind profile, $u_* \sim U_0$ and $u \sim U_0$. Thus, from Eq. 5.8, $w_e \sim U_0$, which is consistent with the CFD simulations.

Case B: $U_0 > 0$, $B > 0$ (Leeward wall heated)

The heating of the leeward wall creates a plume near the wall which influences the air flow inside the canyon and thus the air exchange at the top interface. The increased in-canyon velocity is shown in Fig 5.3. It shows also how the vortex extends above the roof level when the leeward wall is heated. The CFD simulations were performed under

steady-state conditions. To extract the thermal effects on the residence time of air inside the canyon, the heated case is compared with the mechanically driven flow. First, the flow of the wall plume near the leeward wall is considered. Under these circumstances the tracer is nearly spatially uniformly distributed across the canyon, thus Eq. 5.3 is used to calculate the exchange velocity (CFD method) and Eq. 5.4 to calculate the average residence time of air inside the canyon. The dimensionless residence time ($\tau U_0/H$) is shown as a function of the B parameter in Fig 5.4. When the B parameter of the flow is less than 0.1, τ is near constant, but decreases when the B parameter is larger than 0.1. When the B parameter has reached 50, τ decreases as a function of B raised to the power of -0.5, which is identical to the development of the in-canyon velocity increase by B introduced in Chapter 4. Calculations on the residence time based on the momentum exchange method (Eq. 5.8) and the heat flux method (Eq. 5.5) are also shown in the plot. The results show a good consistency between the methods. These two latter methods are thus considered to be relevant to calculate the air exchange rate between the urban canopy layer and the above ambient air.

The re-circulation of air parcels inside the canyon gives an estimate of the efficiency of the shear layer in dispersing pollutants out of the canyon at the top interface. It is calculated by estimating the ratio of mass flux of tracer flowing up in the vortex versus mass flux of the tracer flowing down in the vortex formed inside the canyon. It thus estimates the amount of tracer removed from the canyon during each circulation of an air parcel traveled within the canyon Fig 5.5 shows the re-circulation ratio as a function of the B parameter. When the B parameter of the flow is less than 0.1, the ratio is 98%,

which means that on average 2% of the tracer is dispersed out of the canyon around each circle. The re-circulation ratio then decreases and when the B parameter is 250, the re-circulation ratio is about 0.75. This decrease clearly shows how the buoyant plume formed near the leeward wall increases the exchange rate at the top interface.

Human exposure to air pollutants is an important factor in determining the quality of life in urban areas (breathability). Turbulence (eddy) viscosity is a measurement of the transfer of momentum in the flow. The magnitude of turbulence viscosity inside the canyon, v_{can}, indicates the amount of mixing between in-canyon air and the above ambient air and thus the ability of the flow the remove pollutants from the canyon. v_{can} inside the canyons is shown in Fig 5.6, with the mass fraction of the tracer inside the canyon. The results show that v_{can}/U_0H increases with increasing B parameter. It also shows how the magnitude of the eddy viscosity can be used to estimate the ability of the environment to disperse pollutants. The importance in including thermal situations when simulating air quality in urban areas is also clear from the figure.

Case C: Windward Wall Heated (Counteracting Flow)

The third case considered is when it is the windward wall that is heated. In that case the buoyancy force near the heated wall is working in a different direction compared with the downwards mechanical force at the windward wall. The flow fields obtained inside the canyon for three different buoyancy cases are shown in Fig 5.7. For mechanically driven flows ($B = 0.13$) the flow at the windward wall is downwards so the mechanical force is larger than the buoyancy force and a single vortex is formed inside

the canyon. When the buoyancy is increased and the flow is still in the intermediate regime (B = 13.0), the buoyancy force and the mechanical force at the windward wall are at the same magnitude. The vortex shrinks in volume and another smaller one has been formed near the windward wall. Under this buoyancy level we obtain flux outside of the canyon at the windward wall. When the buoyancy level is increased further and the flow is sufficient to be considered buoyancy driven (B = 130) the small vortex near the windward wall has disappeared and the buoyancy force at the windward wall is dominant. Again, the flux inside the plume and thus the air flow out of the canyon increases by B raised to the power of 0.5 when the flow is buoyancy driven. As we can see in Fig 5.7 we obtain two vortices inside the buoyancy driven canyon. The flow near the wall does not affect all parts of the canyon directly and thus ventilates only part of the canyon.

Under those conditions Fig 5.8 shows how the buoyancy driven plume at the windward wall flows directly out of the canyon and the mixing of released heat from the heated wall into the canyon is limited. Where neither the in-canyon air temperature nor the tracer is spatially uniformly distributed across the canyon the methods introduced in Eqs. 5.3 and 5.5 are not applicable. However, the turbulence viscosity inside the canyon is an indicator of the dispersion of pollutants out of the canyon. Fig 5.9 shows the development with B for the case of a windward heated wall. When the flow is buoyancy driven, v_{can}/U_0H increases with B raised to the power of 0.25 compared to 0.5 when it is the leeward wall which is heated. The increase in in-canyon air temperature is negligible for this case.

Conclusions

The CFD simulations have shown that increased buoyancy inside the urban street canyon increases the turbulent mixing of air at the top interface of the two-dimensional urban street canyon and thus increases the dispersion of pollutants. This result interests architects and urban planners and gives an estimate on the trade-off between the increased in-canyon air temperature and air quality within the built urban environments. The increase in air temperature increases the thermal stress on the inhabitants and the energy demand for cooling of buildings. Fig 5.10 shows the trade-off between in-canyon temperature increase and the reduction of pollution inside the canyon when it is the leeward wall which is heated. It shows a rapid decrease (80%) in pollution concentration when the temperature difference between the in-canyon air temperature and the ambient air temperature is only about 2 K. When the air temperature difference increases further the decrease in pollution concentration does not decrease dramatically. One might argue that a 2 K increase in in-canyon temperature is justifiable because of the tremendous decrease in in-canyon pollutant concentration. For the windward wall heated case the local in-canyon air temperature does not increase at all where the heated wall plume is just near the wall but heating the windward wall is less effective in removing pollutants from the urban canyons (considering the turbulence viscosity). The street orientation and the choice of building façade materials can thus affect the air exchange and thus the residence time of air inside the urban environment. The next chapter focuses on the effects of horizontal advection on the exchange of tracer between the adjacent street canyons.

Figures

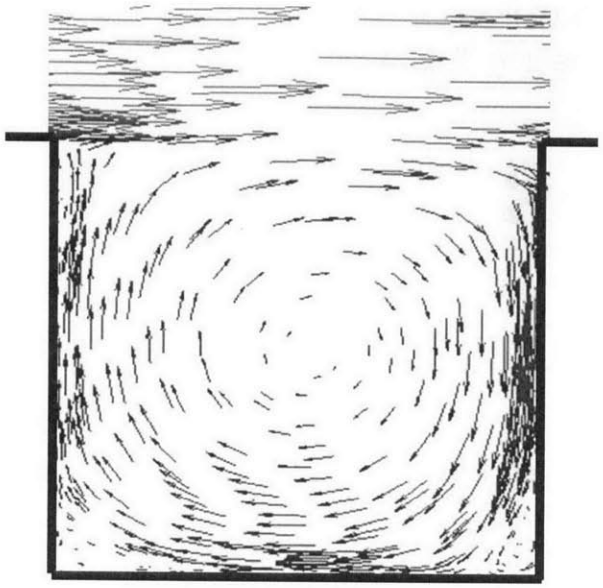

Fig 5.1 The vortex inside the street canyon is driven by the free stream ambient velocity above the canyon (mechanically forced flow). The mixing of air occurs at the top interface, i.e., in the turbulent shear layer.

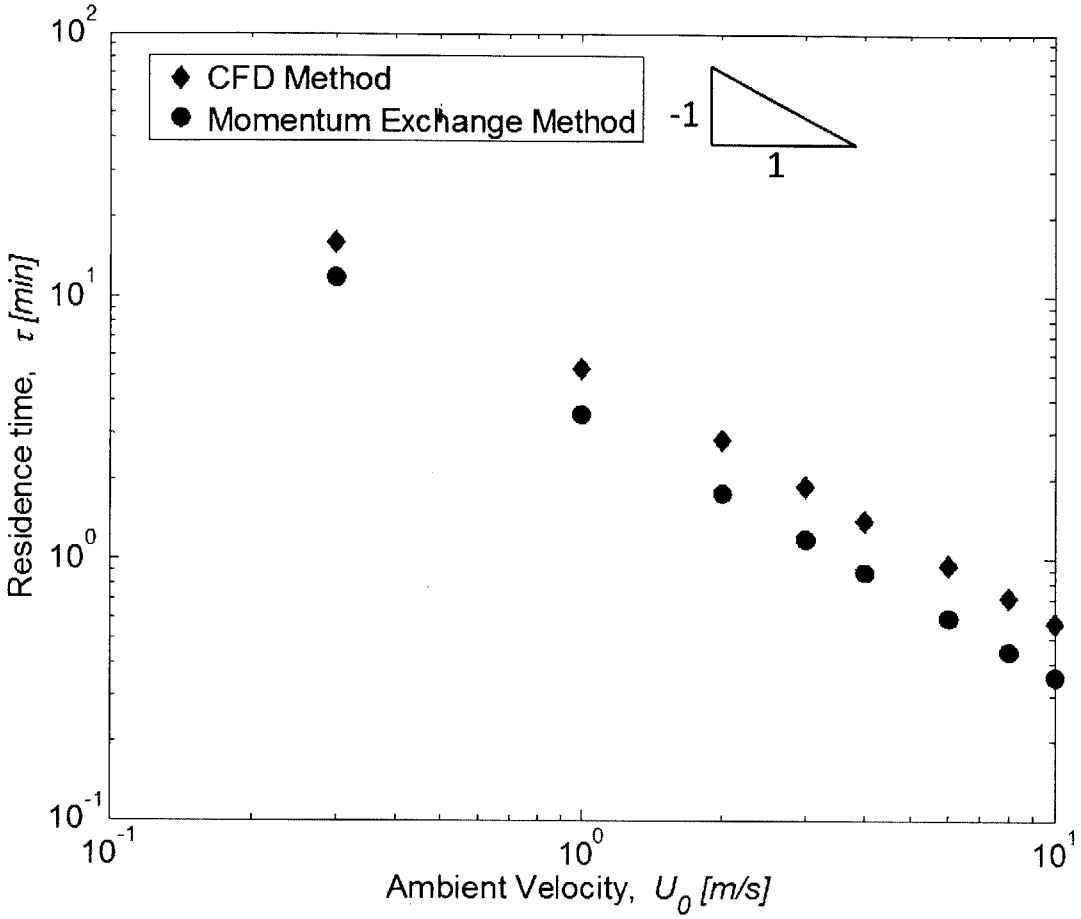

Fig 5.2 The residence time inside a two-dimensional urban street as a function of U_0. The flow is purely mechanically driven. The residence time decreases linearly with the ambient velocity, U_0.

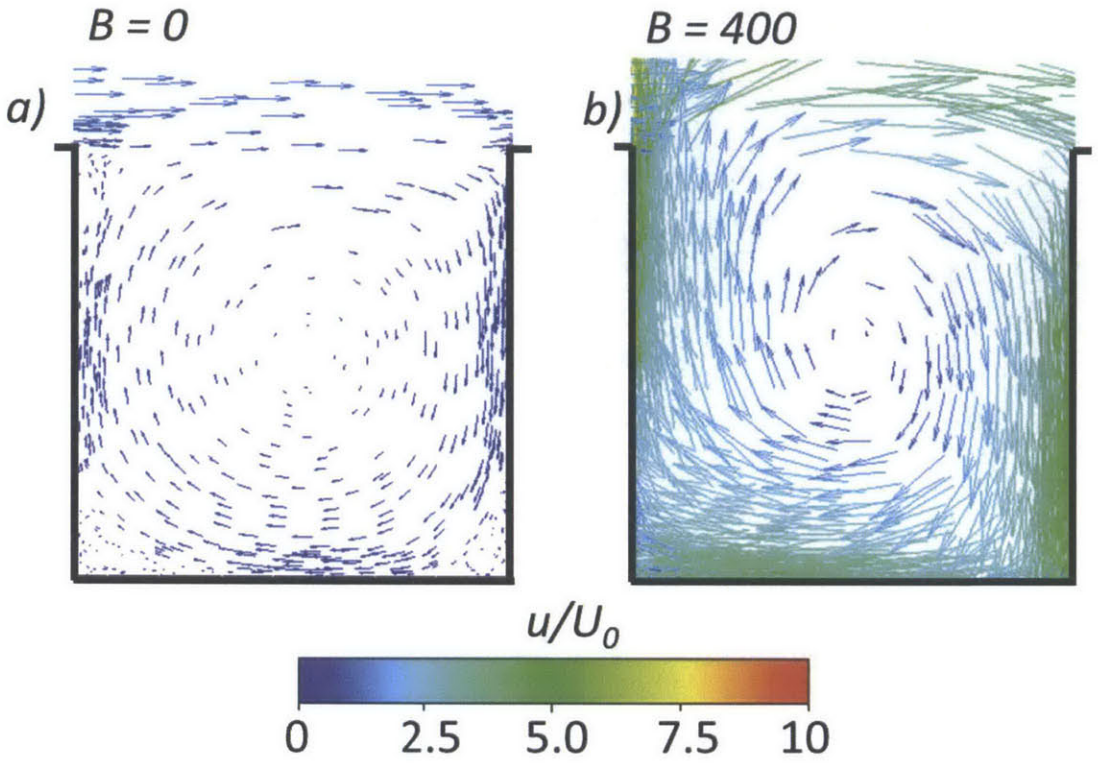

Fig 5.3 The flow structure inside a) a purely mechanically driven canyon, and b) a canyon with the leeward wall heated.

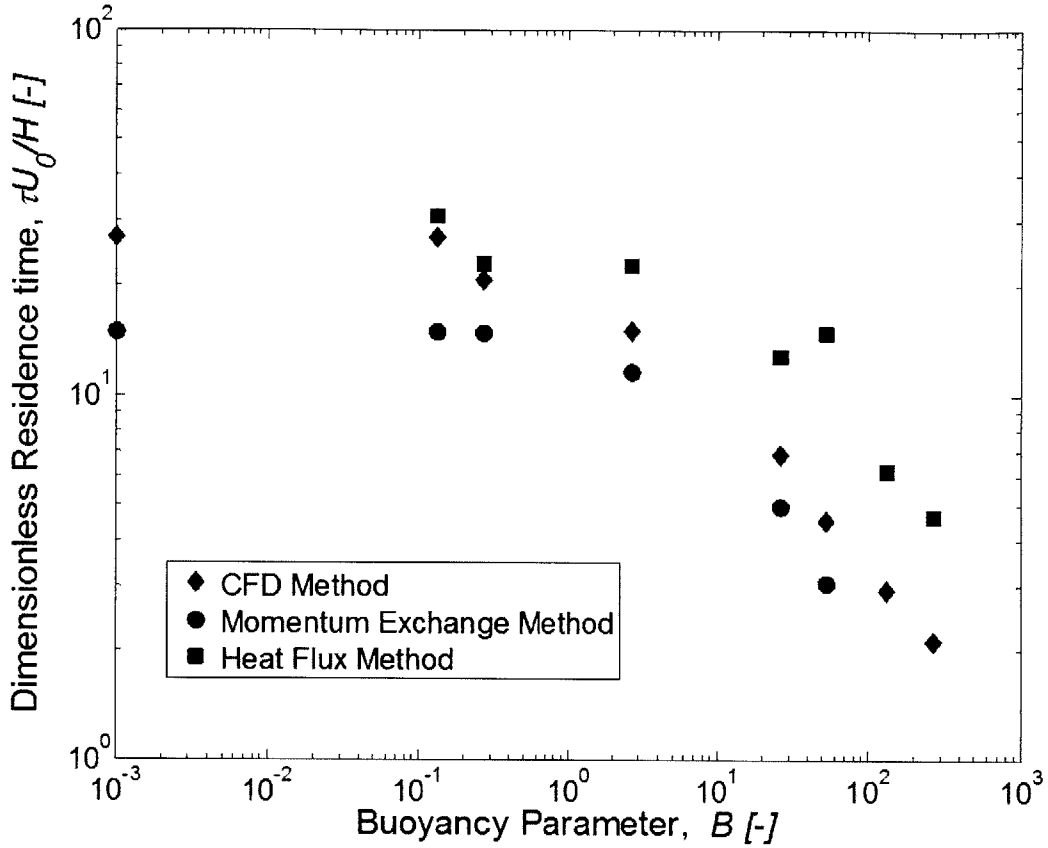

Fig 5.4 The dimensionless residence time inside the canyon as a function of the buoyancy parameter, when it is the leeward wall which is heated.

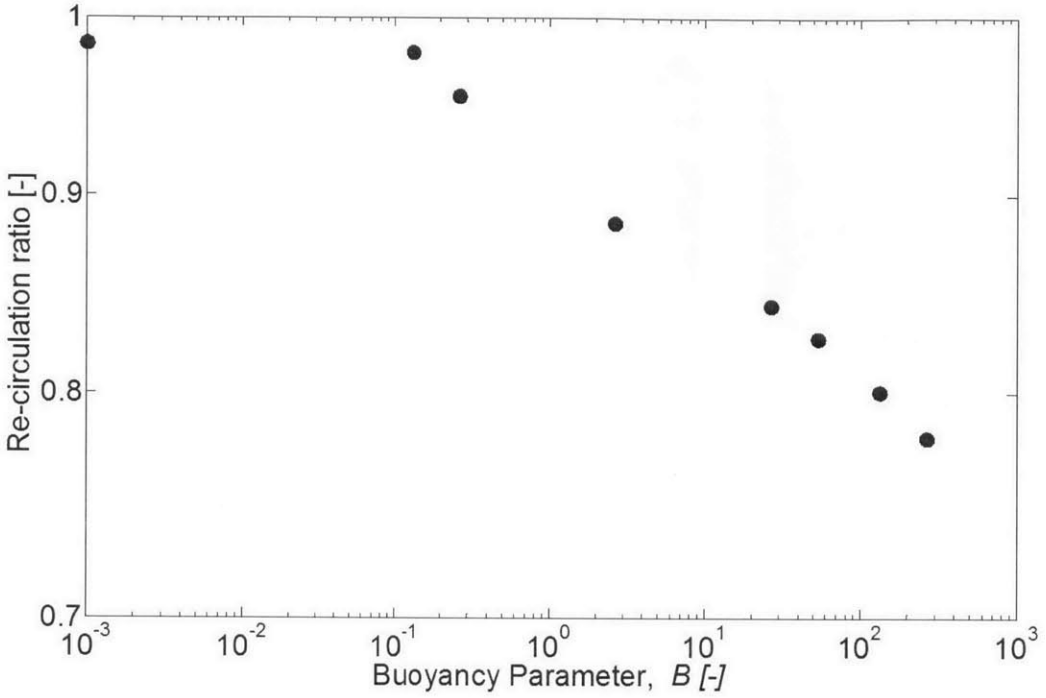

Fig 5.5 The re-circulation ratio of particles as a function of the *B* parameter.

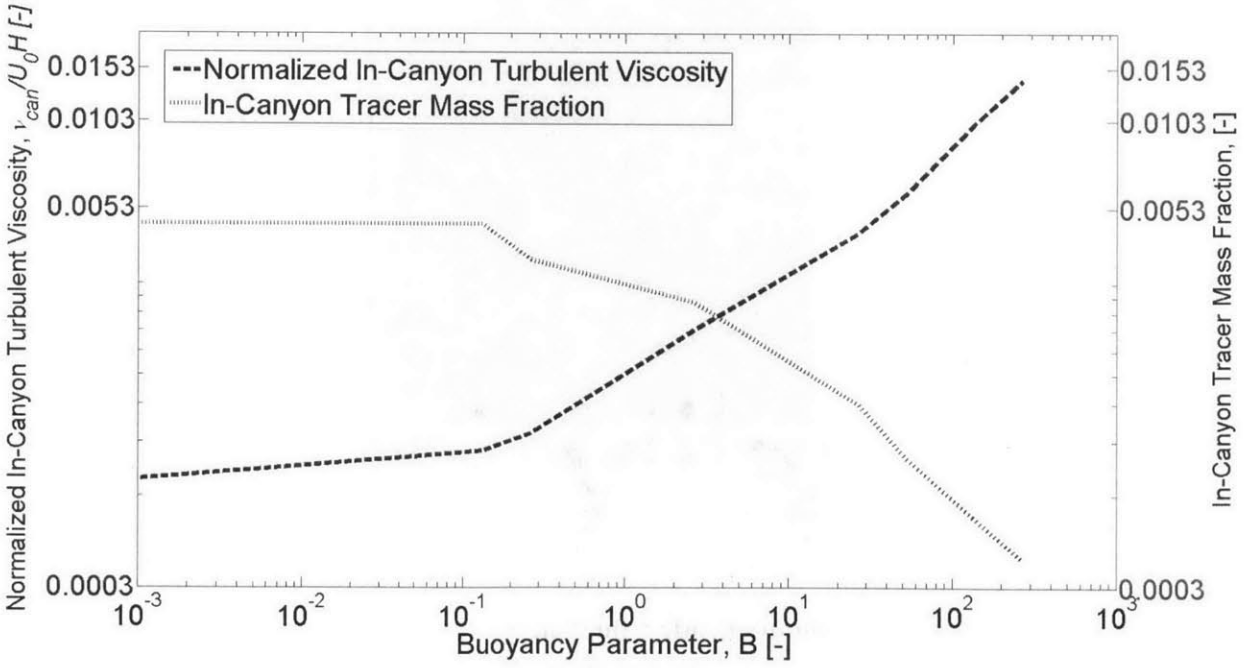

Fig 5.6 The relationship between the in-canyon tracer mass fraction and the normalized in-canyon turbulence viscosity as function of *B*.

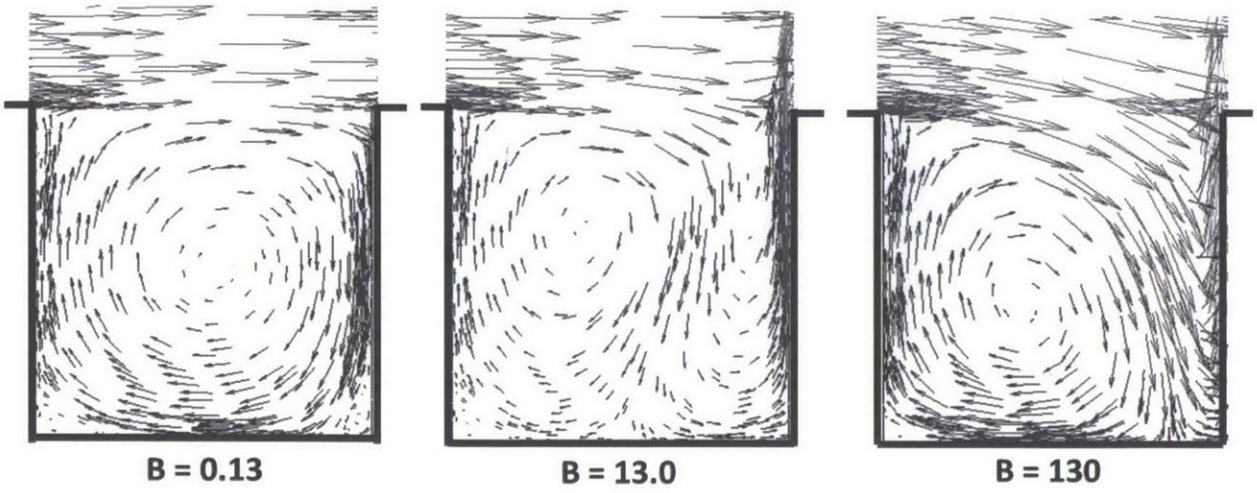

Fig 5.7 The flow field inside the canyon for three different buoyancy levels, when the windward wall is heated.

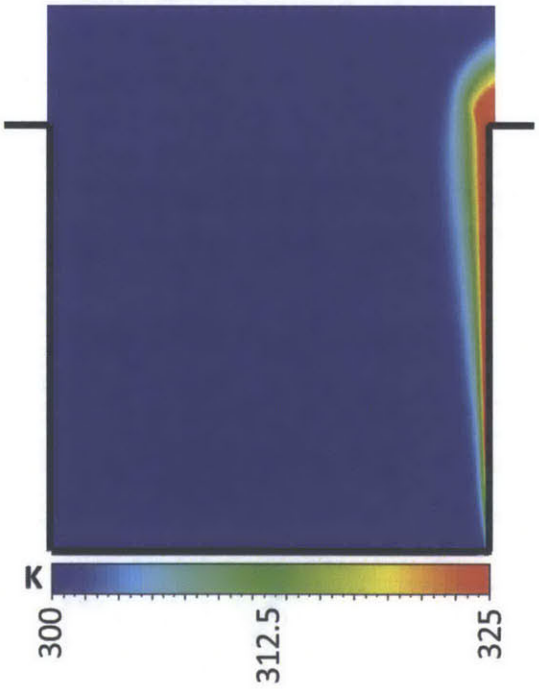

Fig 5.8 The temperature contours inside a buoyancy driven canyon with the windward wall heated (B = 130).

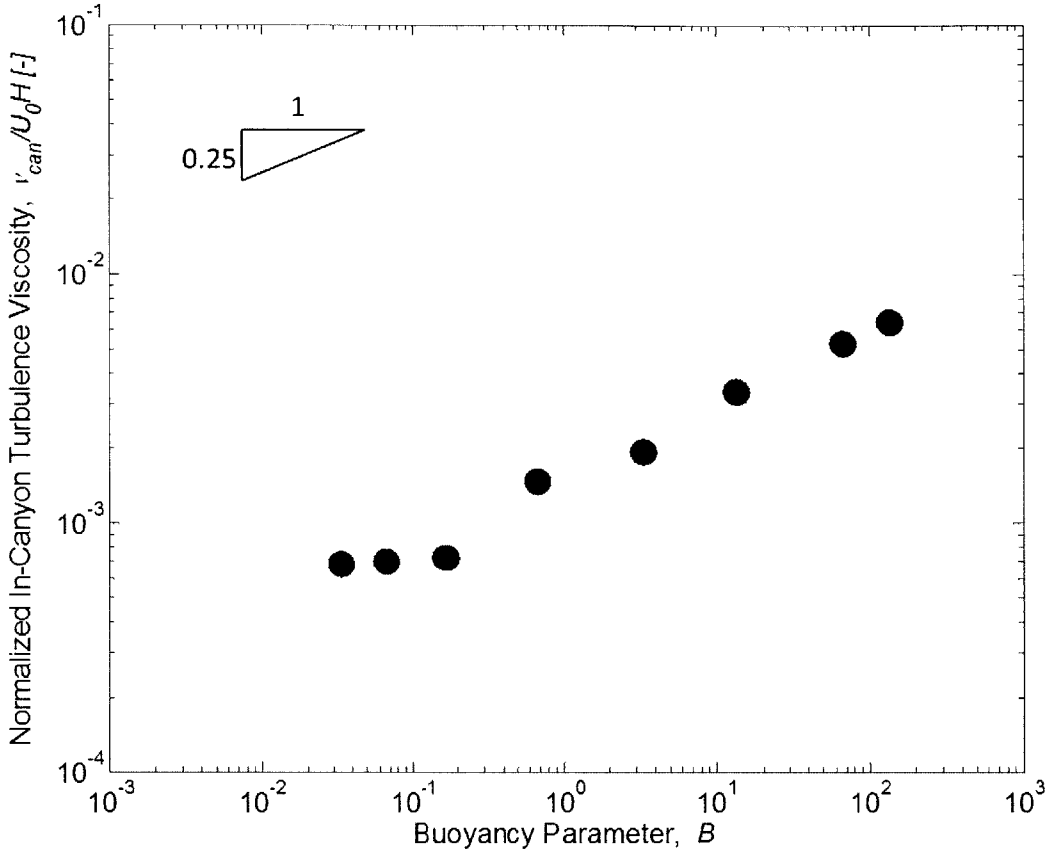

Fig 5.9 The normalized in-canyon turbulence viscosity as a function of B when the windward wall is heated. v_{can} is an indicator of the ability of the flow to disperse pollutants out of the canyon.

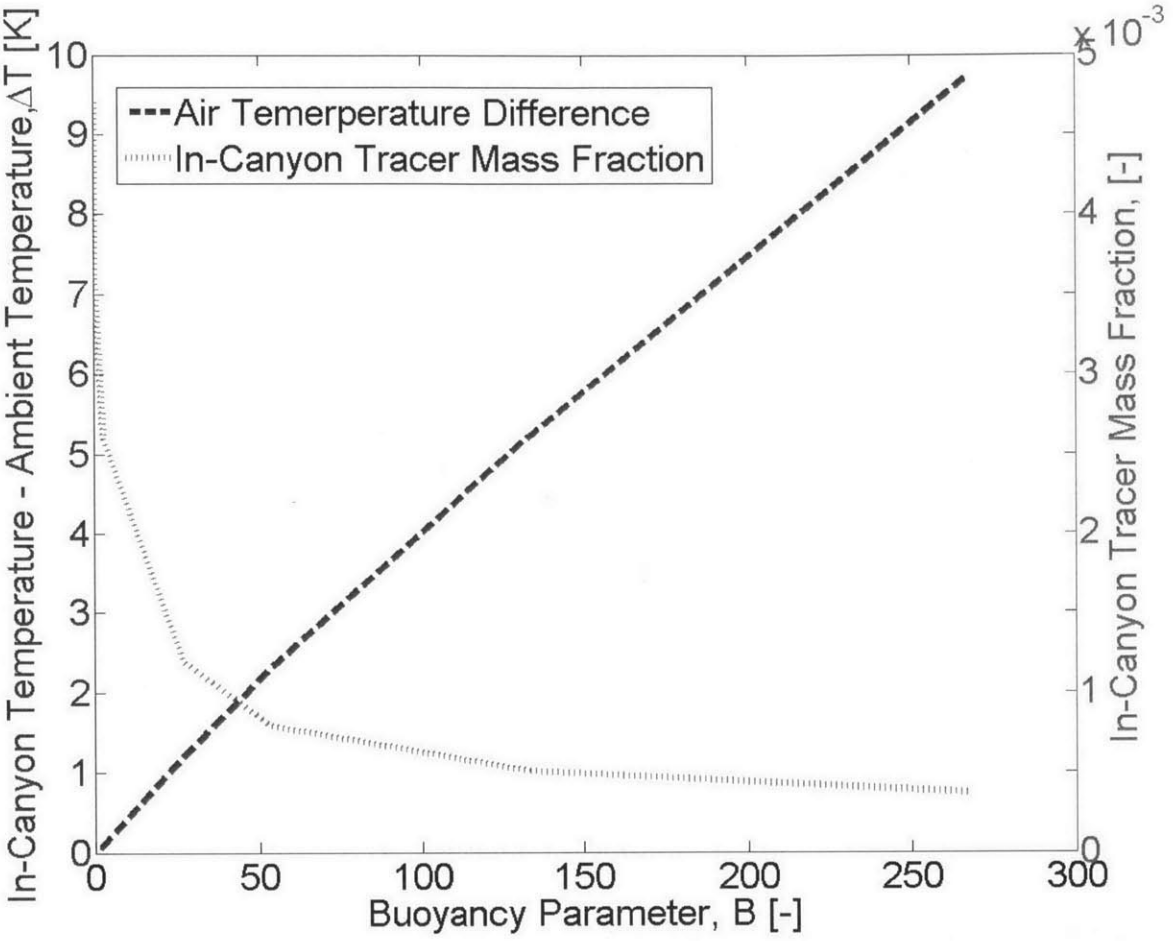

Fig 5.10 The difference in in-canyon temperature and ambient air temperature and the in-canyon tracer mass fraction as a function of the parameter. The leeward wall is heated.

Chapter 6: Effects of Horizontal Advection on Mixing of Air Pollutants in the Built Urban Environments

Abstract

Increased urbanization leads to larger and denser cities which have raised public health concerns due to increased human exposure to air pollutants. Horizontal transport of air pollutants is one factor that affects the air quality within the built urban environments. In general, the main sources of air pollutants within the built urban environment are burning of fossil fuels in vehicles and industrial facilities. Chemical accidents and even chemical terrorist attacks are also risk factors because of increased transport of hazardous materials with trains or trucks near or within urban environments. This study focuses on the transport, mixing and exchange of air pollutants between ten adjacent two-dimensional urban street canyons. Computational Fluid Dynamics (CFD) simulations are applied to simulate the flow in the ten street canyons. Four steady-state cases are considered where the density of the released pollutants is varied between the simulations.

Introduction

Energy and material consumptions and vehicular transportation within urban areas affect the air quality. Most cities have developed and are developing on an industrial basis which leads to concentration of power plants, industrial facilities and other manufacturing enterprises which emit pollutants. The US Environmental Protection Agency (EPA [78]) has defined the six most common air pollutants that can harm human health and cause damage to the environment: ozone (O_3), particulate matter (PM), carbon

monoxide (CO), nitrogen oxides (NO_x), sulfur dioxide (SO_2) and lead (Pb). The first four of these pollutants can be directly linked to human activities in urban areas and the last two pollutants are also common in urban areas due to their emission from airports, power plants and industrial facilities.

The increased urbanization around the world in recent decades and the prediction that the same development will continue increases the public health risk in urban areas. The urbanization has been more rapid than the promising technology improvements that are being developed to reduce the amount of pollutants in the air. A recent study (Lamsal et al. [79]) that NO_2 concentration increases by a factor of two to five when the population increases from 1 million to 10 million people. The range depends on the location of the city. The number of people living in urban areas in the developing countries is increasing rapidly (United Nations [1]). The infrastructure in those countries is hardly prepared for this rapid urbanization. For example, coal accounts for 70% of the energy mix in China (EIA [78]) against 40% in the USA (Energy and You [81]). Access to health services for the inhabitants in the developing countries is limited, which can lead to greater impacts of air pollutants on the public health than in the developed countries.

In this chapter the goal is to estimate the role of horizontal transport of pollutants within the built urban environments. CFD simulations are performed to simulate the flow and estimate the concentration of air pollutants in canyons with a nominal aspect ratio of unity.

Background

The most obvious effects of horizontal transport (advection) of pollutants are the transport of fine particulate matter from wildfires and the transport of ashes from volcano eruptions. For example, wildfires in Quebec, Canada, in May 2010 affected the air quality in the New York and New England areas ([82]), and recent wildfires in Indonesia led to record levels of hazardous air pollution in Singapore and Malaysia, where the smog was transported horizontally by the synoptic wind ([83]). The volcano eruption in Eyjafjallajokull in Iceland in 2010 affected the air quality and air traffic in Europe due to transport of fine ash from the volcano (Flentje et al. [84]). Another aspect of advection is the thermal effects from upstream land uses on the downstream conditions (urban heat advection). Measurements in Baltimore, MD (Zhang [85]) and De Bilt in the Netherlands (Brandsma et al. [86]) show increase in air temperatures when the wind direction is from other surrounding towns or built urban environments.

In this chapter the focus is on the horizontal transport of pollutants on a smaller scale, i.e., within the urban environment. Belcher [87] reviews the important fluid dynamics processes which determine the dispersion of pollutants at the neighborhood scale (1–2 km). At that scale turbulent mixing and mean flow transport control the transport and dispersion of pollutants. Several studies, both field and computational, have been performed on this issue in real urban environments.

Field tracer experiments in Birmingham, UK, were performed by Britter et al. [88] to investigate the pollutant dispersion in a real urban area. The released tracer was sampled in air bags distributed downstream from the tracer release. The experiments

show a rapid rise but a slow decrease in concentration of constituents in canyons downstream of the release canyon. The maximum measured concentration was comparable with results obtained from Gaussian plume models (Seinfeld and Pandis [65]). Another urban tracer dispersion experiment was performed in London, UK, in 2004 (Martin et al. [89]) where the goal was to predict the decay in pollution with respect to distance from the pollutant sources. The measured concentration was compared with three screening dispersion models, which showed the models can give reasonable upper-bound estimates for the maximum measured concentration. More field experiments that concentrate on pollutant dispersion in real environments have been conducted, for example, in New York, NY (Allwine [90]), Salt Lake City, UT (Allwine [91]) and Oklahoma City, OK (Overview of Joint Urban 2003[92]).

Urban air quality modeling assessment have traditionally been performed within operational models that are bulk-integrated, such as OSPM (Berkowicz [93]), AERMOD (AERMOD [94], Cimorelli [95], Perry [96]) and ADMS-urban (Carruthers [97]). More recently CFD has been applied to the problem. Sabatino et al. [98] performed CFD simulations (FLUENT) on pollutant dispersion within idealized urban-type geometries (3D) and compared the results with the atmospheric ADMS-urban dispersion model. The two approaches show similar concentration fields. Hanna et al. [99] applied five CFD simulations models on an area around Madison Square Garden (3D) in Manhattan, NY, and compared their performance in simulating atmospheric flow and dispersion of pollutants. The five models used were CFD-Urban (Coirier [100], JP2.11 [101]), FLACS (Hanna et al. [102]), FLUENT-EPA ([103]), FEM3MP (Gresho and Chan [104], Calhoun

[105]) and FEFLO-Urban (MUST [106], Camelli [107]). The results indicate that all the five models are qualitatively similar.

What makes research on the dispersion, mixing and transport of pollutants in urban areas challenging is the fact that local configurations and geometries of the street canyons affect the air flow. Our goal is to investigate the advection effects generally. The simplest and most generic way to do so is to simulate the flow in two dimensions where the synoptic wind is perpendicular in urban street canyons with infinite length in the span-wise direction. Such simulations are limited in some ways, such as omitting the double-eddy circulation (Biak and Kim [108]) and 3D lateral and secondary flows (Hunter et al. [109], Leitl and Meroney [110]). In 2D the one and only way for a pollutant to be transferred between adjacent street canyons is through mixing of air and pollutants at the roof level.

Chapter 5 shows how the buoyancy forces created inside an urban street canyon affect the amount of mixing between in-canyon air and the above ambient environment. The atmospheric instability created inside the canyon due to heating of the surfaces is thus a key factor in determining air quality inside the urban canopy. The atmospheric conditions inside the urban canopy layer can be evaluated by calculating the Richardson number, $Ri = -\frac{g'H}{U_0^2}$, where g' (m s-2) is the reduced gravity, $g' = g\frac{\Delta\rho}{\rho_0}$, $\Delta\rho$ the density difference (kg m-3) and ρ_0 the density of the ambient fluid (kg m-3). The temperature of buildings facades and streets impacts the air temperature within the built urban environment. During warm sunny days the facades are heated and due to the fact that

buildings' materials have higher heat capacity than ambient environments the thermal effects are often largest during nights. During cold days and especially after snowfall the urban facades can be colder than the above ambient air which leads to atmospheric stability within the urban canopy layer, which is the worst case for air pollutants to disperse out of the urban environment.

Methods

The computational domain is shown in Fig 6.1. The free stream velocity (synoptic wind) is characterized by horizontal velocity U_0 perpendicular to the ten adjacent urban street canyons (normal to their axis) being simulated. U_0 is measured at $1H$ above the street canyons Inside each canyon there is a pollutant source located centrally in-between the walls ($L/2$), $0.035H$ above the street of the canyon where H is the height of the canyon and L is the length of the canyon. The domain height above the canyons and the upstream and the downstream lengths are $10H$.

The finite volume (Appendix 2) CFD code ANSYS FLUENT 13.0 is used in this study. The standard k-ε turbulence closure (Appendix 3) is used to solve the Reynolds-averaged Navier-Stokes (RANS) equations and the advection-diffusion module to compute the diffusive of mass flux. The transport equations for the turbulence kinetic energy, k, and the rate of dissipation, ε, can be found in the ANSYS Theory Guide [53]. Our goal is to establish the role of the advection term and upstream air quality conditions in determining the air quality in the downstream canyons under steady state conditions in a generic way. Thus, it is concluded that the RANS model with a k-ε closure is sufficient

to achieve the goals. Salim et al. [111] compared results on atmospheric pollutant dispersion in an urban street canyon between RANS, large eddy simulations (LES) and wind tunnel measurements, and found that the steady-state RANS turbulence models gave qualitative agreement to the wind tunnel measurements.

The mechanical boundary conditions are the following at the inlet: the wind velocity, turbulent kinetic energy and turbulent dissipation rate profiles are defined as in Richards and Hoxey [54]

$$U(z) = \frac{u_*}{\kappa} ln\left(\frac{z+z_0}{z_0}\right), \quad \textbf{6.1}$$

$$k = \frac{u_*^2}{\sqrt{C_\mu}}, \quad \textbf{6.2}$$

$$\varepsilon(z) = \frac{u_*^3}{\kappa(z+z_0)}, \quad \textbf{6.3}$$

where z (m) is the height above the ground, u_* the friction velocity (m s1), κ the von Karman constant (0.40), z_0 the roughness length as before (m), z the height above canyons (m) and C_μ a constant in the standard k-ε model. The outlet is defined as a pressure outlet with a zero gauge pressure. The top boundary is defined as a wall with no shear stress. The upstream and downstream roofs, the streets and the walls are defined as smooth walls with no slip shear conditions.

The mesh tool provided by the Ansys Fluent Workbench is used for generating the mesh. The cells are quadrilateral with sides $0.01H$ to $0.03H$. Smaller grid sizes are defined near the surfaces of the computational domain, while larger grid sizes are

permitted at some distance away from the surfaces (Ansys [53]). The grid cells expand from the surfaces with an expansion factor of 1.05. Adequate sensitivity experiments were performed to ensure that the computational domain does not bias the results.

The mass-flux (0.2 kg m-2s-1) of released tracer is defined as a mass-flow inlet boundary for the ten sources. The mass-flux was chosen such as that did not affect the flow inside the canyon. The advection-diffusion module is used to model the dispersion of the pollutants. The general form of the conservation equation given in Ansys [53] is

$$\frac{\partial}{\partial t}(\rho Y_p) + \nabla \cdot (\rho \vec{v} Y_p) = -\nabla \cdot \vec{J}_p, \qquad \textbf{6.4}$$

where Y_p is the mass fraction of species p, ρ the mixture density (kg m-3), $\vec{J}_p$ the mass diffusion flux of species p (kg s-1) and $\vec{v}$ the velocity vector (m s-1). For turbulent flows, the mass diffusion flux of species p is calculated in Fluent as

$$\vec{J}_p = -\left(\rho D_p + \frac{\mu_t}{Sc_t}\right) \nabla Y_p, \qquad \textbf{6.5}$$

where D_p is the diffusion coefficient for species p in the mixture, μ_t the turbulent viscosity (m2 s-1) and Sc_t the turbulent Schmidt number.

The shear stress between the ambient free stream flow above the street canyons and the in-canyon air drives a circulation (vortex) inside the canyon. The turbulence at the roof level is high and mixing of air between ambient air and in-canyon air occurs.

Results and Discussion

The CFD simulations can provide insight into the role of advection and air pollution dispersion within an urban area. In order to isolate other effects, uniform conditions within the urban environment with respect to geometric configurations, buoyancy level and tracer mass-fluxes are assumed. Fig 6.1 shows the computational domain and how the pollution is calculated. Tracer is released in each canyon and they are tracked downstream. The figure shows how the tracers aggregate in the downstream canyons. To take one example, $C_{4,6}$ is the tracer concentration in canyon 6 due to the tracer released in canyon 4. This method evaluates the aggregation of air pollutants and also tracks the location of the origin source. The problem is simulated for four Richardson numbers; one neutral (Ri = 0) case and three cases under unstable atmospheric conditions (Ri = -1.9, -3.7, -37)

First, the flow structure inside the canyons for the four cases is considered. Fig 6.2 shows the flow field inside canyon 5 for the four cases as an example. The size of the vectors indicates the strength of each vortex. The released material has neutral buoyancy and does not affect the flow inside the canyon. The vortex is central in the canyon and its height is equal to the height of the canyon. The released pollutants are thus mixed in and out of the canyon at the roof level. When the density of the tracer is decreased the air speed inside the canyon increases as well. The mechanical flow still creates a vortex inside the canyon through the shear stress above the canyon. The mechanical flow transports the pollutants towards the leeward wall where it affects the speed of the flow through buoyancy which causes the height of the vortices to rise above the canyon. The

mixing of pollutants is thus not only due to shear stress at the roof level, as for the neutral case, but rather the bulk flow at the leeward wall transports some amount of the pollution out of the canyon. Fig 6.3 shows how the material released inside canyon 1 is transported in the downstream direction for the four cases being considered. The colors display the mass fraction of the tracer. The figure shows how the height of the plume above the canyon increases with increased buoyancy levels. The height of the plume can be used to estimate the height of the urban boundary layer which is the layer above an urban area which is directly affected by the build environment. The height of the urban boundary layer is of interest where it determines the volume into which the pollutants are mixed and diluted. In Fig 6.4 the heights of the four plumes above the canyons are plotted. For the neutral case ($Ri = 0$) the height of the plume increases due to dispersion of pollutants. It increases from 2.5 m above canyon 1 to 14.5 m above canyon 10. If the most buoyant case ($Ri = -37.0$) is considered the height increases from 4 m above canyon 1 to about 30 m above canyon 10 which means that the pollutants have more volume in which to be diluted. Fig 6.5 shows the average tracer concentration inside each canyon and how the tracer released upstream affects the tracer concentration in the downstream canyons. For the neutral case the average tracer concentration increases in each downstream canyon. The pollution increases by 80% between canyon 1 and canyon 10. That indicates that the advection term greatly impacts the level of air pollution in an urban area. However, the figure shows how the average concentration inside the canyons is near constant for the three buoyant cases.

The turbulence kinetic energy, k_{can}, inside the canyon is a parameter used to estimate the level of dispersion and transport of pollutants out of the canyons. Fig 6.6 shows the distribution of the turbulence kinetic energy inside canyon 5 for the four different buoyant cases. For the neutral case the largest turbulence kinetic energy is just above the canyon and it is there that the mixing of air and pollutants is occurring. When the buoyancy level increases, generation of turbulence also occurs inside the canyon through the buoyancy of the released material. The increase in the average turbulence kinetic energy inside the canyon between the neutral case and the most buoyant case is about 26 times. The relationship between the average tracer concentration inside the canyons and the turbulence kinetic energy is shown in Fig 6.7. The best fit gives us the following relationship

$$\boldsymbol{C(k) \sim 0.02k^{-0.48}}, \qquad \textbf{6.6}$$

This indicates that the average concentration inside the canyon decreases by increased turbulence kinetic energy raised to the power of -0.5.

Finally, the effects of the buoyancy intensity on the exchange velocity is calculated which was introduced in Chapter 5. The following equation defines the rate of exchange of air between the canyon and above air

$$\boldsymbol{Q = (C_{in} - C_{amb})w_e L}, \qquad \textbf{6.7}$$

where Q is the mass flow rate (kg m-1s-1), C_{in} the average pollution inside the canyon (kg m-3), C_{amb} the average ambient pollution (kg m-3), w_e the rate of air exchange

between ambient (m s-1) and canyon air, and L the width of the canyon (m). Fig 6.8 shows the calculated exchange velocity as a function of Ri and the best fit indicates that the exchange velocity increases with Ri raised to the power of 0.5.

Let's consider an artificial case where the pollutant is CO (which is of a similar density to air) and the urban area is under neutral buoyancy condition. The best fit for the neutral case simulation introduced in Fig 6.5 is $C(n) \sim 1.046n^{0.23}$ where C is the concentration and n is the number of the canyon. Let each canyon and its upstream building span 20 m. Consider as an example Los Angeles, which is one of the largest built-up urban areas in the world, covering 1,214 km2 or about 34 km in length assuming the built area to be a square. According to these assumptions, Los Angeles is thus built of about 1,700 street canyons and the most downstream canyon should then be six times more polluted than the first canyon during neutral weather conditions (no buoyancy effects).

Conclusions

By CFD simulations the role of advection in determining air quality within an idealized built urban environment has been estimated and also the effects of buoyancy. For the neutral case the increase in air pollution in the tenth canyon is 80% compared with the air pollution in the first canyon. The trend around the world is that urban areas are growing. The urban environment is simplified into two-dimensional urban street canyons and the focus is set on the case when the flow is perpendicular to the canyons which is the worst direction for air pollutants to disperse and be transported from street

canyons accordingly to Sabbatino et al. [107]. Despite the two-dimensional approach simulations give a quantitative estimate of the removal of air pollutants from street canyons and transport of air pollutants within a built urban environment. More field experiments and laboratory experiments on the effects of horizontal advection of pollutants on the air quality within the built urban environments are needed. Such experiments are necessary to increase the understanding on the risk factors within the built urban environments.

Figures

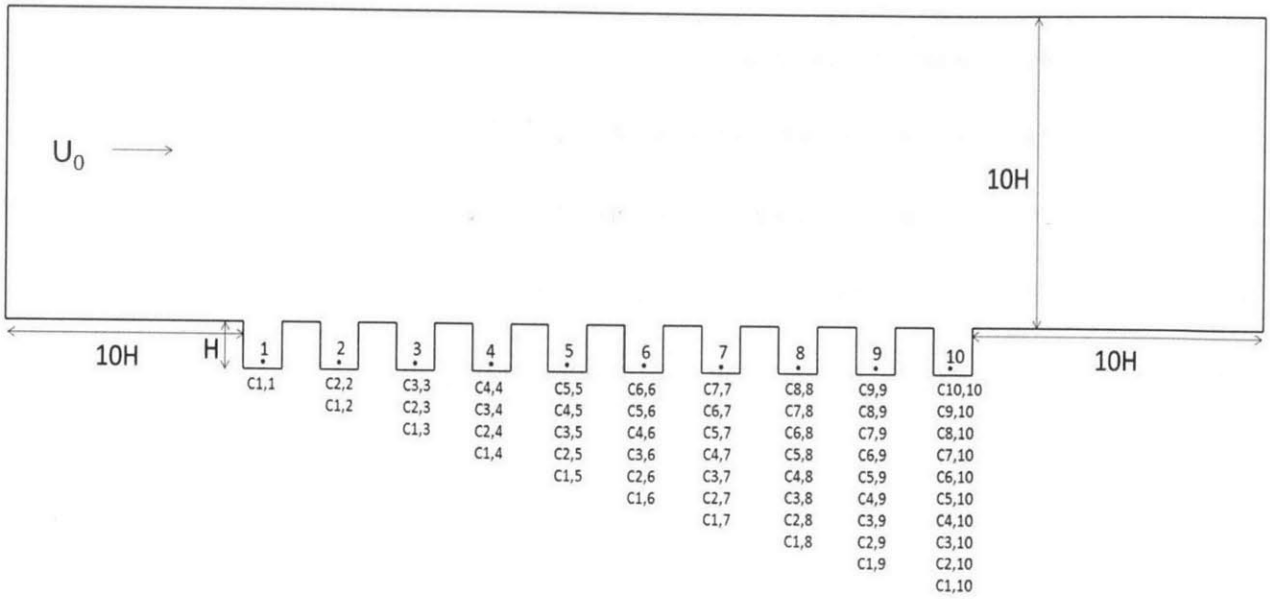

Fig 6.1 The ten adjacent canyons and the computational domain. The same amount of a tracer is released inside each canyon.

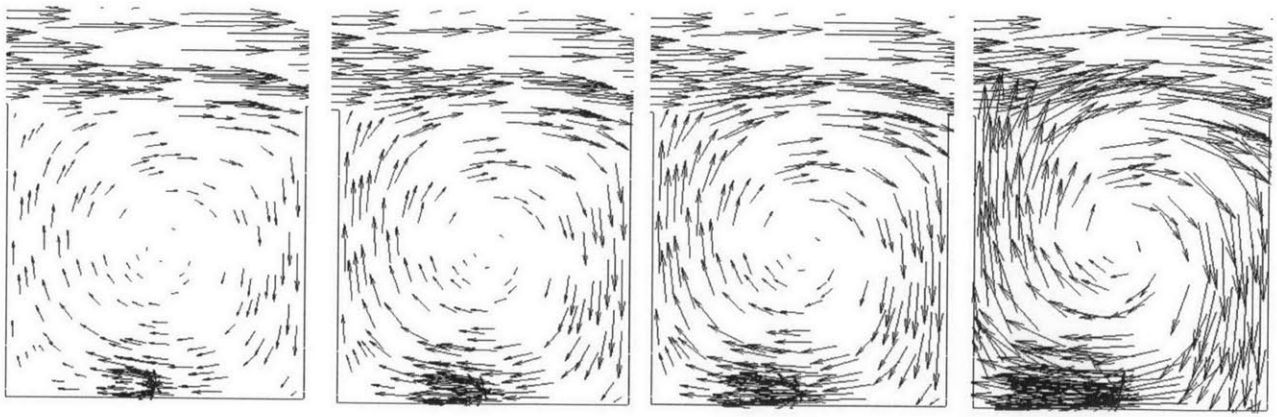

Fig 6.2 The flow field in canyon number 5 for the four Richardson numbers (0, -1.9, -3.7, -37).

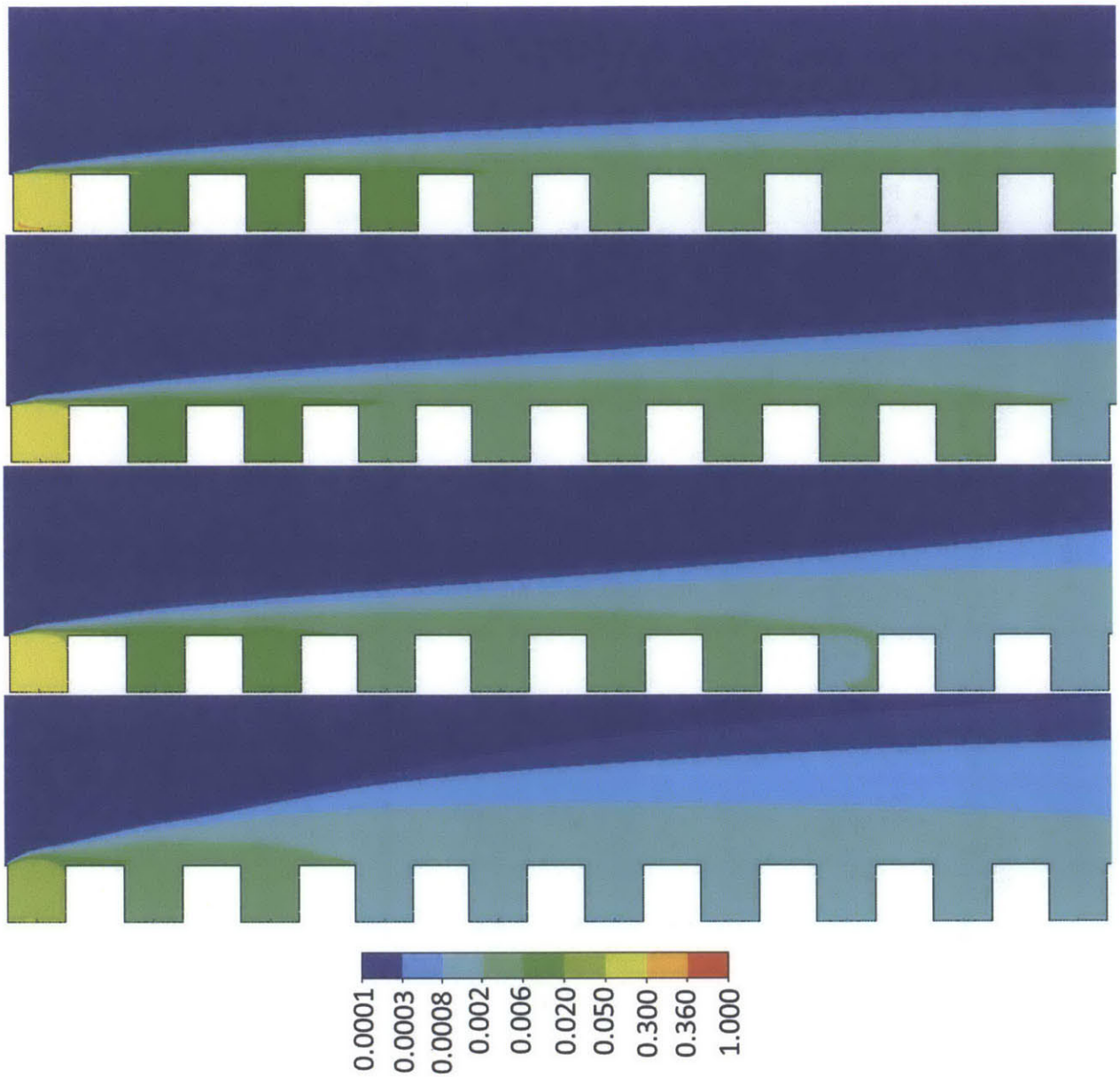

Fig 6.3 The mass fraction of pollutant released inside canyon 1 on a logarithmic scale for the four *Ri* values (0, -1.9, -3.7, -37).

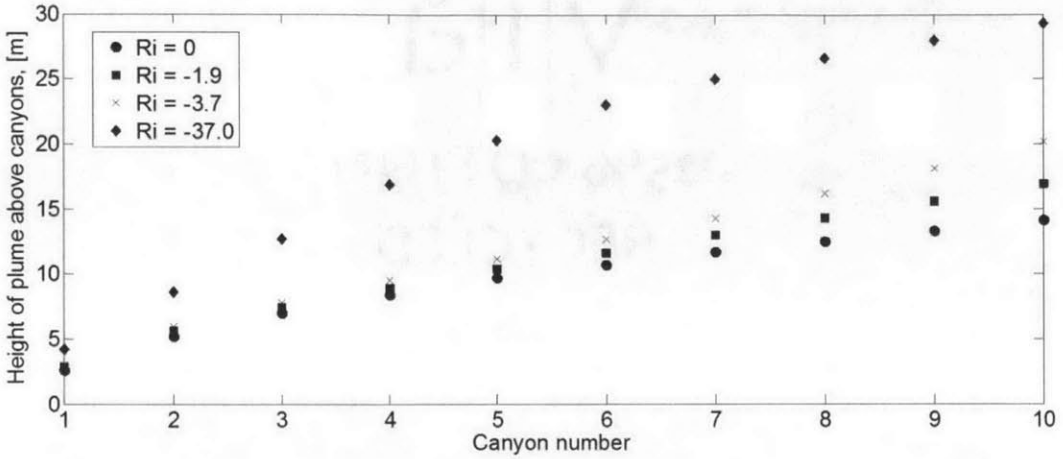

Fig 6.4 The height of the plume above the canyons. The height determines the volume in which the pollutants are diluted.

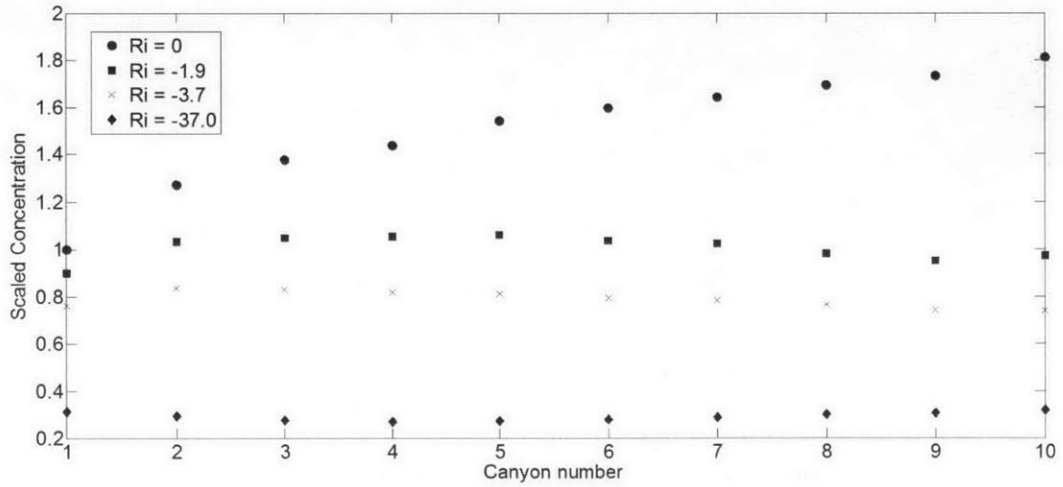

Fig 6.5 The average concentration inside the ten canyons with aspect ratio 1. Similar results obtained for canyons with aspect ratios 0.5 and 2.

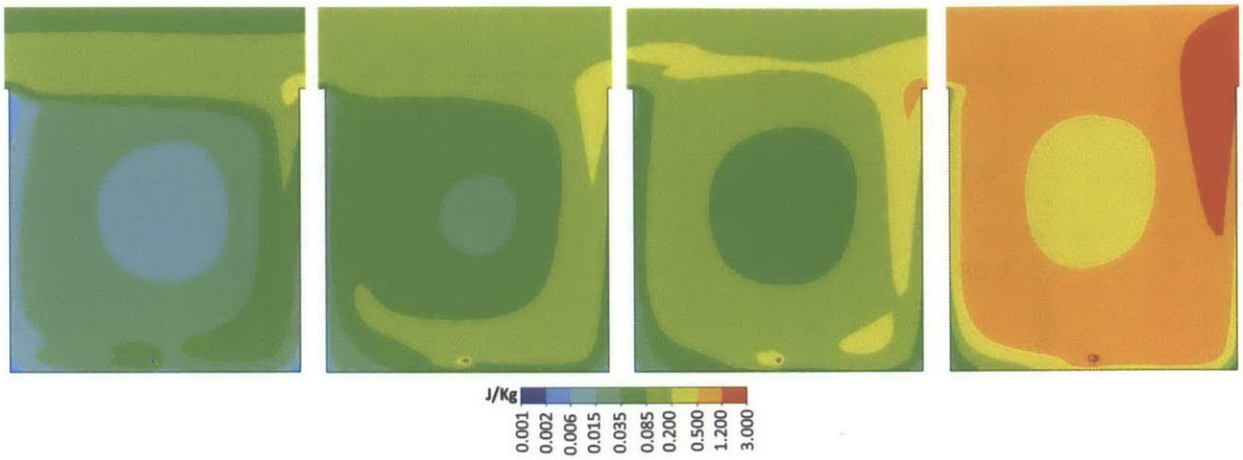

Fig 6.6 The turbulence kinetic energy in- and above canyon 5 for four *Ri* values.

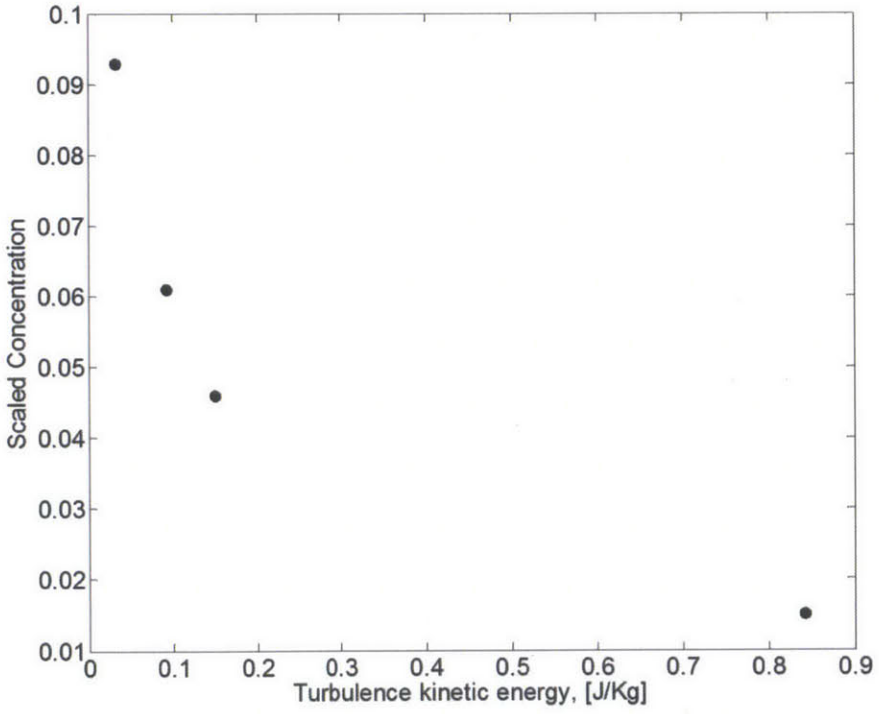

Fig 6.7 The relationship between the average in-canyon scaled concentration and the turbulence kinetic energy.

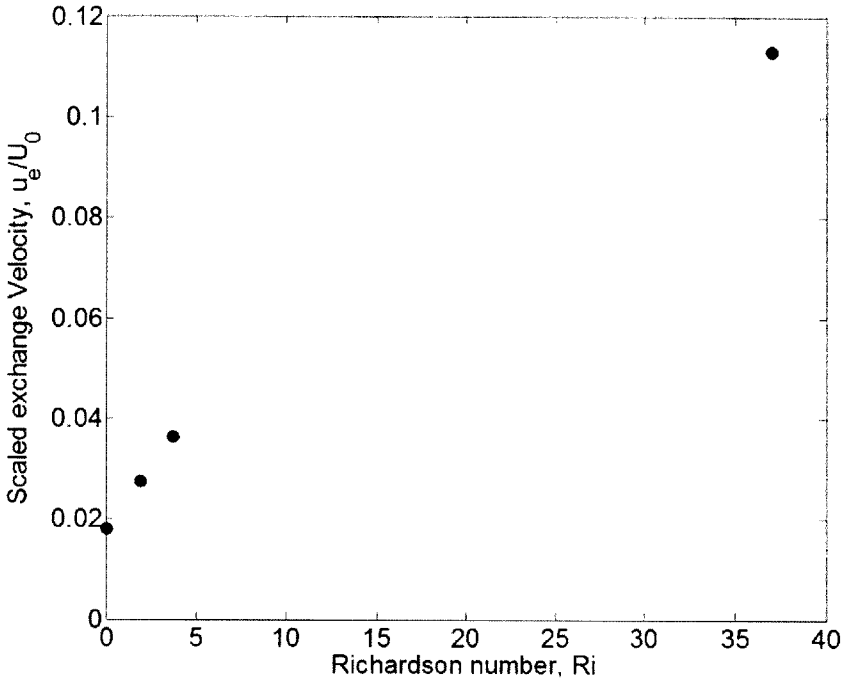

Fig 6.8 The calculated exchange velocity as a function of the Richardson number.

Chapter 7: Conclusions, Summary and Future Research Directions

This study shows how thermal contrasts in urban environments introduce buoyancy that can be the driving force in determining the air flows within the built urban environments. Assessing urban air quality the thermal conditions need to be considered as well as advection. The buoyancy parameter, B, is used to classify the importance of the buoyancy and to evaluate under what synoptic wind and thermal circumstances it is necessary to account for the buoyancy. Buoyancy driven plumes above urban areas were considered in Chapter 2. It was shown how the mass flux inside the plume can alone be responsible to meet environmental standards on air pollution concentration inside cities. In the calculations the buildings and the drag caused by them is not considered. Chapter 3 focused on a street scale field experiment performed in Singapore during the summer of 2012. It shows how the air flow inside an urban street canyon is influenced by the thermal situations inside it. The heated surfaces of the street canyon affect the mechanically driven air flow inside the canyon. Because of limited data, CFD simulations were introduced in Chapter 4 where the importance of the buoyancy relative to the mechanical force, on the air flow has been extended beyond other studies. The buoyancy parameter, B, first introduced in Dallman et al. [37], is used to estimate the balance between the mechanical force and the buoyancy force on the in-canyon air flow in wind-buoyancy driven flow. The flow is considered to be purely mechanically driven when B is less than 0.1, in an intermediate regime when B is between 0.1 and 50, and purely

buoyancy driven when B is larger than 50. The air exchange at the top interface of an urban street canyon was then calculated in Chapter 5. The air quality in a city (breathability) and the thermal stress on the inhabitants are important health factors for the population. The exchange velocity and the residence time are appropriate parameters to estimate the breathability of an urban area. Finally, the importance of the horizontal advection of air pollutants on the air pollution concentration was simulated in Chapter 6. It shows how the concentration of a passive tracer increases in the downstream direction.

There are several situations where buoyancy can affect the air flow within the built urban environments. Low albedo façade materials increase the buoyancy effects in the built urban environments. Natural ventilation of buildings has become more popular in increasing urbanized areas, due to requirements on green buildings and to reduce energy cost. One method to increase the air flow of buildings is to utilize rising heated air (convection). Solar chimneys have been applied for natural ventilation of buildings for centuries, for example in the Middle East. Chimneys are used to increase the effects of the rising heated air, which leads to increased flow of air inside the buildings. Solar chimneys apply the heat from the sun to warm up façades near the buildings and by that providing air flow through the buildings. Both CFD simulations as well as experiments on the effects of the solar chimneys on the indoor air have been performed (Gan and Riffat [113], Ong [114], Zhou et al. [115], Bassiouny and Koura [116], Balocco [117], Chen et al. [118]). These studies show the ventilation increases with the chimney wall temperature and heat gain. Recently a wind tower was built in the Masdar City in Abu Dhabi to ventilate the city ([119]). Abu Dhabi is located in a desert of generally low

synoptic winds. Utilizing convection is thus straightforward. During low synoptic wind periods the tower draws air from the streets due to convection and when the wind is blowing the tower can push air down to increase the air flow at the street level.

Two additional scenarios will now be considered to encourage further research in this field. First, the two extreme cases at the city scale are considered, i.e., an air flow inside the urban canopy layer which is purely mechanically driven versus air flow which is purely buoyancy driven, to give an estimate on the importance of each force separately. Chapter 5 applied a method first introduced by Bentham and Britter [77] to calculate the exchange velocity at the top interface of the urban canopy layer. A method introduced by Michaux and Vauquelin [30] and applied in Chapter 2 deals with plumes originating in a circular source. Results on the exchange velocities from the two sources can be compared and an estimate on what synoptic wind is needed compared with the heat flux in a buoyant source to disperse the same amount of air pollutants from an urban area will be obtained. Thus, imagine a typical circular downtown area with 1 km diameter, with the average building height of 25 m and the frontal density of 0.5 (Bentham and Britter [77]). Using the method introduced in Chapter 5 and the calculations on a buoyant plume originated in an area source from Chapter 2, it is possible to compare the effects of the mechanically driven flow and the buoyancy driven flows on the air exchange rate. Fig 7.1 shows the exchange velocity as a function of the heat flux (Q) and the above ambient air velocity (U_0). The graph quantifies the effects of Q and U_0 (buoyancy and mechanical forcing) on w_e. For example a city with an average heat flux of 250 W m-2 and no

ambient wind leads to an exchange velocity of about 0.45 m s-1, which is also obtained in a city with no heat flux and ambient velocity of 10 m s-1.

Finally, CFD simulations are applied at street scale (Chapter 4 and 5) to address the thermal effects on the flow inside a two-dimensional urban street canyon. We consider now the two extreme cases (purely mechanically driven and purely buoyancy driven). The flow structure inside the canyons is shown in Fig 7.2. All of the three surfaces are heated in the purely buoyant case, leading the formation of two vortices in inside the canyon. The results on the exchange velocity are then introduced in Fig 7.3. As an example, to obtain an exchange velocity of 0.06 m s-1, the ambient velocity needs to 4 m s-1 or the heat flux 200 W m-2. These simulations show further the importance of the buoyancy and why it needs to be considered in air quality and plume models and other atmospheric dispersion models that are applied on urban areas to evaluate the policy on air quality.

The approach in this thesis was to simplify the configurations of the built urban environments into two-dimensional urban street canyons and thus make it possible to investigate in a general way the physical processes of interests without the effects of complex configurations. City centers and downtown areas consist in many places of tall buildings and are surrounded by low raised suburban areas. In order to answer the questions raised in this study locally, either expensive and sophisticated field experiments or CFD simulations need to be performed. The work done by Hanna et al. [99] in Manhattan and by Fernando et al. [39] in Phoenix are examples of such experiments. More work can be done to investigate the thermal effects in the real built urban

environments. Due to complex flow systems around individual buildings and the interplay between buildings, heat can be trapped at certain locations within urban areas, for example in wakes behind buildings. At those locations the buoyancy effects on the flow is strong. The effects of the unsteady synoptic wind flow, the unequal heat fluxes within an urban area and different building configurations are all factors that affect the physical questions asked in this thesis and need further considerations, but despite that the results introduced in this study are useful and a motivation for further research in this field. The following research tasks are suggested to further extend the research introduced in this thesis:

- Perform a field experiment of a similar set-up as introduced in Chapter 3 over a longer period of time. The field experiment should be performed at a location with low synoptic winds and high thermal effects to extend the buoyancy effects beyond what was obtained in the current experiment.

- Perform unsteady CFD simulations with respect to free stream wind magnitudes and directions to investigate if and then under what conditions the unsteadiness dominates and/or eliminates the thermal impacts.

- Perform three-dimensional CFD simulations on an urban area (at least 200 m times 200 m) to investigate if the three air flow regimes exist in a real environment. Factors such as building density, frontal density and heights of buildings should be considered.

- Perform three-dimensional CFD simulations at an urban area to evaluate for how long time and how far downstream at average an air parcel travels within the urban environment before it is removed from the urban canopy layer at the top interface. Factors such as building density, frontal density and heights of buildings should be considered.

Figures

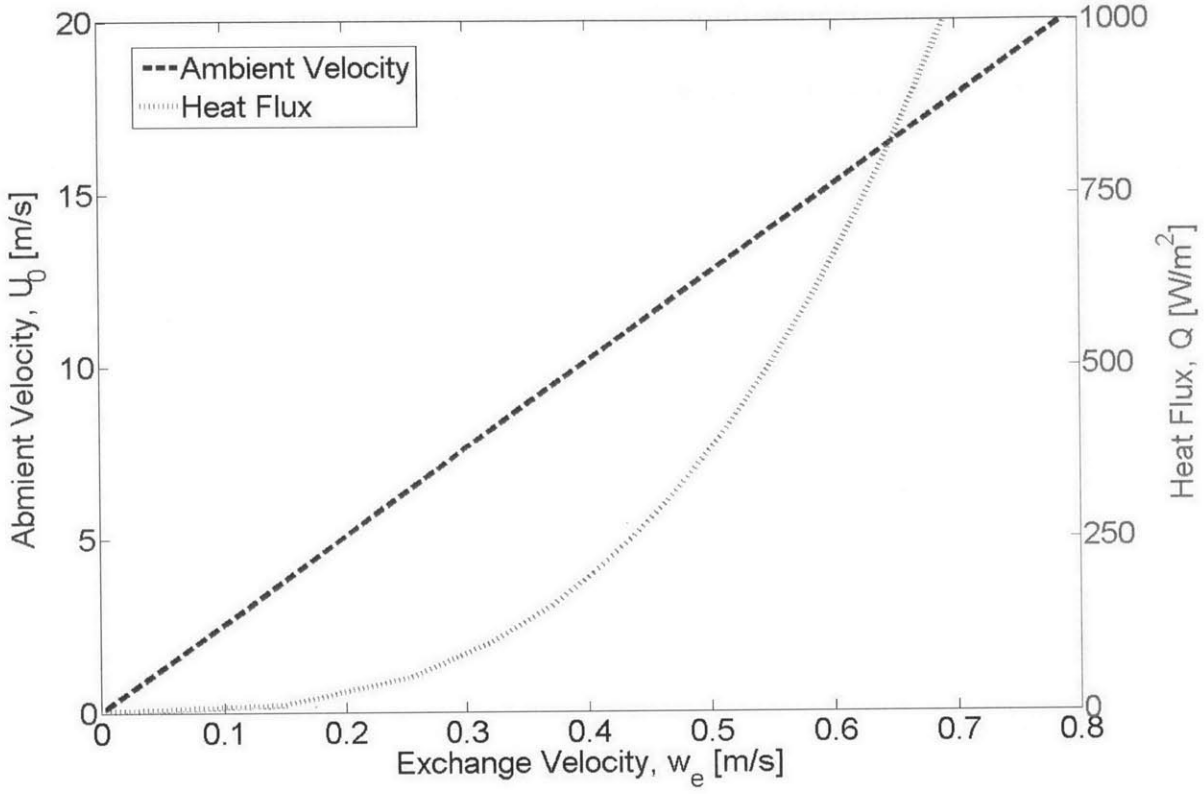

Fig 7.1 The effects of mechanically and buoyancy driven flows on the exchange velocity, w_e.

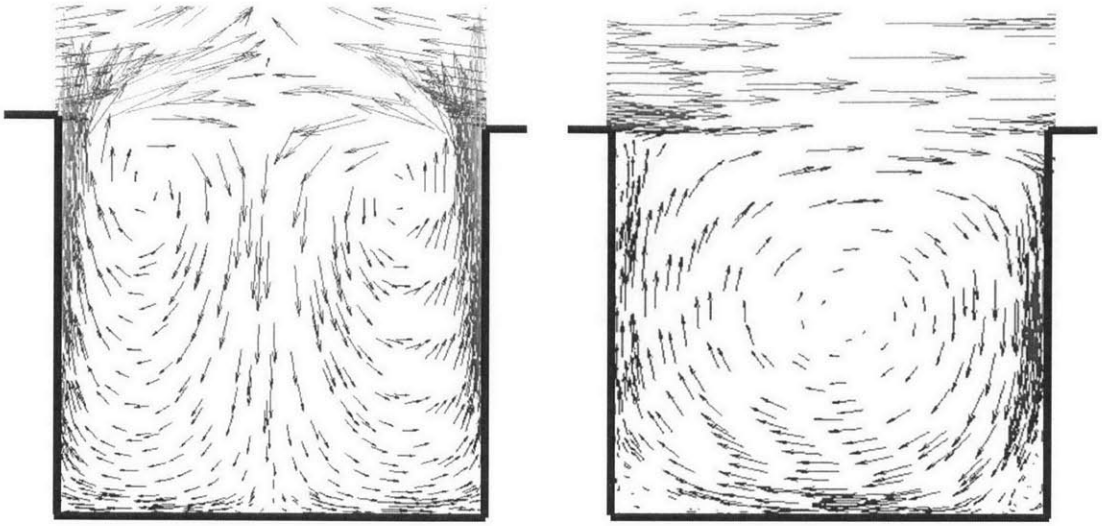

Fig 7.2 Purely buoyancy driven and purely mechanically driven street canyons.

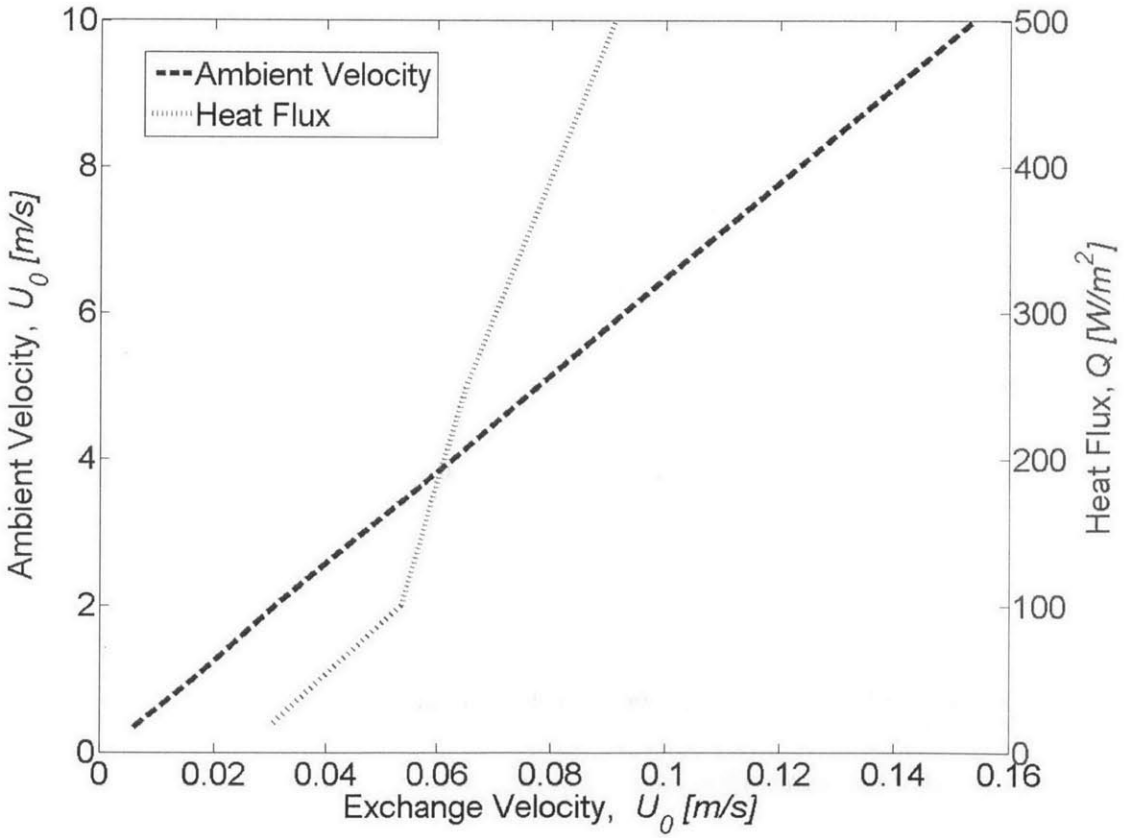

Fig 7.3 The exchange velocity inside a purely mechanically driven canyon and a buoyancy driven canyon.

Appendix 1 – Theoretical Considerations

The following deduction is based on the work published in Dallman et al. [37]. For a skimming flow regime (or a flow in transition between skimming flow and wake interference) the horizontal and vertical velocities in a canyon are in general proportional to each other. Thus for a mechanically driven flow the following relationship exists:

$$\boldsymbol{\beta}\, \boldsymbol{w_m/H} \approx \boldsymbol{u_m/L} \sim \boldsymbol{U_0/L}$$

where $\beta \approx 1$ (see Dallman et al. [37]), H the height of the canyon (m), w_m the characteristic in-canyon vertical mechanical velocity (m s-1), u_m the characteristic in-canyon horizontal velocity (m s-1), U_0 the ambient free stream velocity perpendicular to the axis of the canyon (m s-1) and L the width of the canyon (m).

Now consider the case when U_0 is weak and the temperature of the walls are not equal ($T_1 \neq T_2$). Under these situations a buoyancy driven circulation is dominant with a characteristic in-canyon horizontal velocity, u_t (m s-1), and a characteristic in-canyon vertical velocity, w_t (m s-1). The buoyancy circulation velocity vector, $\underline{u_t} = (u_t,\ w_t)$, can be estimated by applying the equation for vorticity generation, i.e.,

$$\boldsymbol{D\underline{\omega}/Dt} = \boldsymbol{\underline{\omega}\nabla\underline{u}} + \boldsymbol{\nabla p \times \nabla(1/\rho)} + \boldsymbol{\nu\, \nabla^2\underline{\omega}},$$

where $\underline{\omega}$ is the vorticity (s-1), ρ the ambient fluid density (kg m-3), p the ambient pressure (Pa) and ν the kinematic viscosity (m2 s-1). The contribution of vorticity due to vortex stretching ($\underline{\omega}\nabla\underline{u}$) is neglected and the diffusion of the vorticity term ($\nu\, \nabla^2\underline{\omega}$) only considers flow in two dimensions. Then:

$$D\underline{\omega}/Dt \sim \nabla p \times \nabla(1/\rho) \sim \nabla \times \underline{b},$$

where $\underline{b} = g\,\alpha\,\Delta T$ is the buoyancy (m s-2), g is the gravitational acceleration (m s-2), α the thermal expansion coefficient (K-1) and $\Delta T = T_2 - T_1$ (K). Considering the vorticity around the canyon axis, the y-component, and assuming a quasi-steady flow, the equation can be reduced to

$$\underline{u_t} \cdot \nabla \omega_y \sim -\frac{\partial \underline{b}}{\partial x},$$

where

$$\omega_y \sim -(\partial u/\partial z - \partial w/\partial x)$$

$$\sim -[\, u_t/H + w_t/L \,]$$

$$\sim -[\, u_t/H + u_t/H\,(H/L)^2 \,]$$

$$\sim -(u_t/H)[1 + (H/L)^2].$$

For $H/L \lesssim 1$, with $u_t/L \sim w_t/H$, the relationship is:

$$\underbrace{u_t \frac{\partial \omega_y}{\partial x}} + \underbrace{w_t \frac{\partial \omega_y}{\partial z}} \sim -\underbrace{\frac{\partial b}{\partial x}}$$

$$-\frac{u_t}{L}\frac{u_t}{H}\left[1 + \left(\frac{H}{L}\right)^2\right] - \frac{w_t}{H}\frac{u_t}{H}\left[1 + \left(\frac{H}{L}\right)^2\right] \sim -\frac{g\,\alpha\,\Delta T}{L}.$$

Then, the scale for thermal circulation is

$$u_t \sim \left(\frac{g\,\alpha\,\Delta T\,H}{[1+(H/L)^2]}\right)^{1/2}.$$

Considering the case where both buoyant circulation and mechanically forced circulation exist, the balance is given by

$$B = \left(\frac{g\,\alpha\,\Delta T\,H}{u_0{}^2\,[1+(H/L)^2]}\right),$$

where B is the dimensionless buoyancy parameter.

Appendix 2 – Finite Volume Method

Sources: Ansys Fluent Theory Guide [53], *Ferziger and Peric* [120], *and Strang* [121]:

Considering the general conservation equation

$$\frac{\partial(\rho\varphi)}{\partial t} + \nabla \cdot \rho\varphi\vec{V} = -\nabla \cdot \vec{q}_{\varphi} + S_{\varphi}$$

Where φ is any specific quantity, ρ is the fluid density (kg m-3), $\vec{V}$ is the velocity vector (m s-1), S is the generation of the specific quantity per unit volume and $\vec{q}_{\varphi}$ a transport term (diffusion etc.).

The idea behind the finite volume method is to integrate the equation and discretize the integrated equation instead of discretizing the equation on the differential form. Integrating the conservation equation gives:

$$\frac{\partial}{\partial t}\int_{CV} \rho\varphi \, dV + \int_{CS} \rho\varphi(\overrightarrow{V} \cdot \vec{n})dA = -\int_{CS} \vec{q}_{\varphi} \cdot \vec{n}dA + \sum \int_{CV} S_{\varphi}dV,$$

where CV is the control volume and CS the control surface.

The volume integral is calculated by integration of the volume of CV. The simples way is to take mean value of the integrand, i.e.,

$$\int_{CV} S_{\varphi}dV = \overline{S_{\varphi}} \cdot \Delta V$$

The surface integrals are calculated from the net flux through the CV boundaries (grids). In two dimensions we have four faces and six in three dimensions. Different schemes are

used to solve the equations. The one we use is the upwind method which approximates the value of scalars at nodes upwind of the face. For further considerations see for example Ferziger and Perić [120].

Appendix 3 – k-ε Turbulence Model

Source: Ansys Fluent Theory Guide [53]

The RANS equations:

$$\frac{d\rho}{dt} + \frac{d}{dx_i}(\rho u_i) = 0$$

$$\frac{d}{dt}(\rho u_i) + \frac{d}{dx_j}(\rho u_i u_j) = -\frac{dp}{dx_j}\left[\mu(\frac{du_i}{dx_j} + \frac{du_j}{dx_i} - \frac{2}{3}\delta_{ij})\right] + \frac{d}{dx_j}(-\rho\overline{u_i' u_j'})$$

The last term in the second equation is the Reynolds stresses, which must be modeled in order to close the equation.

The Boussinesq hypothesis is the method used in k-ε models.

$$-\rho(-\rho\overline{u_i' u_j'}) = \mu_t\left(\frac{\partial u_i}{\partial x_j} + \frac{\partial u_j}{\partial x_i}\right) - \frac{2}{3}(\rho k + \mu_t\frac{\partial u_k}{\partial x_k})\delta_{ij}$$

The turbulence kinetic energy, k, and its rate of dissipation, ε, are obtained from the following transport equations:

$$\frac{d}{dt}(\rho k) + \frac{d}{dx_i}(\rho k u_i) = \frac{d}{dx_j}\left[\left(\mu + \frac{\mu_t}{\sigma_k}\right)\frac{dk}{dx_j}\right] + G_k + G_b - \rho\varepsilon - Y_M + S_k$$

$$\frac{d}{dt}(\rho\varepsilon) + \frac{d}{dx_i}(\rho\varepsilon u_i) = \frac{d}{dx_j}\left[\left(\mu + \frac{\mu_t}{\sigma_\varepsilon}\right)\frac{d\varepsilon}{dx_j}\right] + C_{1\varepsilon}\frac{\varepsilon}{k}(G_k + C_{3\varepsilon}G_b) - C_{2\varepsilon}\rho\frac{\varepsilon^2}{k} + S_\varepsilon$$

G_k: Generation of turbulence kinetic energy due to mean velocity gradients.

G_b: Generation of turbulence kinetic energy due to buoyancy

$$G_b = -g_i \frac{\mu_t}{\rho Pr_t} \frac{\partial \rho}{\partial x_i}$$

where, g is gravity (m s-2), μ_t turbulent viscosity (kg m-1s-1) and Pr_t the Prandtl number.

Y_M: The contribution of the fluctuating dilatation in compressible turbulence to the overall dissipation rate.

$C_{1\varepsilon}$, $C_{2\varepsilon}$, $C_{3\varepsilon}$: Constants.

σ_k, σ_ε: The turbulent Prandtl numbers for k and ε.

S_k, S_ε: User defined source terms.

References

[1] "World Urbanization Prospects, the 2011 Revision." [Online]. Available: http://esa.un.org/unup/. [Accessed: 17-Nov-2013].

[2] "The 2011 United Nations Demographic Yearbook - Google Search." [Online]. Available: https://www.google.com/search?q=The+2011+United+Nations+Demographic+Yearbook&ie=utf-8&oe=utf-8&aq=t&rls=org.mozilla:en-US:official&client=firefox-a&channel=fflb. [Accessed: 11-Mar-2014].

[3] D. W. Dockery, C. A. Pope 3rd, X. Xu, J. D. Spengler, J. H. Ware, M. E. Fay, B. G. Ferris Jr, and F. E. Speizer, "An association between air pollution and mortality in six U.S. cities," *N. Engl. J. Med.*, vol. 329, no. 24, pp. 1753–1759, Dec. 1993.

[4] "Blackest day," *The Economist*. [Online]. Available: http://www.economist.com/blogs/analects/2013/01/beijings-air-pollution. [Accessed: 07-Nov-2013].

[5] D. LeComte, "Global Weather Highlights 2010: Flooding, Heatwaves, and Fires," *Weatherwise*, vol. 64, no. 3, pp. 21–28, 2011.

[6] D. Li and E. Bou-Zeid, "Synergistic Interactions between Urban Heat Islands and Heat Waves: The Impact in Cities Is Larger than the Sum of Its Parts*," *J. Appl. Meteorol. Climatol.*, vol. 52, no. 9, pp. 2051–2064, Sep. 2013.

[7] Y.-H. Kim and J.-J. Baik, "Maximum Urban Heat Island Intensity in Seoul," *J. Appl. Meteorol.*, vol. 41, no. 6, pp. 651–659, Jun. 2002.

[8] D. K. Papanastasiou and C. Kittas, "Maximum urban heat island intensity in a medium-sized coastal Mediterranean city," *Theor. Appl. Climatol.*, vol. 107, no. 3–4, pp. 407–416, Feb. 2012.

[9] T. R. Oke, "City size and the urban heat island," *Atmospheric Environ. 1967*, vol. 7, no. 8, pp. 769–779, Aug. 1973.

[10] H. Kim, J.-S. Ha, and J. Park, "High Temperature, Heat Index, and Mortality in 6 Major Cities in South Korea," *Arch. Environ. Occup. Health*, vol. 61, no. 6, pp. 265–270, 2006.

[11] J. Allegrini, V. Dorer, and J. Carmeliet, "Wind tunnel measurements of buoyant flows in street canyons," *Build. Environ.*, vol. 59, pp. 315–326, Jan. 2013.

[12] X.-X. Li, R. E. Britter, T. Y. Koh, L. K. Norford, C.-H. Liu, D. Entekhabi, and D. Y. C. Leung, "Large-Eddy Simulation of Flow and Pollutant Transport in Urban

Street Canyons with Ground Heating," *Bound.-Layer Meteorol.*, vol. 137, no. 2, pp. 187–204, Nov. 2010.

[13] *United Nations Environment Programme (UNEP). http://www.unep.org/urban_environment/issues/urban_air.asp. Retrieved online 09/26/2013.*.

[14] L. Howard, *The Climate of London: Deduced from Meteorological Observations Made in the Metropolis and at Various Places Around it.* Harvey and Darton, J. and A. Arch, Longman, Hatchard, S. Highley [and] R. Hunter, 1833.

[15] R. B. Stull, *An introduction to boundary layer meteorology.* Springer, 1988.

[16] S. R. Gaffin, "Variations in New York City's urban heat island strength over time and space," *Theor. Appl. Climatol.*, vol. 94, no. 1–2, p. 1, 2008.

[17] M. Roth, "Review of urban climate research in (sub)tropical regions," *Int. J. Climatol.*, vol. 27, no. 14, pp. 1859–1873, 2007.

[18] B. B. Hicks, W. J. Callahan, and M. A. Hoekzema, "On the Heat Islands of Washington, DC, and New York City, NY," *Bound.-Layer Meteorol.*, vol. 135, no. 2, pp. 291–300, May 2010.

[19] D. R. Streutker, "Satellite-measured growth of the urban heat island of Houston, Texas," *Remote Sens. Environ.*, vol. 85, no. 3, pp. 282–289, May 2003.

[20] K. Schäfer, S. Emeis, H. Hoffmann, and C. Jahn, "Influence of mixing layer height upon air pollution in urban and sub-urban areas," *Meteorol. Z.*, vol. 15, no. 6, pp. 647–658, Dec. 2006.

[21] S. Srivastava, S. Lal, D. B. Subrahamanyam, S. Gupta, S. Venkataramani, and T. A. Rajesh, "Seasonal variability in mixed layer height and its impact on trace gas distribution over a tropical urban site: Ahmedabad," *Atmospheric Res.*, vol. 96, no. 1, pp. 79–87, Apr. 2010.

[22] M. Simpson, S. Raman, J. K. Lundquist, and M. Leach, "A study of the variation of urban mixed layer heights," *Atmos. Environ.*, vol. 41, no. 33, pp. 6923–6930, Oct. 2007.

[23] L. Bianco, "Convective boundary layer depth: Improved measurement by Doppler radar wind profiler using fuzzy logic methods," *J. Atmospheric Ocean. Technol.*, vol. 19, no. 11, p. 1745, 2002.

[24] A. A. Bidokhti, "Estimation of urban mixed layer height in Zanjan using LIDAR observations and numerical modeling," *Proc. Indian Acad. Sci. Earth Planet. Sci.*, vol. 117, no. 6, p. 925, 2008.

[25] D. G. Steyn, M. Baldi, and R. M. Hoff, "The Detection of Mixed Layer Depth and Entrainment Zone Thickness from Lidar Backscatter Profiles," *J. Atmospheric Ocean. Technol.*, vol. 16, no. 7, pp. 953–959, Jul. 1999.

[26] L. Menut, C. Flamant, J. Pelon, and P. H. Flamant, "Urban Boundary-Layer Height Determination from Lidar Measurements Over the Paris Area," *Appl. Opt.*, vol. 38, no. 6, pp. 945–954, Feb. 1999.

[27] J. S. Turner, *Buoyancy effects in fluids*. Cambridge University Press, 1979.

[28] F. M. White, *Fluid mechanics*. New York: McGraw-Hill, 2008.

[29] B. R. Morton, G. Taylor, and J. S. Turner, "Turbulent Gravitational Convection from Maintained and Instantaneous Sources," *Proc. R. Soc. Lond. Ser. Math. Phys. Sci.*, vol. 234, no. 1196, pp. 1–23, Jan. 1956.

[30] G. Michaux and O. Vauquelin, "Solutions for turbulent buoyant plumes rising from circular sources," *Phys. Fluids*, vol. 20, no. 6, p. 066601, Jun. 2008.

[31] P. N. Papanicolaou and E. J. List, "Investigations of round vertical turbulent buoyant jets," *J. Fluid Mech.*, vol. 195, pp. 341–391, 1988.

[32] B. R. Morton, "Forced plumes," *J. Fluid Mech.*, vol. 5, no. 01, pp. 151–163, 1959.

[33] U. EPA, "US Environmental Protection Agency." [Online]. Available: http://www.epa.gov/. [Accessed: 17-Dec-2013].

[34] "Density, Car Ownership, and What It Means for the Future of Los Angeles | Streetsblog Los Angeles." [Online]. Available: http://la.streetsblog.org/2010/12/13/density-car-ownership-and-what-it-means-for-the-future-of-los-angeles/. [Accessed: 15-Dec-2013].

[35] "Publications & Research | Land Transport Authority." [Online]. Available: http://www.lta.gov.sg/content/ltaweb/en/publications-and-research.html. [Accessed: 15-Dec-2013].

[36] "Carbon Monoxide NAAQS | US EPA." [Online]. Available: http://www.epa.gov/ttn/naaqs/standards/co/s_co_index.html. [Accessed: 16-Dec-2013].

[37] A. Dallman, S. Magnusson, R. E. Britter, L. Norford, D. Entekhabi, and H. J. S. Fernando, "Conditions for Thermal Circulation in Urban Street Canyons," *Build. Environ.*, vol. (submitted for publication), 2014.

[38] R. E. Britter and S. R. Hanna, "Flow and Dispersion in Urban Areas," *Annu. Rev. Fluid Mech.*, vol. 35, no. 1, pp. 469–496, 2003.

[39] H. J. S. Fernando, D. Zajic, S. Di Sabatino, R. Dimitrova, B. Hedquist, and A. Dallman, "Flow, turbulence, and pollutant dispersion in urban atmospheres," *Phys. Fluids*, vol. 22, no. 5, p. 051301, 2010.

[40] J.-F. Sini, S. Anquetin, and P. G. Mestayer, "Pollutant dispersion and thermal effects in urban street canyons," *Atmos. Environ.*, vol. 30, no. 15, pp. 2659–2677, Aug. 1996.

[41] C. Biltoft, "Customer Report for Mock Urban Setting test - Google Scholar," *Tech Rep 2001 WDTC-FR-01-121 US Army Dugway Proving Ground Dugway Utah.*

[42] D. Zajic, H. J. S. Fernando, M. J. Brown, and E. R. Pardyjak, "On flows in simulated urban canopies," *Environ. Fluid Mech.*, pp. 1–29.

[43] T. R. Oke, "Street design and urban canopy layer climate," *Energy Build.*, vol. 11, no. 1, p. 103, 1988.

[44] A. F. Mills, *Heat Transfer*. Pearson Education, 1999.

[45] J.-J. Kim and J.-J. Baik, "A Numerical Study of Thermal Effects on Flow and Pollutant Dispersion in Urban Street Canyons," *J. Appl. Meteorol.*, vol. 38, no. 9, pp. 1249–1261, Sep. 1999.

[46] S.-B. Park, J.-J. Baik, S. Raasch, and M. O. Letzel, "A Large-Eddy Simulation Study of Thermal Effects on Turbulent Flow and Dispersion in and above a Street Canyon," *J. Appl. Meteorol. Climatol.*, vol. 51, no. 5, pp. 829–841, May 2012.

[47] S. Magnusson, A. Dallman, D. Entekhabi, R. E. Britter, L. Norford, and H. J. S. Fernando, "On Thermally Forced Flows in Urban Street Canyons," *Environ. Fluid Mech.*, vol. (Accepted), 2014.

[48] X.-X. Li, R. E. Britter, L. K. Norford, T.-Y. Koh, and D. Entekhabi, "Flow and Pollutant Transport in Urban Street Canyons of Different Aspect Ratios with Ground Heating: Large-Eddy Simulation," *Bound.-Layer Meteorol.*, vol. 142, no. 2, pp. 289–304, Feb. 2012.

[49] P. Louka, S. . Belcher, and R. . Harrison, "Coupling between air flow in streets and the well-developed boundary layer aloft," *Atmos. Environ.*, vol. 34, no. 16, pp. 2613–2621, 2000.

[50] P. Louka, G. Vachon, J.-F. Sini, P. G. Mestayer, and J.-M. Rosant, "Thermal Effects on the Airflow in a Street Canyon – Nantes'99 Experimental Results and Model Simulations," *Water Air Soil Pollut. Focus*, vol. 2, no. 5–6, pp. 351–364, Sep. 2002.

[51] E. Solazzo and R. E. Britter, "Transfer processes in a simulated urban street canyon," *Bound. - Layer Meteorol.*, vol. 124, no. 1, p. 43, 2007.

[52] X. M. Cai, "Effects of wall heating on flow characteristics in a street canyon," *Bound. - Layer Meteorol.*, vol. 142, no. 3, p. 443, 2012.

[53] ANSYS Inc., "ANSYS Fluent 14.0 Theory Guide." 2012.

[54] P. J. Richards and R. P. Hoxey, "Appropriate boundary conditions for computational wind engineering models using the k-ϵ turbulence model," *J. Wind Eng. Ind. Aerodyn.*, vol. 46–47, pp. 145–153, Aug. 1993.

[55] I. P. Castro and A. G. Robins, "The flow around a surface-mounted cube in uniform and turbulent streams," *J. Fluid Mech.*, vol. 79, no. 02, pp. 307–335, 1977.

[56] "WHO | World Health Organization," *WHO*. [Online]. Available: http://www.who.int/en/. [Accessed: 12-Feb-2014].

[57] J. E. Vena, "Air Pollution as a Risk Factor in Lung Cancer," *Am. J. Epidemiol.*, vol. 116, no. 1, pp. 42–56, Jul. 1982.

[58] Pope III C, Burnett RT, Thun MJ, Calle EE, Krewski D, Ito K, and Thurston GD, "Lung cancer, cardiopulmonary mortality, and long-term exposure to fine particulate air pollution," *JAMA*, vol. 287, no. 9, pp. 1132–1141, Mar. 2002.

[59] "The Mortality Effects of Long-Term Exposure to Particulate Air Pollution in the United Kingdom." [Online]. Available: http://www.comeap.org.uk/39-page/linking/51-the-mortality-effects-of-long-term-exposure-to-particulate-air-pollution-in-the-united-kingdom. [Accessed: 12-Feb-2014].

[60] S. H. L. Yim and S. R. H. Barrett, "Public Health Impacts of Combustion Emissions in the United Kingdom," *Environ. Sci. Technol.*, vol. 46, no. 8, pp. 4291–4296, Apr. 2012.

[61] P. Kumar, L. Morawska, W. Birmili, P. Paasonen, M. Hu, M. Kulmala, R. M. Harrison, L. Norford, and R. Britter, "Ultrafine particles in cities," *Environ. Int.*, vol. 66, pp. 1–10, May 2014.

[62] P. Kumar, A. Robins, S. Vardoulakis, and R. Britter, "A review of the characteristics of nanoparticles in the urban atmosphere and the prospects for developing regulatory controls," *Atmos. Environ.*, vol. 44, no. 39, pp. 5035–5052, Dec. 2010.

[63] B. R. Gurjar, A. Jain, A. Sharma, A. Agarwal, P. Gupta, A. S. Nagpure, and J. Lelieveld, "Human health risks in megacities due to air pollution," *Atmos. Environ.*, vol. 44, no. 36, pp. 4606–4613, Nov. 2010.

[64] "Train accidents stir worries about crude transport," *The Big Story*. [Online]. Available: http://bigstory.ap.org/article/train-accidents-stir-worries-about-crude-transport. [Accessed: 19-Feb-2014].

[65] J. H. Seinfeld and S. N. Pandis, *Atmospheric Chemistry and Physics: From Air Pollution to Climate Change*. John Wiley & Sons, 2012.

[66] A. C. Chamberlain, "Transport of Lycopodium Spores and Other Small Particles to Rough Surfaces," *Proc. R. Soc. Lond. Ser. Math. Phys. Sci.*, vol. 296, no. 1444, pp. 45–70, Jan. 1967.

[67] N. A. Esmen and M. Corn, "Residence time of particles in urban air," *Atmospheric Environ. 1967*, vol. 5, no. 8, pp. 571–578, Aug. 1971.

[68] W. G. N. Slinn, "Residence time of particles in urban air," *Atmospheric Environ. 1967*, vol. 7, no. 7, pp. 763–765, Jul. 1973.

[69] W. Humphries and J. H. Vincent, "An experimental investigation of the detention of airborne smoke in the wake bubble behind a disk," *J. Fluid Mech.*, vol. 73, no. 03, pp. 453–464, 1976.

[70] J. E. Fackrell, "Parameters characterising dispersion in the near wake of buildings," *J. Wind Eng. Ind. Aerodyn.*, vol. 16, no. 1, pp. 97–118, Jan. 1984.

[71] W. C. Cheng, C.-H. Liu, and D. Y. C. Leung, "Computational formulation for the evaluation of street canyon ventilation and pollutant removal performance," *Atmos. Environ.*, vol. 42, no. 40, pp. 9041–9051, Dec. 2008.

[72] S. Simoëns, M. Ayrault, and J. M. Wallace, "The flow across a street canyon of variable width—Part 1: Kinematic description," *Atmos. Environ.*, vol. 41, no. 39, pp. 9002–9017, Dec. 2007.

[73] J. Richmond-Bryant, S. S. Isukapalli, and D. A. Vallero, "Air pollutant retention within a complex of urban street canyons," *Atmos. Environ.*, vol. 45, no. 40, pp. 7612–7618, Dec. 2011.

[74] K. J. Allwine and J. E. Flaherty, "Joint Urban 2003: Study Overview and Instrument Locations," Pacific Northwest National Laboratory (PNNL), Richland, WA (US), PNNL-15967, Aug. 2006.

[75] W. C. Cheng, C.-H. Liu, and D. Y. C. Leung, "On the correlation of air and pollutant exchange for street canyons in combined wind-buoyancy-driven flow," *Atmos. Environ.*, vol. 43, no. 24, pp. 3682–3690, Aug. 2009.

[76] K.-H. Kwak and J.-J. Baik, "Diurnal variation of NOx and ozone exchange between a street canyon and the overlying air," *Atmos. Environ.*, vol. 86, pp. 120–128, Apr. 2014.

[77] T. Bentham and R. Britter, "Spatially averaged flow within obstacle arrays," *Atmos. Environ.*, vol. 37, no. 15, pp. 2037–2043, May 2003.

[78] "Six Common Air Pollutants | Air & Radiation | US EPA." [Online]. Available: http://www.epa.gov/air/urbanair/. [Accessed: 03-Oct-2013].

[79] L. N. Lamsal, R. V. Martin, D. D. Parrish, and N. A. Krotkov, "Scaling Relationship for NO2 Pollution and Urban Population Size: A Satellite Perspective," *Environ. Sci. Technol.*, vol. 47, no. 14, pp. 7855–7861, Jul. 2013.

[80] "China - Analysis - U.S. Energy Information Administration (EIA)." [Online]. Available: http://www.eia.gov/countries/cab.cfm?fips=CH. [Accessed: 03-Oct-2013].

[81] "Energy and You." [Online]. Available: http://www.epa.gov/cleanenergy/energy-and-you/. [Accessed: 03-Oct-2013].

[82] "Smoke from Canadian fires blankets NY, New England," *Boston.com*, 31-May-2010.

[83] "Indonesian forest fire and haze risk remains high," *Eco-Business*. [Online]. Available: http://www.eco-business.com/opinion/indonesian-forest-fire-and-haze-risk-remains-high/. [Accessed: 04-Oct-2013].

[84] H. Flentje, H. Claude, T. Elste, S. Gilge, U. Köhler, C. Plass-Dülmer, W. Steinbrecht, W. Thomas, A. Werner, and W. Fricke, "The Eyjafjallajökull eruption in April 2010 – detection of volcanic plume using in-situ measurements, ozone sondes and lidar-ceilometer profiles," *Atmos Chem Phys*, vol. 10, no. 20, pp. 10085–10092, Oct. 2010.

[85] D. L. Zhang, "Upstream urbanization exacerbates urban heat island effects," *Geophys. Res. Lett.*, vol. 36, no. 24, p. L24401, 2009.

[86] T. Brandsma, G. P. Können, and H. R. A. Wessels, "Empirical estimation of the effect of urban heat advection on the temperature series of De Bilt (The Netherlands)," *Int. J. Climatol.*, vol. 23, no. 7, pp. 829–845, 2003.

[87] S. E. Belcher, "Mixing and transport in urban areas," *Philos. Trans. - R. Soc. Math. Phys. Eng. Sci.*, vol. 363, no. 1837, p. 2947, 2005.

[88] R. E. Britter, S. D. Sabatino, F. Caton, K. M. Cooke, P. G. Simmonds, and G. Nickless, "Results from Three Field Tracer Experiments on the Neighbourhood Scale in the City of Birmingham UK," *Water Air Soil Pollut. Focus*, vol. 2, no. 5–6, pp. 79–90, Sep. 2002.

[89] D. Martin, C. S. Price, I. R. White, G. Nickless, K. F. Petersson, R. E. Britter, A. G. Robins, S. E. Belcher, J. F. Barlow, M. Neophytou, S. J. Arnold, A. S. Tomlin, R. J. Smalley, and D. E. Shallcross, "Urban tracer dispersion experiments during the second DAPPLE field campaign in London 2004," *Atmos. Environ.*, vol. 44, no. 25, pp. 3043–3052, Aug. 2010.

[90] K. J. Allwine, *Urban dispersion program MSG05 field study: summary of tracer and meteorological measurements*. 2006.

[91] K. J. Allwine, "Overview of URBAN 2000: A multiscale field study of dispersion through an urban environment," *Bull. Am. Meteorol. Soc.*, vol. 83, no. 4, p. 521, 2002.

[92] "Overview of Joint Urban 2003—An atmospheric dispersion study in Oklahoma City - Google Scholar." [Online]. Available: http://scholar.google.com/scholar?hl=en&q=Overview+of+Joint+Urban+2003%E2%80%94An+atmospheric+dispersion+study+in+Oklahoma+City&btnG=&as_sdt=1%2C22&as_sdtp=. [Accessed: 04-Oct-2013].

[93] R. Berkowicz, "OSPM — A Parameterised Street Pollution Model," in *Urban Air Quality: Measurement, Modelling and Management*, R. S. Sokhi, R. S. José, N. Moussiopoulos, and R. Berkowicz, Eds. Springer Netherlands, 2000, pp. 323–331.

[94] "AERMOD—description of model formulation - Google Scholar." [Online]. Available: http://scholar.google.com/scholar?q=AERMOD%E2%80%94description+of+model+formulation&btnG=&hl=en&as_sdt=0%2C22. [Accessed: 05-Oct-2013].

[95] A. J. Cimorelli, "AERMOD: A dispersion model for industrial source applications. Part I: General model formulation and boundary layer characterization," *J. Appl. Meteorol.*, vol. 44, no. 5, p. 682, 2005.

[96] S. G. Perry, "AERMOD: A dispersion model for industrial source applications. Part II: Model performance against 17 field study databases," *J. Appl. Meteorol.*, vol. 44, no. 5, p. 694, 2005.

[97] D. J. Carruthers, "UK-ADMS: A new approach to modelling dispersion in the earth's atmospheric boundary layer," *J. Wind Eng. Ind. Aerodyn.*, vol. 52, p. 139, 1994.

[98] S. Di Sabatino, R. Buccolieri, B. Pulvirenti, and R. Britter, "Simulations of pollutant dispersion within idealised urban-type geometries with CFD and integral models," *Atmos. Environ.*, vol. 41, no. 37, pp. 8316–8329, Dec. 2007.

[99] S. R. Hanna, "Detailed simulations of atmospheric flow and dispersion in downtown Manhattan: An application of five computational fluid dynamics models," *Bull. Am. Meteorol. Soc.*, vol. 87, no. 12, p. 1713, 2006.

[100] W. J. Coirier, "A computational fluid dynamics approach for urban area transport and dispersion modeling," *Environ. Fluid Mech.*, vol. 5, no. 5, p. 443, 2005.

[101] "JP2.11 CFD Modeling for Urban Area Contaminant Transport and Dispersion: Model Description and Data Requirements (2006 - Annual2006_6urban)." [Online]. Available: https://ams.confex.com/ams/Annual2006/techprogram/paper_99711.htm. [Accessed: 04-Oct-2013].

[102] S. R. Hanna, O. R. Hansen, and S. Dharmavaram, "FLACS CFD air quality model performance evaluation with Kit Fox, MUST, Prairie Grass, and EMU observations," *Atmos. Environ.*, vol. 38, no. 28, pp. 4675–4687, Sep. 2004.

[103] "Applications of CFD simulations of pollutant transport and dispersion within ambient urban building environments: Including homeland security. - Google Scholar." [Online]. Available: http://scholar.google.com/scholar?hl=en&q=Applications+of+CFD+simulations+of+pollutant+transport+and+dispersion+within+ambient+urban+building+environments%3A+Including+homeland+security.&btnG=&as_sdt=1%2C22&as_sdtp=#. [Accessed: 04-Oct-2013].

[104] P. M. GRESHO and S. T. CHAN, "Projection 2 Goes Turbulent - and Fully Implicit," *Int. J. Comput. Fluid Dyn.*, vol. 9, no. 3–4, pp. 249–272, 1998.

[105] R. Calhoun, "Flow around a complex building: Experimental and large-eddy simulation comparisons," *J. Appl. Meteorol.*, vol. 44, no. 5, p. 571, 2005.

[106] "13.12 Simulation of the MUST field experiment using the FEFLO-URBAN CFD model (2004 - AFAPURBBIO_5urban)." [Online]. Available:

https://ams.confex.com/ams/AFAPURBBIO/techprogram/paper_79468.htm. [Accessed: 04-Oct-2013].

[107] F. Camelli, "Assessing maximum possible damage for contaminant release events," *Eng. Comput.*, vol. 21, no. 7, p. 748, 2004.

[108] J.-J. Baik and J.-J. Kim, "A Numerical Study of Flow and Pollutant Dispersion Characteristics in Urban Street Canyons," *J. Appl. Meteorol.*, vol. 38, no. 11, pp. 1576–1589, Nov. 1999.

[109] L. J. Hunter, G. T. Johnson, and I. D. Watson, "An investigation of three-dimensional characteristics of flow regimes within the urban canyon," *Atmospheric Environ. Part B Urban Atmosphere*, vol. 26, no. 4, pp. 425–432, Dec. 1992.

[110] B. M. Leitl and R. N. Meroney, "Car exhaust dispersion in a street canyon. Numerical critique of a wind tunnel experiment," *J. Wind Eng. Ind. Aerodyn.*, vol. 67–68, pp. 293–304, Apr. 1997.

[111] S. M. Salim, R. Buccolieri, A. Chan, and S. Di Sabatino, "Numerical simulation of atmospheric pollutant dispersion in an urban street canyon: Comparison between RANS and LES," *J. Wind Eng. Ind. Aerodyn.*, vol. 99, no. 2–3, pp. 103–113, Feb. 2011.

[112] S. Di Sabatino, "Flow and pollutant dispersion in street canyons using FLUENT and ADMS-Urban," *Environ. Model. Assess.*, vol. 13, no. 3, p. 369, 2008.

[113] G. Gan and S. B. Riffat, "A numerical study of solar chimney for natural ventilation of buildings with heat recovery," *Appl. Therm. Eng.*, vol. 18, no. 12, pp. 1171–1187, Dec. 1998.

[114] K. S. Ong, "A mathematical model of a solar chimney," *Renew. Energy*, vol. 28, no. 7, pp. 1047–1060, Jun. 2003.

[115] X. Zhou, J. Yang, B. Xiao, and G. Hou, "Experimental study of temperature field in a solar chimney power setup," *Appl. Therm. Eng.*, vol. 27, no. 11–12, pp. 2044–2050, Aug. 2007.

[116] R. Bassiouny and N. S. A. Koura, "An analytical and numerical study of solar chimney use for room natural ventilation," *Energy Build.*, vol. 40, no. 5, pp. 865–873, 2008.

[117] C. Balocco, "A simple model to study ventilated facades energy performance," *Energy Build.*, vol. 34, no. 5, pp. 469–475, Jun. 2002.

[118] Z. D. Chen, P. Bandopadhayay, J. Halldorsson, C. Byrjalsen, P. Heiselberg, and Y. Li, "An experimental investigation of a solar chimney model with uniform wall heat flux," *Build. Environ.*, vol. 38, no. 7, pp. 893–906, Jul. 2003.

[119] "In Abu Dhabi, a Simple Wind Tower Cools the Desert," *greengopost.com*. [Online]. Available: http://greengopost.com/in-abu-dhabi-a-simple-wind-tower-cools-the-desert/. [Accessed: 16-Dec-2013].

[120] J. H. Ferziger and M. Perić, *Computational Methods for Fluid Dynamics*. Springer London, Limited, 2002.

[121] G. Strang, *Computational Science and Engineering*. Wellesley-Cambridge Press, 2007.